CBM

Compressed Baryonic Matter
experiment
at FAIR

PROGRESS REPORT

2009

CBM Progress Report 2009

ISBN 978-3-9811298-7-8

Editors: Walter F. J. Müller and Volker Friese

Printed in Darmstadt by GSI Darmstadt

This work was supported by the EU Integrated Infrastructure Initiatives HadronPhysics (I3HP) and HadronPhysics2 (grant No. 227431), the EU INTAS initiative (grant 06-1000012-8729), the Ministry of Science and Technology of China (grant 2008CB817707), the National Natural Science Foundation of China (grants 10620210287, 10610285, 10675072, 10775082, and 10875120), the Bundesministerium für Bildung und Forschung, Germany (06DR9059D, 06FY1731, 06HD190i, 06MN229I, 06WU9195I), GSI Helmholtzzentrum für Schwerionenforschung GmbH, the Helmholtz International Center for FAIR, the Helmholtz Alliance HA216/EMMI, the Helmholtz Research School H-QM, the Romanian NASR/CAPACITATI-Modul III contract nr. 42 and NASR/PARTENERIATE contract no. 71-144, the Russian Foundation for Basic Resqearch (grant 08-01-00800), and the Federal Agency of Russia for Atomic Energy (Rosatom).

Preface: FAIR News

FAIR modular start version

In 2009 the FAIR project experienced a complicated phase due to a dramatic cost increase for civil construction and the accelerator complex. Some of the additional costs result from the ground conditions. The Federal Republic of Germany and the State of Hesse announced to cover these site-dependent construction costs of 110 Mio Euro outside the FAIR project. Nevertheless, the FAIR phase A had to be staged in order to fit into the available budget. The so called modular FAIR start version consists of the following parts: SIS100 (module 0), the CBM-HADES underground cave and the APPA experimental hall (module 1), the Super-FRS and the fixed target area (module 2), the anti-proton facility including the collector ring (module 3), the Low-Energy Branch at the Super-FRS, NESR and FLAIR (module 4), and the RESR (module 5). Only the modules 0 – 3 will be realized in the first stage. The SIS300 accelerator will come in phase B, but the accelerator tunnel (in module 0) will be built large enough to host both SIS100 and SIS300. The FAIR modular start version will provide research opportunities for the four scientific pillars of FAIR (APPA, CBM, NuSTAR and PANDA). All FAIR experiments will be able to start their research programmes as soon as the first beams from SIS100 are available. Of course, as stated in the FAIR convention, the final goal is the full realization of FAIR including SIS300 which will provide high-energy beams for CBM and parallel operation of several experiments.

Russia signs FAIR contract

A major breakthrough towards the realization of FAIR was the decision of the Russian Federal Government on the Russian participation in FAIR on February 27, 2010. Russia approved the FAIR Convention and a contribution to FAIR construction by an amount of 178 Mio Euro (prices of January 2005). Now we are looking forward to the formation of the FAIR GmbH in 2010, and the start of construction in 2011.

Board of FAIR Collaborations constituted

In order to strengthen the scientific community within FAIR and help to coordinate research activities and funding issues, the Board of FAIR Collaborations (BFC) was constituted. The BFC consists of two representatives of each of the four scientific pillars of FAIR (APPA, CBM, NuSTAR, and PANDA), which will meet regularly to discuss common issues and joint initiatives.

FAIR experiment representatives at the BFC start-up meeting on March 3, 2010. From left to right: Christoph Scheidenberger (NuSTAR), Juha Äystö (NuSTAR), Dieter H.H. Hoffmann (HEDgeHOB/APPA), Peter Senger (CBM), Yuri Zaitsev (CBM), Ulrich Wiedner (PANDA), Reiner Krücken (NuSTAR), Klaus Peters (PANDA), Marek Pajek (SPARC/APPA)

Peter Senger, March 2010

Contents

Status of the CBM experiment at FAIR

P. Senger
GSI Darmstadt, Germany

Exploring the QCD phase diagram

The goal of present and future heavy-ion collision experiments at high beam energies is the precise scanning of the QCD phase diagram. The measurements at RHIC and LHC concentrate on the region at very high temperatures and almost zero baryon-chemical potential. The complementary approach is to explore the QCD phase diagram in the region of high net-baryon densities. Such experiments allow to address fundamental physics questions: What are the properties of very dense nuclear matter? Is there a first order phase transition between hadronic and partonic matter? Is there a critical or a triple point, and, if yes, where are these points located? Is there a chiral phase transition, and, if yes, does it coincide with the deconfinement phase transition? Are there new QCD phases such as "quarkyonic" matter? Figure 1 illustrates possible phases of strongly interaction matter.

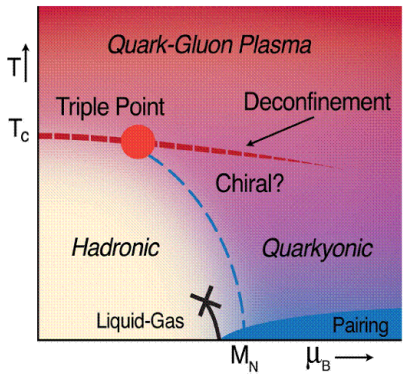

Figure 1: Sketch of a possible QCD phase diagram

The discovery potential of nuclear matter experiments at intermediate beam energies triggered new experimental activities at the major heavy-ion laboratories: the beam energy scan program at RHIC, the fixed-target NA61/SHINE experiment at CERN-SPS, the NICA collider project at JINR in Dubna, and the fixed-target Compressed Baryonic Matter (CBM) experiment at FAIR. The collider experiments at RHIC and NICA have the advantage of a constant acceptance as function of beam energy. On the other hand, when running at low beam energies, collider experiments are restricted to the measurement of abundantly produced particles due to limitations in luminosity. The same is true for the experiment NA61/shine at the SPS which is limited by the detector rate capability. In contrast, the experiments at FAIR are designed for extremely high luminosities, enabling the systematic measurement of multi-differential cross sections with unprecedented statistics even for rare diagnostic probes like multi-strange hyperons, lepton pairs, charmonium and open charm.

CBM and HADES within the modular FAIR start version

The full realization of the CBM research program requires beams from SIS300 (up to energies of 45A GeV), but the experiments can already be started at SIS100 using the upgraded HADES detector and an initial implementation of CBM. The upgrade of HADES with timing RPC detectors is already in progress. The SIS-100 accelerator at FAIR will deliver heavy-ion beams with energies up to 14A GeV. This energy range is ideally suited to produce and to investigate net-baryon densities as they are expected to exist in the core of a neutron star. For the first time, penetrating probes like dileptons and multi-strange particles such as Ω-hyperons will be used to systematically study the properties of baryonic matter in this beam energy range. The 29 GeV proton beams from SIS-100 will permit to perform pioneering measurements on (open) charm production at threshold energies and detailed studies of charm propagation in cold nuclear matter. Figure 2 depicts the HADES detector together with a start version of the CBM detector system.

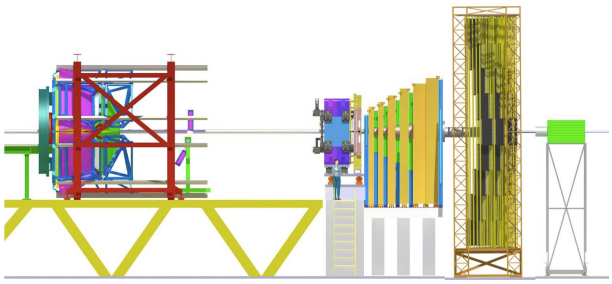

Figure 2: Experimental setups for measurements at SIS-100 consisting of the HADES detector (left) and an initial version of the CBM detector (right, "muon option")

R&D activities for CBM

The experimental task of the CBM detector system is to identify hadrons and leptons in collisions with up to 700 charged primary particles per event in the acceptance of the setup. Event rates of up to 10 MHz are needed for high statistics measurements of rare probes such as charmonium. These experimental conditions require fast and

radiation hard detectors, free-streaming read-out electronics, an ultra-fast online event-selection based on future CPU/GPU architectures, and a high-speed data acquisition (DAQ) system. The full version of the CBM detector system designed for measurements at SIS-300 is sketched in Fig. 3. The CBM setup will be equipped both with electron and with muon detectors.

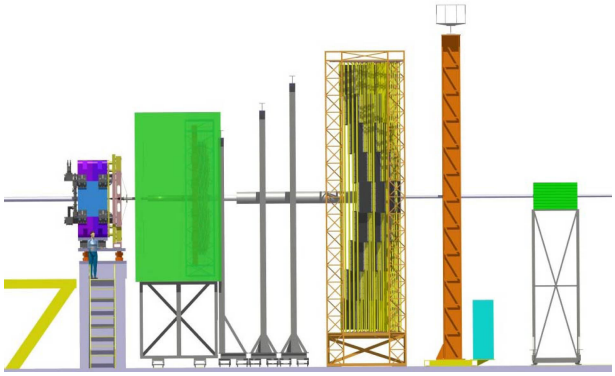

Figure 3: Experimental setup for measurements at SIS-300 ("electron version"). From left to right: dipol magnet with MVD and STS, RICH, 3 TRD stations, ToF-RPC, ECAL and PSD.

The Silicon tracking and vertexing system. The core of the CBM experimental setup is the Silicon Tracking System (STS) based on double-sided micro-strip sensors. The arrangement under study comprises 8 planes distributed within a distance of 1 m, located in a magnetic dipole field. The challenge is to built a radiation hard (up to $10^{15}\,\mathrm{n_{eq}}/cm^2$) and low-mass (well below 8 % radiation length) detector system which enables the reconstruction of primary and secondary tracks with an efficiency of 90 % or above. The simulation model of the STS was improved by implementing a detailed layout of the sensor arrangement within the stations and taking into account a realistic detector response. The track reconstruction routines were modified to cope with the new detector geometry and with charge sharing between neighbouring strips. Several prototype Silicon microstrip detector stations coupled to a free-streaming data read-out and a common data acquisition system were successfully tested at GSI with a proton beam.

The Micro-Vertex Detector (MVD) will provide high-precision vertexing for open charm measurements. The R&D on the MVD concentrates on the development of radiation hard and fast Monolithic Active Pixel Sensors (MAPS). A radiation hardness of better than $3 \times 10^{13}\,\mathrm{n_{eq}}/cm^2$ and a vertex resolution of 50 μm were achieved, both values being close to the experimental requirements for open charm measurement. A prototype MAPS with massive parallel read-out was successfully tested with a pion beam at CERN.

Electron measurements. Detailed feasibility studies of electron-pair measurements were performed based on a compact Ring-Imaging Cherenkov (RICH) detector. Although the compact RICH is substantially reduced both in volume and in the number of readout channels with respect to the initial design, its performance is not significantly deteriorated. These studies also took into account a segmented layout of the TRD detector including frames and support structures. The detector R&D resulted in a real-size prototype TRD with a double-sided pad plane, which was tested successfully with radioactive sources. A demonstrator of a RICH photon counter consisting of a MAPMT with 64 channels read-out via a self-triggered nXYter chip was successfully tested with the GSI proton beam.

Muon measurements. The layout of the muon detection system within the GEANT simulations was improved by taking into account a realistic detector module arrangement and their mechanical support structure. The track reconstruction algorithms were adapted to this new geometry. Simulations based on the improved layout of the STS and the muon system demonstrate the feasibility of vector meson measurements via the dimuon decay channel in central Au+Au collisions at FAIR energies. A muon detector start version was developed for charmonium measurements in proton-nucleus collisions at SIS100. The detector R&D concentrates on the construction and test of prototype gaseous detectors based on GEM technology. Two prototype GEM detectors read out by a free-streaming FEE and DAQ system were successfully tested with the GSI proton beam.

Hadron identification. Hadrons will be identified in CBM by measuring the particle momentum with the STS in the magnetic field and its time-of-flight using a wall of timing Resistive Plate Chambers (RPC). The R&D on prototype timing RPCs concentrates on high rate capability, low-resistivity material, long-term stability and the realization of large arrays with overall excellent timing performance. Various prototype RPC time-of-flight detectors were successfully tested in 2009 with a proton beam at GSI in Cave B.

Projectile spectator detector. The task of the Projectile Spectator Detector (PSD) is to determine the centrality of the collision and the orientation of the reaction plane. Simulations were performed in order to calculate the response of the PSD to projectile protons, neutrons and fragments, and to optimize the reaction plane resolution.

First level event selection. All main reconstruction packages (STS, MuCh, TRD, RICH and vertexing) were significantly optimized and parallelized resulting in a speed-up of the event reconstruction by 2-3 orders of magnitude. Therefore, the First Level Event Selection (FLES) can be based on the information delivered by several or even all subdetectors.

Dark rates of irradiated Monolithic Active Pixel Sensors

M. Deveaux[1], D. Doering[1], M. Domachowski[1], S. Ottersbach[1], J. Stroth[1], and F. M. Wagner[2]
[1]Goethe University Frankfurt/Main, Germany; [2]Forschungsneutronenquelle Heinz Maier-Leibnitz(FRM-II), TU München, Garching, Germany

Due to the high collision rates foreseen, the vertex detector of Compressed Baryonic Matter experiment will be exposed to very high radiation doses. We studied, if the damage caused by this radiation might provoke a crucial increase in the dark rate of the detector.

The Compressed Baryonic Matter (CBM)-experiment aims to explore the properties of hadronic matter in the region of highest baryonic densities. One of the major probes of the experiment are open charm particles, which are produced close to the kinematical threshold at CBM beam energies (10-40 AGeV). Reconstructing those rare and short lived ($c\tau \sim 100\ \mu$m) particles calls for a vacuum compatible vertex detector with an outstanding spatial resolution ($\lesssim 5\ \mu m$) and very low material budget ($\lesssim 0.3\ \mathrm{X}_0$). To match those requirements, we aim to build an actively cooled detector based on ultra light and highly granular Monolithic Active Pixel Sensors (MAPS).

Within one year of operation, the sensors will be exposed to very high radiation doses of $\gtrsim 10^{13}\ \mathrm{n_{eq}/cm^2}$ and $\gtrsim 3$ Mrad. The question how to extend their radiation tolerance to those values triggered a common R&D program of the IPHC (Strasbourg), GSI and the Goethe University Frankfurt/Main. In the context of this program, we observed that non-ionizing radiation damage causes Random Telegraph Signal (RTS) [1]. This non-gaussian noise was found to dominate the dark rate of the detector, which remains only tolerable if the detector is moderately cooled. This conclusion was so far restricted to sensors which were exposed exclusively to non-ionizing neutron radiation. The question, if the predicted additional ionizing doses would worsen the situation remained to be studied.

This study was performed with MIMOSA-18 sensors obtained from IPHC Strasbourg. The sensors host four matrices with 256×256 SB-pixels and 10 μm pixel pitch each, which are read out within 6.5 ms. They were irradiated with fission neutrons at the MEDAPP facility of the FRM-II reactor. Moreover, some of the chips were exposed to a dose of $\sim$10 keV X-rays at the irradiation facility of the Karlsruhe Institute of Technology. After the irradiations, we compared the dark rates of non-irradiated sensors with the ones of sensors irradiated with either $1.3 \times 10^{13}\ \mathrm{n_{eq}/cm^2}$ or 200 krad. Moreover, a sensor being consecutively irradiated with both, $1.3 \times 10^{13}\ \mathrm{n_{eq}/cm^2}$ or 200 krad was available. The moderate ionizing dose was chosen as MIMOSA-18, which was initially designed for other purposes, does not feature radiation hardened pixels.

The sensors were tested by measuring their dark rate as a function of the temperature. We counted a false hit if a pixel indicated a signal above 150 $\mathrm{e^-}$ ENC in the absence of a particle source. This value represents a limit up to which a MAPS detector should still be reasonably efficient. The temperature was measured at the cooling support of the test cards used. Cross checks suggest that, despite a bias by several °C towards room temperature, the true chip temperature was well reproduced.

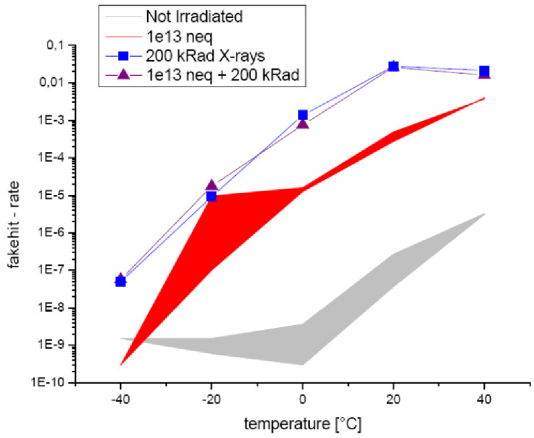

Figure 1: *Dark rate of irradiated MIMOSA-18 sensors as function of radiation dose and temperature.*

The results of our measurements are displayed in Figure 1. It is shown that irradiation increases the dark rate of the sensors at all temperatures. Unlike our initial assumptions this holds in particular for ionizing irradiation which increases the dark rate by several orders of magnitude with respect to the one of the non-irradiated chip. However, a cooling to -20 °C is sufficient to dim the dark rate to an acceptable value below 10^{-4}. We believe that the foreseen improvements in terms of readout speed will further reduce the dark rate as the faster sampling acts as a high pass filter which partially suppresses RTS.

We intend to use the results obtained as input for the MVD-digitizer [2]. This will allow for a detailed simulation study of the impact of the effects observed on CBM.

References

[1] M. Deveaux et al., "Radiation hardness studies on Monolithic Active Pixel Sensors", GSI Scientific Report 2008, FAIR-Experiments-19

[2] C. Dritsa et al., "Detector response simulation of the CBM Micro Vertex Detector", GSI Scientific Report 2008, FAIR-Experiments-21

Construction and test of the demonstrator of the CBM-Micro-Vertex-Detector

M. Deveaux[1], S. Amar-Youcef[1], J. Baudot[2], N. Bialas[1], N. Chon-Sen[2], H. Düring[1], I. Fröhlich[1], M. Goffe[2], J. Michel[1], C. Müntz[1], C. Schrader[1], P. Scharrer[1], S. Seddiki[1,2], J. Stroth[1], and T. Tischler[1]

[1]Goethe University Frankfurt/Main, Germany; [2]Institut Pluridisciplinaire Hubert Curien, Strasbourg, France

Reconstructing open charm with the CBM-experiment requires a vertex detector with outstanding rate capability, spatial resolution and low material budget. The MVD-demonstrator project studied the feasibility of building such a detector.

The CBM-experiment aims to explore the properties of hadronic matter in the region of highest baryonic densities. One of the major probes of the experiment are open charm particles, which are produced close to the kinematical threshold at CBM beam energies (10-40 AGeV). Reconstructing those rare and short lived ($c\tau \sim 100\ \mu$m) particles calls for a vacuum compatible vertex detector with an outstandingly high spatial resolution ($\lesssim 5\ \mu m$) and very low material budget ($\lesssim 0.3\ \mathrm{X}_0$). To match those requirements, we aim to build an actively cooled detector based on ultra light and highly granular Monolithic Active Pixel Sensors (MAPS).

The MVD-demonstrator project [1] aimed to study the integration of up to four MIMOSA-20 sensors into a detector ladder. MIMOSA-20, which was designed by IPHC Strasbourg, provides a pixel matrix with 640×320 pixels with $30 \times 30\ \mu\mathrm{m}^2$ pitch. The chip is readout within 2.2 ms via two serial analog outputs submitting each $50\ \mathrm{Mpixel/s}$. Slow control is done via a JTAG interface. Sensors thinned down to $50\ \mu$m were successfully operated conjointly with the PLUME-collaboration [2] but not chosen for the MVD-demonstrator for reasons of risk management. Due to a (meanwhile solved) problem in the chip production, the noise of the MIMOSA-20 sensors used was increased to a disappointing value of $\sim 23\ \mathrm{e}^-$ ENC.

The demonstrator was built by wire bonding a three layer flexprint cable top of two sensors. Two of the objects obtained were glued on the opposite faces of a cooling support formed from the highly heat conductive TPG and the ultra light and stiff carbon foam RVC. This support is to transport the heat of the sensors towards a liquid cooled heat sink located outside the acceptance of the future MVD. The sensor control was performed by a dedicated add-on board of the HADES-TRB2, which hosts among others four 12-bit ADCs sampling the analogue data stream of the sensors, a VIRTEX4 FPGA and an 1 GB SDRAM module.

The demonstrator was intensely tested in laboratory. Vacuum compatibility to fairly below 10^{-6} mbar was demonstrated with the vacuum vessel of the IKF technology lab. The cooling concept of the ladder was validated despite the disappointing performances of the rather simplistic heat sink. First attempts to operate MIMOSA-20 via the flex print cables showed an unusually high noise of 45 e^- ENC, which could be reduced to the expected $\lesssim 23\ e^-$ ENC with an FPGA-based common mode filter.

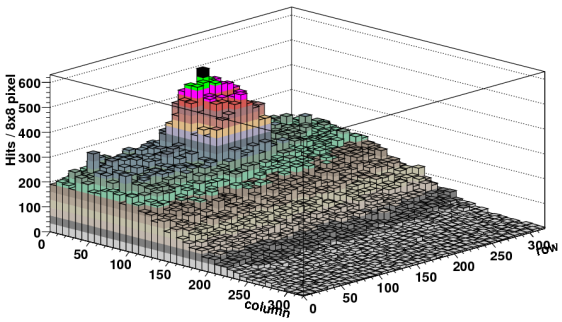

Figure 1: *Number of hits as function of the pixel coordinate as recorded in beam with the CBM-MVD demonstrator.*

The demonstrator was tested with ~ 120 GeV pions at the CERN-SPS. Two single sided MVD-demonstrators were operated with continuous read out. Trigger signals and additional time stamps obtained from the IPHC TAPI beam telescope were encoded into their data stream and allow for an offline synchronization with data obtained from this telescope. The readout clock of the demonstrators was set to $20\ \mathrm{Mpixel/s}$ (corresponding to 5.5 ms readout time), which reduced the data rate of the demonstrators from $2.4\mathrm{Gbit/s}$ to $960\ \mathrm{Mbit/s}$.

According to our data analysis, the good noise performances observed in the laboratory could be reproduced in the beam. Moreover, we observed the shadow of the trigger scintillator (see figure 1), which is located on top of a background formed from untriggered particle hits. A preliminary evaluation of the spatial resolution (σ) of the demonstrator was carried out by correlating the hits observed in both stations. We measured $\sigma \lesssim 5.6\ \mu$m which, probably due to the increased noise of MIMSOA-20, does not fit the ultimate resolution ($\sim 2\ \mu$m) expected for this sensor. However, the results match the requirements of CBM, which validates the concept of the MVD-demonstrator.

References

[1] S. Amar-Youcef et al., "R&D for the demonstrator of the CBM-Micro-Vertex-Detector", GSI Scientific Report 2008, FAIR-Experiments-18

[2] http://www.iphc.cnrs.fr/plume.html.

Development of very light pixel arrays based on fast and radiation tolerant CMOS sensors for the CBM vertex detector*

M. Winter, for the Strasbourg team[1] and M. Deveaux, for the Frankfurt team[2]
[1]Institut Pluridisciplinaire Hubert Curien, Strasbourg, France; [2]Goethe University, Frankfurt/Main, Germany

The Micro-Vertex Detector (MVD) of the CBM experiment requires very light detector stations equipped with highly granular and thin pixel sensors adapted to hostile running conditions. CMOS pixel sensors of the MIMOSA series are being developed for several years in ordre to match the challenging specifications of the MVD. Breakthroughs were achieved in 2009, which concern the fast sensor read-out architecture and its non-ionising radiation tolerance. A significant step was also made towards very light sensor arrays.

Full scale sensor with zero-suppression

MIMOSA-26, the first full scale sensor featuring fast read-out with integrated zero-suppression, was fabricated and tested extensively. It is composed of 1152 columns read out in parallel, each made of 576 pixels (18.4μm pitch) and terminated with a discriminator. The discriminator outputs are processed through an integrated zero-suppression logic. The 665,000 pixels of the sensor cover an active area exceeding 1×2 cm^2 and are read out in $\sim 110\mu s$. More than 30 chips were characterised. A fabrication yield of $\sim$ 90% was measured. The total sensor noise (N) was evaluated to 13-14 e$^-$ENC.

6 sensors were assembled in a telescope configuration and installed on a $\sim$ 100GeV particle beam at the CERN-SPS. A detection efficiency of $\gtrsim$ 99.5% was measured with discriminator threshold values ($\sim$ 5 N) high enough to maintain the rate of noise fluctuations above threshold around 10^{-4} (typically 40 to 80 pixels per frame). These performances validate the architecture for its extension to shorter read-out times like those required for the MVD.

Non-ionising radiation tolerant sensor

A new fabrication process was investigated in 2008 with the MIMOSA-25 prototype, featuring a high resistivity epitaxial layer. The latter could thus be depleted, resulting in substantial charge collection efficiency and non-ionising radiation tolerance improvements. The sensor, which features 20μm pitch pixels, was studied with $\sim$ 100GeV particles at the CERN-SPS, before and after irradiation with $\sim$ 1MeV neutrons. The result of the study is summarised in figure 1, which displays the signal-to-noise ratio (SNR) of the cluster seed pixels before and after an exposure to a fluence of 3·10^{13} n$_{eq}$/cm^2.

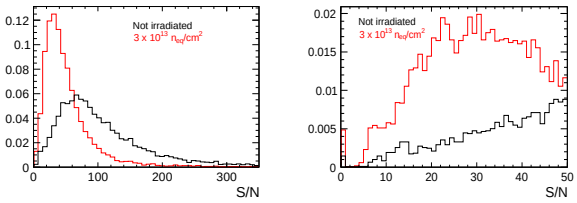

Figure 1: SNR of MIMOSA-25 before (black lines) and after (red lines) irradiation (fluence of 3·10^{13} n$_{eq}$/cm^2). The right figure is a zoom of the left one.

The SNR before irradiation ($\sim$ 60-65) is more than twice higher than in case of a usual, low resistivity, epitaxial layer. After an exposure equivalent to 3·10^{13} n$_{eq}$/cm^2, the SNR is still $\sim$ 30-35, translating into a detection efficiency of $\sim$ 99.5%. A fluence of $\gtrsim 10^{14}$ n$_{eq}$/cm^2 is therefore likely to be tolerable, which would well fullfil the MVD specifications.

3D integrated technologies

The performances of CMOS sensors are expected to still improve with vertical integration technologies. First prototypes were designed and fabricated in a 2-tier, 130 nm, process. Several different chips were realised, with expected read-out times of a few μs. One of them is foreseen to be interconnected with a sensing tier featuring a depleted epitaxial layer as for *MIMOSA-25* (see previous section). The chips are currently being manufactured and will be tested during 2010.

Ultra-light pixelated ladders

The development of very light sensor arrays was initiated via the Hadron Physics 2 project. It aims at unsupported, flexible, sensor rows featuring a material budget of $\lesssim$ 0.15% of radiation length. The concept consists in assembling a row of $\sim 35\mu m$ thin pixel sensors on a very thin flexible cable and in wrapping the device in a very thin polymerised film. These rows would next be mounted on the mechanical (and cooling) support. The first prototype, which should allow commissioning the procedure, is being fabricated.

References

[1] M. Winter et al., 2008 GSI annual report.

[2] M. Winter et al., DESY PRC report, Novembre 2009.

*Work supported by EU within the projects EUDET (FP-6) and Hadron Physics 2 (FP-7).

Progress with performance simulations of the CBM Silicon Tracking System

A. Kotynia[1] and J.M. Heuser[2]
[1]Univ. Frankfurt, Germany; [2]GSI, Darmstadt, Germany

Efficient charged particle tracking and high momentum resolution are central performance requirements of the CBM Silicon Tracking System (STS). The aim of the ongoing layout studies is to design a highly granular and low-mass detector system which can track up to 1000 charged particles that are typically generated in one central Au+Au collision at 25 GeV/u projectile energy. A low-mass detector is crucial to achieve a momentum resolution down to 1%. Progress has been made with optimizations of the detector geometry and with the implementation of realistic detector response functions.

Detector layout studies

The STS comprises eight tracking stations located 30, 35, 40, 50, 60, 75, 95 and 100 cm downstream of the target. The stations have a modular structure and are constructed from 300 μm thick double-sided silicon microstrip sensors. Groups of sensors (sectors) are individually read out with electronics located at the perimeter of the stations. Signals from the sectors are sent through thin aluminum-polyimide micro-cables to the front-end electronics (Fig. 1).

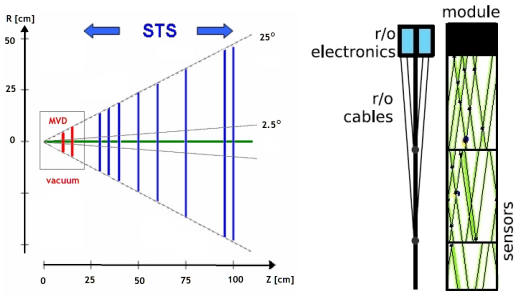

Figure 1: Left:Schematical layout of the STS. Right: One module with read-out electronics.

Three variations of this layout have been studied.

1. Following a modified arrangement of the Micro Vertex Detector (MVD) with its detector stations at 5 and 10 cm distance from the target, it is possible to place the first STS station at 20 cm. In order to have enough space for mechanical support structures, the distance between the STS stations should not be less than 7 cm. Taking this into account, the STS stations have been redistributed to the z positions 20, 27, 34, 44, 60, 75, 90, 100 cm. This results in an increased track finding efficiency (+2%), together with a momentum resolution improving from 1.37% to 1.12%.

2. Due to the fact that the current track reconstruction software requires four consecutive hits in the STS, a geometry with one additional station has been studied as well. In spite of the expectation one more station does not improve the tracking results significantly. The efficiency increases by about 1% but the momentum resolution worsens from 1.12% to 1.20%.

3. In the tracking modules detectors with a width of 6 cm and a strip pitch of 60 μm are applied. The strip length has been matched to a maximum occupancy of less than 5% what results in a vertical size of one sector between 2 to 18 cm. The strips on the front side are tilted by 7.5° and on the back side by -7.5° creating a stereo angle of 15°. Every strip can cross between 100 and 800 strips on the opposite side of a sector. This results in a large number of fake or combinatorial hits. To reduce this effect, a special geometry with shorter strips has been prepared. The strip lengths vary between 1 cm in inner parts of the tracking stations and 6 cm in their outer parts. In such a geometry, the number of fake hits is reduced by a factor of two, from 5.7k to 2.7k per central event.

Performance studies

The performance of the STS has been evaluated with realistic detector response functions implemented. Signal sharing between strips together with charge collection inefficiency and Lorentz shift due to the presence of the magnetic field, channel dead time, and single-channel inefficiencies are present in the simulations. For more details see [1]. The efficiency of the cluster finding method only depends on the particle's incident angle. For angles below 20° the hit finding efficiency drops from 98% for ideal digitization to 95% in the realistic case.

Next steps

In order to improve the hit finding efficiency, we consider tilting the outer parts of all STS stations by 20° around the vertical axis. This should assure hit finding efficiencies above 95% for all parts of the tracking stations.

References

[1] A. Kotynia, J.M. Heuser and W. Müller, *Simulation of realistic detector responce in the CBM Silicon Tracking System*, CBM Progress Report 2009

Simulation of realistic detector response in the CBM Silicon Tracking System

A. Kotynia[1], J.M. Heuser[2], and W. Müller[2]
[1]Univ. Frankfurt, Germany; [2]GSI, Darmstadt, Germany

The Silicon Tracking System of the CBM Experiment consists of eight tracking layers of silicon detectors. Each layer is an array of vertical modules containing 300 μm thick double-sided silicon strip sensors. The strip pitch is 60 μm on both sides. The sensors are segmented into 1024 strips per side. On either side the strips are tilted by +7.5° or -7.5° with respect to the vertical edge, creating 15° stereo angle between the opposite sides. This allows reconstructing multiple hits from the same sensor at the expense of a poorer spatial resolution in the vertical direction, keeping high resolution in horizontal direction for better reconstruction of the particle momenta.

Detector response simulations

The simulations which have been developed include the complete chain of physical processes caused by a charged particle traversing the detector – from charge creation in the silicon to the digitized output signals. Fig. 1 illustrates the simulated track originating from a minimum ionizing particle in the silicon detector, where every point along the track represents a charge packet. The track is constructed using finite steps to exploit fine granularity in the energy deposition. In the second phase, the charge packets are collected on the strips. A random noise sample is added to the charge signal, according to a Gaussian distribution whose standard deviation should be considered as an equivalent noise charge of the detector system.

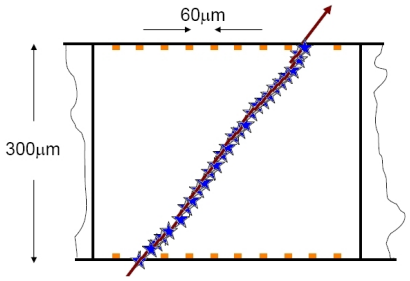

Figure 1: Simulated track of a minimum ionizing particle in the silicon detector (arrow). The orange rectangles represent the read-out strips.

The presence of a magnetic field in the region where the detectors operate influences the collection of the charge on the strips. Due to the Lorentz force on the charge carriers, electrons and holes produced along the track of a crossing particle are collected at an angle ϑ_L (Lorentz angle) with respect to the track. In our STS configuration ϑ_L is 1.5° for holes and 7.5° for electrons. For a more detailed description of the Lorentz force see [1].

The center-of-gravity algorithm (1) allows to obtain the position of the incident particle in the sensor. Using this method, it is possible to estimate the particle position as the weighted average of the position x_i of the n strips included in one cluster with the S_i being the corresponding signals:

$$x = \frac{\sum_{i=1}^{n} S_i x_i}{\sum_{i=1}^{n} S_i} \quad (1)$$

This procedure has been performed independently for both sensor sides. Two clusters found on opposite sides are associated with a particle hit, under the condition that the fired strips on one side have a point of intersection with the fired strips on the other side. This method results in strong dependance of the hit finding efficiency on the particle crossing angle, which is presented in Fig. 2 together with the distribution of cluster sizes in the first STS station. The results were obtained with a noise width of 0.5k electrons and a threshold of 4k electrons.

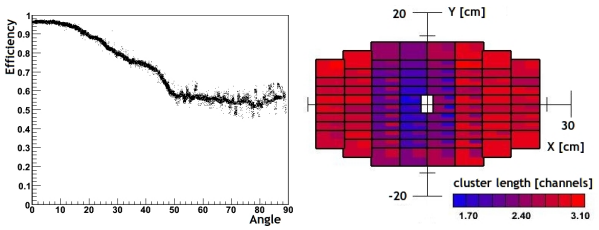

Figure 2: Left: Hit finding efficiency as a function of the particle crossing angle. Right: Number of fired strips per cluster on first STS station.

Single channel inefficiencies occur as a result of the readout electronic's dead time. According to the newest predictions for the actual behaviour of the STS prototype readout electronics, the channel dead time significantly depends on the pulse amplitude and varies between 100 and 1000 ns. Moreover, the measurements of the pulse length have been done for three settings "fast", "mid" and "slow" corresponding to the discharge time. Those settings result in different noise values. Preliminary studies of the hit finding efficiency show that for the "fast" setup in the inner parts of stations one and two 6% of the hits are lost, while for the outer parts of the stations the number of lost hits drops down to 1%. The influence of this effect on the track reconstruction is to be studied further.

References

[1] Nuc. Instr. Meth. A497 (2003) 389-396

Construction of a reference telescope from prototype components of the CBM Silicon Tracking System

J.M. Heuser[1], V. Kleipa[1], W. Müller[1], W. Niebur[1], C.J. Schmidt[1], C. Simons[1], and A. Lymanets[2]
[1]GSI, Darmstadt, Germany; [2]Univ. Frankfurt, Germany

A reference tracking telescope has been developed and constructed in preparation of in-beam tests with forthcoming prototype modules of the CBM Silicon Tracking System. A first test in a 2 GeV proton beam took place at GSI in Fall 2009 [1].

Assembly of a tracking station

A tracking station is realized on an 8-layer printed circuit board that features the full readout of a *CBM02B2* [2] double-sided prototype silicon microstrip detector with 2×256 orthogonal strips of 50 μm pitch (Fig. 1). Four self-triggering n-XYTER [3] readout chips have been directly wire-bonded to the detector. The detector is glued into a squared opening in the board resting on a machined-in balcony structure of about 100 μm width. Two chips read out one detector side. The 10 cm by 10 cm board also houses the external *ADC* converter and *DC* power converters. It is connected to a CBM readout controller [4] with two high-density flat/twisted-pair cables. The detector bias is provided through a coaxial cable.

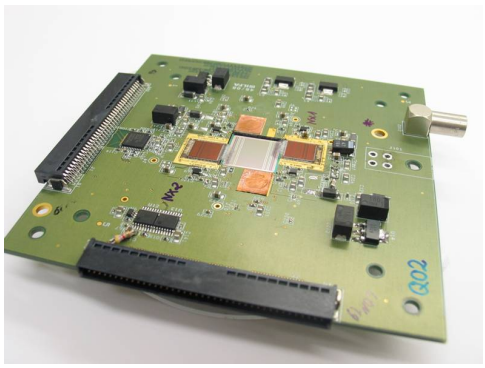

Figure 1: A reference tracker board comprising a double-sided *CBM02B2* prototype detector wire-bonded to four n-XYTER readout chips, two per side.

The four readout chips dissipate up to 20 W. The tracker board has therefore to be cooled to avoid excessive temperatures of chips and silicon detector that would result in unstable operation, high leakage current and noise, particularly in a concealed space like in an experimental setup. On the tracker board, the readout chips are brought in thermal contact with a copper inlay reaching to the back side of the board. The board is then sandwiched between two aluminum plates with built-in water cooling pipes as shown in Fig. 2. A compact object is created.

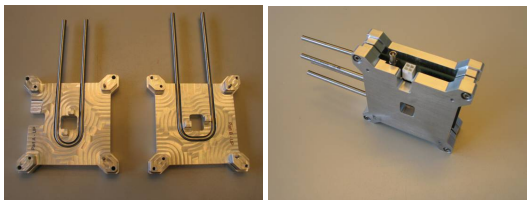

Figure 2: A tracker board mounted between cooling plates.

Three tracker boards have been mounted in an aluminum shielding box. They were then connected to the low and high-voltage supplies, the control and readout system as well as the water cooling and temperature monitoring system. The completed setup as operated in the laboratory and on the beam line is shown in Fig. 3.

Setup of a reference tracking telescope

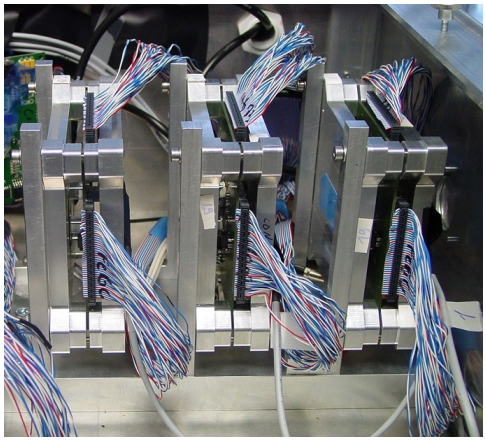

Figure 3: Three tracking stations on the beam line.

References

[1] V. Friese et al., *Operation and performance of the CBM Silicon tracking reference telescope*, CBM Progress Report 2009
[2] J.M. Heuser et al., GSI Scientific Report 2008 p 10
[3] C.J. Schmidt et al., CBM Progress Report 2006 p49
[4] N. Abel et al., GSI Progress Report 2007 p53

Operation and performance of the CBM Silicon Tracking reference telescope

V. Friese[1], J.M. Heuser[1], V. Kleipa[1], S. Linev[1], W. Müller[1], W. Niebur[1], C.J. Schmidt[1], A. Kotynia[2], A. Lymanets[2], A. Wilczek[3], and B. Bozsogi[4]

[1]GSI, Darmstadt, Germany; [2]University of Frankfurt, Germany; [3]University of Silesia, Katowice, Poland; [3]Eotvos Lorand Univ., Budapest, Hungary

A reference tracking telescope consisting of three stations based on double-sided silicon microstrip detectors has been constructed and tested in a 2 GeV proton beam experiment at GSI. This proof-of-principle device designed for charged particle track measurement with high spatial resolution closely integrates silicon sensors with self-triggering front-end electronics. Each station features the full read-out of a *CBM02B2* prototype detector with 2×256 strips of orthogonal orientation and 50 μm strip pitch. Four self-triggering n-XYTER readout chips have been directly wire-bonded to the detector.

Operation of the tracking stations

In the experiment the data streams from several detector systems have been combined using the Data Acquisition Backbone Core framework [1]. An online monitor based on the Go4 system [2] has been used to control the data quality by representing raw spectra (e.g. ADC distributions, channel occupancies) as well as an elementary analysis of e.g. time correlations. The online histograms provide feedback for the correct adjustment of the readout electronics. The ADC spectrum in each channel contains a noise peak and a signal distribution created by the beam particles. By setting the threshold in the chip above the noise most of the registered hits become associated with the incident beam.

Also the stability of the detector settings has been monitored. Temperature stability turned out to be most important for particle detection with constant performance. The tracking stations dissipate up to 20 W (current of up to 4 A at 5 V) and thus must be cooled. The boards were sandwiched between aluminum plates through which chilled water was circulated. Initially, due to periodic switching of water chiller, the temperature of all three tracker stations exhibited sinusoidal time dependence with a period of ∼20 minutes and a full swing of ∼3 $^{\circ}C$ (see Fig. 1 left). Observed temperature variation causes a drift of baseline in the read-out chip, revealing its high temperature coefficient. The right panel of Fig. 1 shows time dependence of baseline position as a result of temperature variation. The peak-to-peak amplitude of the baseline drift comprises 200 ADC counts, exceeding the signal amplitude of a beam particle. The cooling system was exchanged with more stable device and, in addition, an on-line amplitude calibration method was implemented. The high temperature coefficient of the front-end chip will be addressed in the upcoming n-XYTER engineering run.

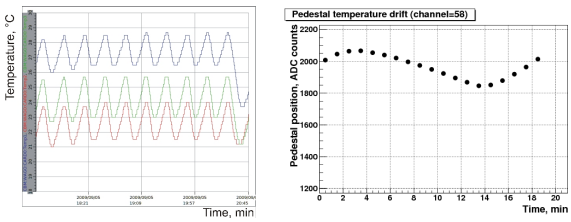

Figure 1: Temperature oscillations tracking stations (left). Pedestal drift in a front-end chip (right).

Offline performance analysis

Advanced tools for offline analysis have been developed. As a first step the raw data files are converted to root files. After such conversion, it is possible to use the current STS digitization and STS hit finding algorithm, developed for the full CBM setup. The hit finding tools include charge sharing beetween neighbouring strips, which provide position resolution better than 15 μm [3]. As an example of the hit distribution the beam profile reconstructed in one of the detector stations is shown in Fig. 2.

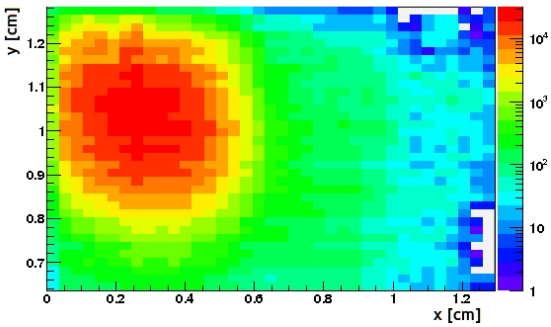

Figure 2: Beam spot reconstructed in a tracking station.

References

[1] Data Acquisition Backbone Core, http://dabc.gsi.de

[2] GSI Object Oriented On-line Off-line system, http://go4.gsi.de

[3] A. Kotynia et al., *Simulation of realistic detector response in the CBM STS*, CBM Progress Report 2009

Progress with the development of double-sided microstrip detectors for the CBM Silicon Tracking System

J.M. Heuser[1], L. Long[2], M. Luleich[2], H. G. Ortlepp[2], and R. Röder[2]
[1]GSI, Darmstadt, Germany; [2]CiS Forschungsinstitut für Mikrosensorik und Photovoltaik GmbH, Erfurt, Germany

The second prototype of a full-size double-sided silicon microstrip detector for CBM's Silicon Tracking System has been developed in cooperation of GSI and CiS. Its dimensions and contact pattern are compatible with the construction of a low-mass demonstrator tracking module by the CBM-MPD STS Consortium [1]. Further activities concern the preparation of a new technology wafer for the exploration of a variety of sensor design improvements towards improved high signal efficiency after high radiation exposure.

Full-size prototype detector CBM03

Based on the first prototype *CBM01* [2] and experience with technology wafer *CBM02* [3], the new design *CBM03* realizes a large double-sided detector with the strips under a stereo angle on both sides. This design is favoured for aspects of the module assembly but requires interconnecting the short corner strips on both sides through lines on a second metal layer to read out the detector from two edges only. The detector matches in its outer dimensions and the layout of its readout pattern with another prototype detector with shorter strips, designed within the CBM-MPD STS Consortium as one of three possible detector types for the CBM Silicon Tracking System. The *CBM03* design has the following features:

- n-type Si material
- double-sided segmentation into strips
- 1024 strips per side
- stereo angle ± 7.5 degree
- 58 μm strip pitch
- AC-coupled readout
- 1 DC pad and 4 AC pads per strip
- poly-silicon resistor plus punch-through biasing
- p-spray insulation on the ohmic side
- two metal layers per side
- 10 guard rings
- outer dimension 6.2 cm by 6.2 cm

The wafer requires 19 masks for production. Processing started early 2010 and the delivery of a batch is expected by Summer 2010.

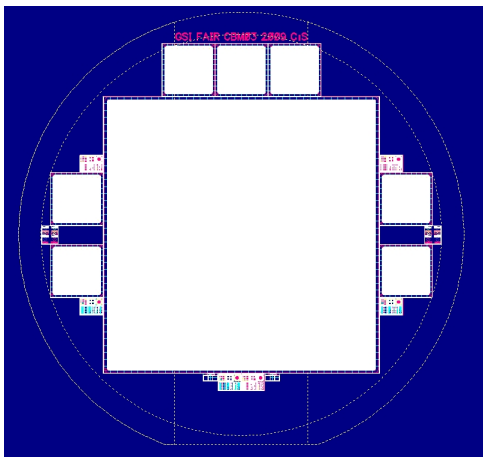

Figure 1: Layout of the *CBM03* wafer (4" diameter) with the main detector in the center and various test structures.

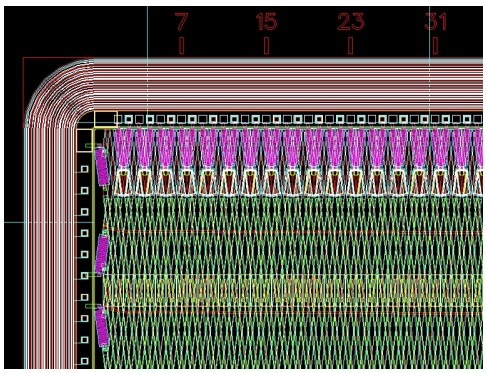

Figure 2: Design of the *CBM03* main detector with strips under ± 7.5 degree stereo angle and double-metal interconnections of the corner strips.

Preparations for a second technology wafer

Various design parameters are the target of a forthcoming second technology wafer. The research project of CiS will develop and implement innovative structures to improve the detectors' radiation tolerance and charge collection efficiency after exposure to high particle fluence as expected in the CBM experiment.

References

[1] http://sunse.jinr.ru/projects/sts/abstract_sts.html
[2] J.M. Heuser et al., GSI Report 2008-1 9
[3] J.M. Heuser et al., GSI Report 2009-1 10

Characterization of CBM prototype microstrip detectors

V. Pugatch[1], M. Borysova[1], A. Chaus[1], J.M. Heuser[2], O. Kovalchuk[1], V. Kyva[1], A. Lymanets[3], A. Melnyk[1], V. Militsiya[1], O. Okhrimenko[1], Yu. Sorokin[1], D. Storozhik[1], V. Perevertailo[4], and V. Zhora[4]

[1]Kiev Inst. for Nucl. Research, Kiev, Ukraine; [2]GSI, Darmstadt, Germany; [3]Goethe University, Frankfurt, Germany; [4]Institute of Microdevices, Kiev, Ukraine

We report on the characterization of CBM prototype microstrip detectors with a laser and radioactive sources and the analysis of their signal amplitude in a proton beam.

Tests with laser and radioactive sources

A quality assurance system for the CBM Silicon Tracking System detector modules has been set up at KINR and used for the assessment of the prototype microstrip detectors CBM01 and CBM02 [1]. The detectors were characterized with radioactive sources (^{226}Ra–α, ^{90}Sr–γ) as well as with a laser beam (640 nm, diameter 10 μm) movable in X and Y-directions. The detectors were read out through micro cables with discrete electronics. The measurements with the α-source as well as with a laser beam have revealed an unexpected behaviour of the interstrip gap response at low voltages for all types of detectors, that might be explained with insufficient charge collection in the surface region of the interstrip gaps. For all types of detectors, the spectra from minimum ionizing particles have a Landau shape at low bias voltage. At a bias exceeding 30 V the signal spectra are of a gaussian shape as shown in Figs. 1 and 2. This requires further studies.

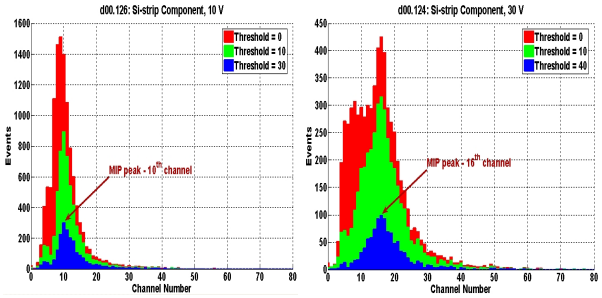

Figure 1: ^{90}Sr β spectra measured on the p side of a CBM01 detector at 10 V (left) and 30 V bias (right).

Tests with 2 GeV proton beam

The signal amplitudes of CBM prototype detectors have been evaluated in Summer 2009 with a 2 GeV proton beam at GSI. The test setup considered here comprised one CBM01 and one CBM02 "baby" detector mounted on individual boards and read out with two n-XYTER chips [2] on two separate general-purpose front-end boards. Isolated single-strip beam hits were selected by delayed coincidences with a reference signal from the auxiliar trigger provided from two crossed scintillators. Hit isolation was ensured by requiring no signal on the adjacent strips (1 from each side) within 45 ns before and after the hit. For isolated single-strip hits Landau spectra with a gaussian component were observed as shown in Fig. 3. The spectra are similar for all channels which tells about the good uniformity of the detector strips and the readout channels. The peak maximum near 155 ADC units corresponds to about 21 ke$^-$ [3], which is close to the expected value of 23 ke$^-$ in the 285 $\pm$10 μm thick detector.

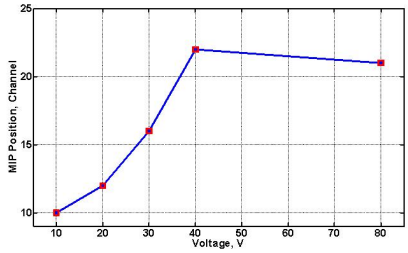

Figure 2: Peak ADC value as function of the bias voltages.

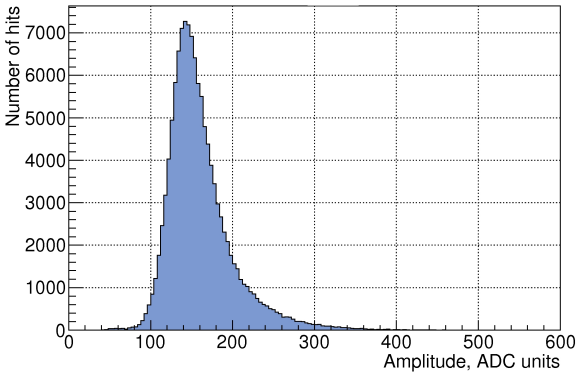

Figure 3: Amplitude spectrum of 1-strip hits on one of the p-strips of a CBM02 test detector, biased with 70 V.

References

[1] CBM Progress Report 2008 pp. 15 and 16

[2] NIM A, 568 (2006) 301-308

[3] C.J. Schmidt et al., *Characterization of the n-XYTER chip and preparations for the engineering run*, this Progress Report

Development of a Quality Assurance System for the Silicon Tracking System

V. Pugatch[1], J. Heuser[2], V. Kyva[1], A. Lymanets[3], G. Melnyk[1], V. Militsiya[1], O. Okhrimenko[1], and Y. Panasenko[1]

[1]KINR, Kyiv, Ukraine; [2]GSI, Darmstadt, Germany; [3]Goethe University, Frankfurt, Germany

Double-sided microstrip sensors of type *CBM02* mounted onto carbon fiber supporting frames and connected through micro-cables to discrete readout electronics have been characterized with the prototype of the quality assurance system that is under development at KINR. Measurements were carried out on the full depletion voltage, the leakage current as well as charge sharing phenomena of adjacent strips.

Full depletion voltage

The point of full depletion is illustrated in the measurement shown in Fig. 1. The two regions (rise and plateau) of the total detector current as a function of the applied reverse bias allow to assess when the detector is fully sensitive across the bulk.

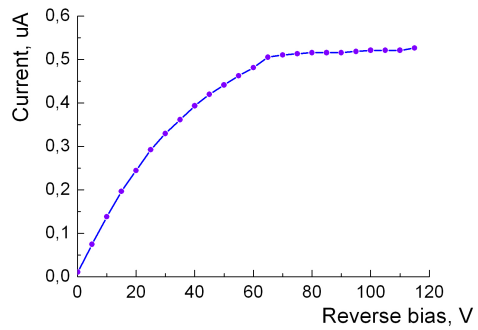

Figure 1: A typical IV-curve measured for one of the *CBM02-B1* sensors indicating full depletion at around 65 V.

Charge sharing of adjacent strips

The investigation with an α-source (^{226}Ra) showed the expected response of the strips: The amplitude of signals grows as the reverse voltage increases. The measurements also revealed a worsening of the energy resolution after having reached full depletion voltage. Coincident α-spectra for pairs of adjacent p-strips irradiated from the p-side have demonstrated an unusual feature of the collected signal at 3.5 V, as seen in Fig. 2.

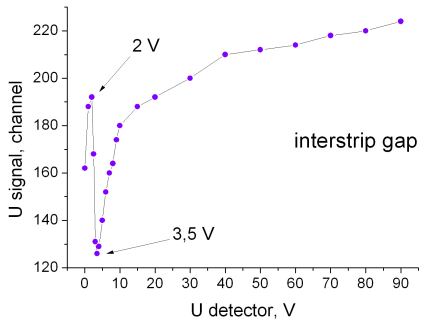

Figure 2: Sum of the signal amplitudes from an α-source in adjacent strips as a function of the bias voltage.

Presumably, both observations are related to a reduction of charge collection efficiency caused by an insensitive $(10-15\ \mu$m) layer in the inter-strip gaps on either side of the sensor. We have to note that the performance of the *CBM01*-type sensors was very similar [1].

Single-strip charge spectra

The sensor response to minimum ionizing particles (MIP) was studied using a β-source (^{90}Sr). From the entire continuous spectrum, only electrons with energies between $1.5-2.3$ MeV were selected and triggering the data acquisition. The spectrum obtained features a typical Landau distribution (Fig. 3).

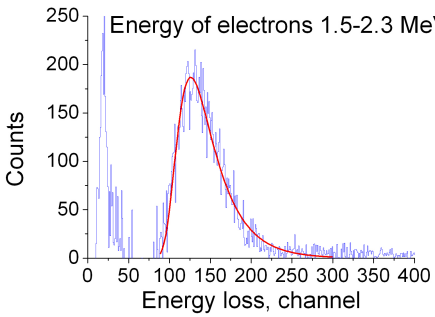

Figure 3: MIP spectrum in one strip at 80 V detector bias.

References

[1] V. Pugatch et al., CBM Progress Report 2008, p. 15.

Simulation study of radiation damage in double-sided silicon microstrip detectors for the CBM Silicon Tracking System

S. Chatterji and J.M. Heuser
GSI, Darmstadt, Germany

We started TCAD simulations last year to understand the radiation damage in Double Sided Silicon Strip Detectors (DSSD) for the CBM Silicon Tracking System. We used the public domain versions from Stanford namely SUPREM for Process Simulation and PISCES for device simulation [1]. The results were reported in the GSI Scientific Report 2008 [2]. Now we are using the three-dimensional TCAD simulation package from Synopsys [3] which we procured through the Europractise Software Service. Synopsys has several subpackages for three-dimensional simulations like Sentaurus Process, Sentaurus Device, Workbench, TecPlot, Inspect etc.

Two- and Three-dimensional simulations

Fig. 1 shows the two-dimensional grid of the DSSD. There are three n-strips on the front side seperated by p-stops, and three p-strips on the back side. It is also possible to simulate transients like passage of Minimum Ionizing Particles (MIPs) through the device. One can see a very dense mesh in the middle of the grid which is required to correctly simulate the passage of the MIP. It is also very important to give a fine mesh at the junction curvatures and at interfaces. This is seen in Fig. 2. We apply a negative bias on the backside and ground the n-strips in order to reversely bias the detector. We have found that the peak electric field occurs at the junction curvature as can be seen from the left panel of Fig. 3. The right panel shows that p-stops are indeed able to isolate the adjacent n-strips under depleted condition. The extension of the studies with a three-dimensional implementation of the detector is illustrated in [4].

Studies of radiation damage

We are ready to simulate the radiation damage in the DSSD by changing the effective substrate concentration using the Hamburg model [5] and also by changing the surface oxide charge.

References

[1] http://home.comcast.net/ john.faricelli/tcad.htm

[2] S. Chatterji et al., GSI Report 2008-1 14

[3] http://www.synopsys.com/home.aspx

[4] S. Chatterji et al., *Microstrip detector design optimization for the CBM Silicon Tracking System*, GSI Progress Report 2009

[5] Nucl. Instr. Meth. Phys. Res. A439 (2000) 282-292

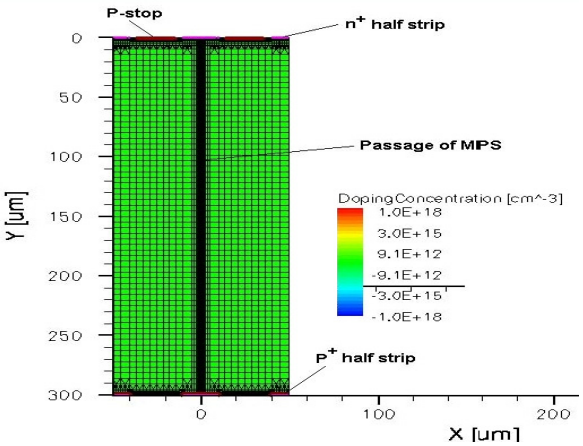

Figure 1: Two-dimensional grid of the simulated DSSD.

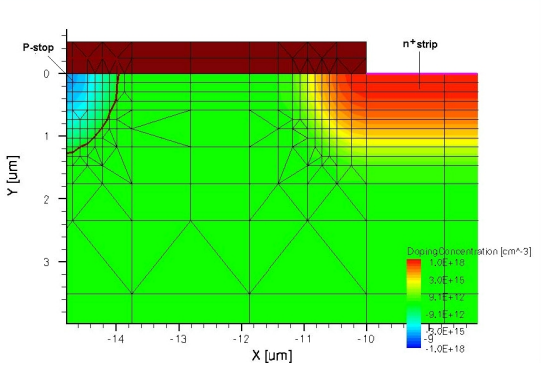

Figure 2: Zoomed frontal view of the simulated DSSD.

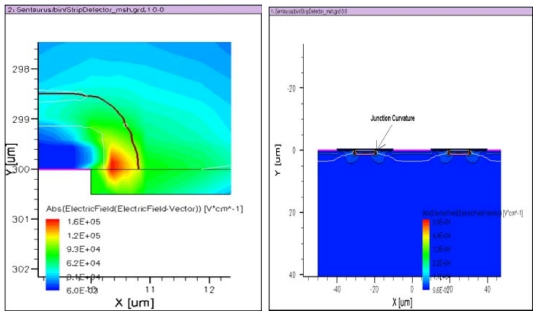

Figure 3: Electric field distribution at the curvature of one of the p-strips (left). Role of p-stops in isolating the adjacent n-strips in non-depleted condition (right).

Microstrip detector design optimization for the CBM Silicon Tracking System

S. Chatterji and J.M. Heuser
GSI, Darmstadt, Germany

We are using the SYNOPSYS [1] package for three-dimensional TCAD simulations to optimize various design parameters of the Double Sided Silicon Strip Detector (DSSD) under development for the CBM Silicon Tracking System.

Three-dimensional device simulations

Building on the experience with two-dimensional simulations in PISCES [2], we developed a three-dimensional grid in TCAD which approximates all the features of our existing prototype detector, like the strip pitch of 50 μm, strip width of 20 μm, strip stereo angle of $\pm$7.5 $^\circ$ with *AC* coupling. A part of the modeled detector is shown in Fig. 1, zooming in on a n-strip and its neighbouring p-stops. The x (horizontal) axis points along the width and pitch of the strips, the y axis along the lenght of the strips and z (vertical) axis along the wafer thickness. The $\pm$7.5 ^{0} stereo angle of the strips is better recognized from Fig. 2 which shows a two dimensional projection (x-y plane) of the grid.

We have simulated transients by passing Minimum Ionizing Particles (MIP) at various angles through the detector. Fig. 3 shows in the left graph the transient charge generated by the passage of the MIP. Many device parameters can be extracted from the simulation. Examples are interstrip capacitances and resistances relevant e.g. for an understanding of the cross talk between channels. The right graph of Fig. 3 shows the interstrip admittance as a function of the applied bias voltage. The value of interstrip resistance comes out to be around 10-20 GΩ which is as per the expected value.

Comparison with measurements

At present the simulations represent existing detector designs. We have started to verify the calculations with measurements of our prototype detectors. The simulation tools will then be used to optimize the next generation of CBM DSSDs already during the design phase.

References

[1] http://www.synopsys.com/home.aspx, http://home.comcast.net/ john.faricelli/tcad.htm

[2] S. Chatterji et al., GSI Report 2008-1 14

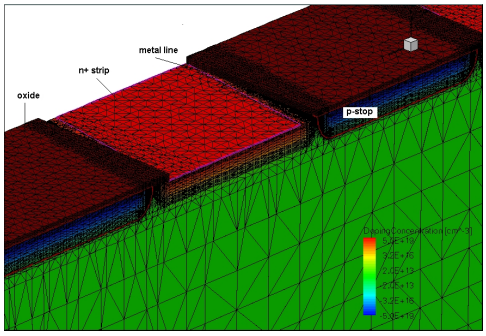

Figure 1: Three dimensional grid of the simulated DSSD.

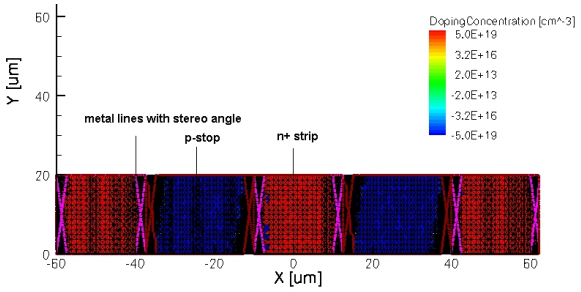

Figure 2: 2-dim. projection of the 3-dim. DSSD grid.

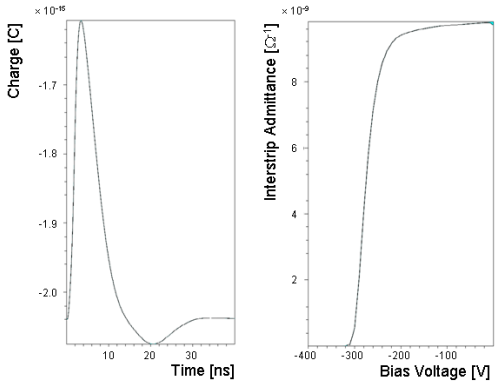

Figure 3: Transient charge generated by passage of MIP through the simulated grid (left). Simulated interstrip admittance versus bias voltage (right).

Development of ultra-thin cables for the CBM Silicon Tracking System

V.M. Borshchov[1], J.M. Heuser[2], Yu.A. Murin[3], O.M. Listratenko[1], M.A. Protsenko[1], I.T. Tymchuk[1], Y.Y. Kostyshyn[1], Y.A. Shulenko[1], A.M. Steblina[1], and the CBM-MPD STS Consortium

[1]State Enterprise Scientific Research Technological Institute of Instrumental Engineering (SE SRTIIE), Kharkov, Ukraine; [2]GSI, Darmstadt, Germany; [3]Joint Institute for Nuclear Research (JINR), Dubna, Russian Federation

Three types of demonstrators for studies of the readout of silicon microstrip detectors with ultra-light cables were developed by participants of the CBM-MPD STS Consortium [1] and manufactured in SE SRTIIE, Kharkov, Ukraine. The cables were made on the basis of adhesiveless aluminium-polyimide foiled dielectrics and assembled using a "chip-on-flex" technology.

Demonstrator 1-a

Demonstrator 1-a (Fig. 1) is a cable with connectors at both ends that attaches to the already existing Demonstrator 0-b [2] built around the double-sided prototype detector CBM01B2. Its purpose is to investigate the effect of the cable length on the signal transmission. Three sets of multilayer cables were designed and manufactured, with lengths of 10 cm, 20 cm and 30 cm. Their main features are:

- 2 signal layers, 1 shielding layer, 1 mesh-spacer;
- signal layers: foiled dielectric FDI-A-24 (aluminium/polyimide 14 μm/10 μm); shielding layer: FDI-A-50 (aluminium/polyimide 30 μm/20 μm); mesh-spacer: 50 μm Kapton, 50% fill factor;
- 64 traces per signal layer, $\sim$100 μm pitch.

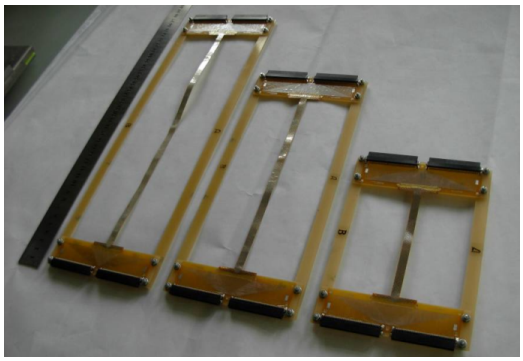

Figure 1: Multilayer analog cables.

During the manufacturing process all cables were tested for shorts/breaks/resistance of the traces using specialized automated test equipment.

Demonstrator 1-b

Demonstrator 1-b (Fig. 2) extends the application of the developed cables to a new object. The cables are connected through tab-bonding to the double-sided prototype detectors CBM02B2. They permit the readout of all 2$\times$256 orthogonal strips of the detector. The demonstrator has been manufactured in three specimen with different cable length.

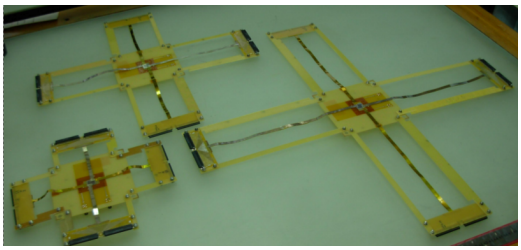

Figure 2: Demonstrators 1-b.

Demonstrator 1-b'

Demonstrator 1-b' (Fig. 3) is a subsequent development of demonstrator 1-b and realizes the first prove-of-principle object to study the concept of the planned CBM silicon tracking modules. It is built around the full-scale double-sided prototype detector CBM01 [3] and realizes the readout of 2$\times$128 strips (1/8th of all detector channels).

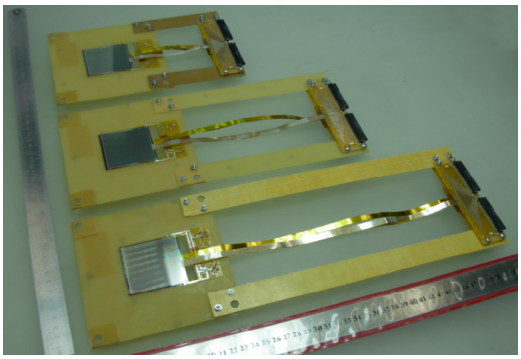

Figure 3: Demonstrators 1-b'.

Various tests planned with the demonstrators in the laboratory and with beam will yield important feedback for the determination of technical requirements of the components for the CBM STS detector modules.

References

[1] http://sunse.jinr.ru/projects/sts/abstract_sts.html
[2] V.M. Borshchov et al., CBM Progress Report 2008 12
[3] J.M. Heuser et al., CBM Progress Report 2007 9

Comparative analysis of CBM-STS ultra light-weight support structures manufactured from prepregs with different Young's Moduli

S.N. Igolkin[1], V.M. Dobulevich[2], Yu.A. Murin[3], J. Heuser[4], and the CBM-MPD STS Consortium

[1]St. Petersburg State University (SPbSU), St. Petersburg, Russia; [2]Central Construction Bureau for Machine-Building, St.-Petersburg, Russia; [3]Joint Institute for Nuclear Research (JINR), Dubna, Russia; [4]GSI, Darmstadt, Germany

The Silicon Tracking System (STS) of the CBM project consists of 8 layers of Si microstrip detectors. The detectors of each layer are combined in modules mounted onto ultra-light carbon fiber space forms with ultra thin microstrip cables transmitting the analog signal from the sensor to the electronic units attached at the back-ends of thus built supermodule, also called *ladder*. To meet the requirements of the experiment, the mechanical support of the ladder should allow the high-precision positioning of the Si detectors within the STS volume ($\approx$ 40 μm along the horizontal axis) with long-term position stability. Also access for maintainance and replacement of detector modules must be ensured.

Ladder space forms

The ladder space forms can be manufactured of carbon fiber prepregs with different Young's modulus and density [1, 2]. The choice of the carbon fiber prepreg to be used for manufacturing the space forms is a trade-off between the cost of the initial material, its availability on the market and the mechanical properties of the final product. To find out the impact of the type of prepreg chosen on the quality of the produced carbon fiber space forms, ANSYS calculations of basic mechanical properties of the space forms manufactured from different prepregs have been performed. With the help of the software package, the construction elements were optimized. The beams and the ribs of the space form were modeled with one-dimensional finite elements.

Carbon fiber materials

The properties of several commercially available high-performance prepregs are summarized in Table 1. For comparison, the mechanical deformation of space forms manufactured from the M40J, M46J, M50J and M55J carbon fibers has been simulated assuming 30% mass percentage of the binding agent ("carbon plastic"). The boundary conditions assumed in calculations were as follows:

- swivel connections at a distance of 40 mm from the ends of the frame;
- frame mounted horizontally;
- sag calculated under a central load of 100 g.

The sag (y and z components) and mass of the space forms are shown in Fig. 1.

Carbon fiber type	Carbon fiber YM [GPa]	Carbon plastic YM [GPa]	Carbon fiber ρ [g/cm^3]	Carbon plastic ρ [g/cm^3]
M55J	540	322	1,91	1,62
M50J	475	285	1,88	1,607
M46J	436	264	1,84	1,586
M40J	377	232	1,77	1,549

Table 1: Young's moduli (YM) and densities of commercially available carbon fibers (TORAYCA) and carbon composites.

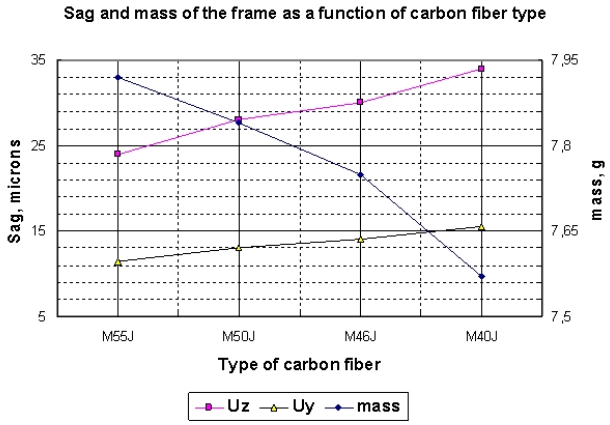

Figure 1: Sag and mass of the 1 m long CBM-STS space form manufactured from different types of prepreg.

Conclusions

The material recommended for production of the space forms is a TORAYCA prepreg with M55J carbon fibers. The R&D effort described was undertaken within the work plan of the ISTC Project # 3540 [3].

References

[1] S.N. Igolkin et al., *Ultra Light-Weight Carbon-Fiber Structures for CBM STS*, CBM Progress Report 2008

[2] S.N. Igolkin et al., *An apparatus for production of intricate shape carbon-fiber articles*, Patent No. 79268 of 12.27.2008, Int. Cl. B29C53/56(206.01).

[3] www.istc.ru

Prototyping of the CBM-STS module

V.M. Borshchov[1], Yu.A. Murin[2], J. Heuser[3], O.M. Listratenko[1], M.A. Protsenko[1], I.T. Tymchuk[1], Y.Y. Kostyshyn[1], L.V. Klimova[1], O.P. Starchenko[1], M.M. Merkin[4], N.N. Egorov[5], S.A.Golubkov[5], and the CBM-MPD STS Consortium

[1]State Enterprise Scientific Research Technological Institute of Instrumental Engineering (SE SRTIIE), Kharkov, Ukraine; [2]Joint Institute for Nuclear Research (JINR), Dubna, Russia; [3]GSI, Darmstadt, Germany; [4]Skobeltsyn Institute of Nuclear Physics of the Moscow State University, Moscow, Russia; [4]Research Institute of Material Science and Technology (RIMST), Zelenograd, Russia

For the prototyping of the CBM-STS module the Demonstrator 2-a was developed by members of the the CBM-MPD STS Consortium and manufactured at SE SRTIIE, Kharkov, Ukraine utilizing aluminum-polyimide cable elements and "chip-on-flex" assembly technology.

Design of Demonstrator 2-a

The demonstrator consists of the following components:

1) Three mock-ups of the full-scale silicon double-sided CBM03 sensors. The sensor replica were manufactured by RIMST (Zelenograd, Russia) within the work plan of the ISTC Project # 3540 dedicated to the development of the prototype CBM STS ladder. The main parameters are: Overall dimensions 62 mm by 42 mm, 1024 strips of 58 μm pitch per side. A subset of the masks for the full detector were used to produce the mock-ups.

2) Four flexible ultra light daisy-chain cables for series connection of the sensors. The cables are made from foiled FDI-A-20 dielectric with 14 μm thick aluminum lines on 10 μm polyimide carrier. The cable comprises 1024 traces of 58 μm pitch.

3) Two flexible multilayer analog cables to connect the sensors to the front-end-board (FEB). They are built from four layers: two signal layers, a shielding layer and a mesh-spacer. The signal layers are made from foiled FDI-A-24 dielectric with 14 μm aluminium on 10 μm polyimide. It comprises 512 lines and two bias lines. The trace pitch is 116 μm. The shielding layer is a FDI-A-50 dielectric with aluminium/polyimide of 30 μm/20 μm. The mesh-spacer is a 50 μm thick Kapton layer.

4) Two FEB mock-ups. Each mock-up of the FEB includes a flexible-rigid multilayer board on which are mounted 8 mock-ups of the readout chips (128 input pads per chip) with spTAB-bonded two-layer fine-pitch chipcables. In addition, the SMD components are mounted on the FEB as well. The multilayer analog cables are connected to the FEB with a pitch-adapter (aluminium traces on oxidized silicon).

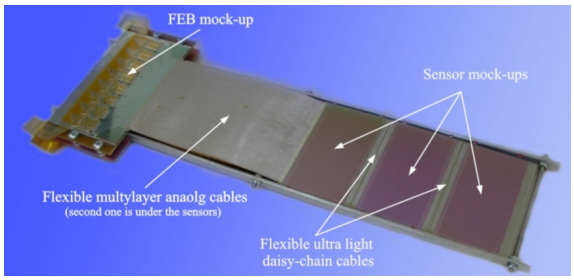

Figure 1: Demonstrator 2-a.

Assembly of Demonstrator 2-a

The assembly has been performed in three stages:

1) Interconnection of sensors with daisy-chain cables: Ultrasonic tab-bonding of daisy-chain cables to the sensor mock-ups (over 8000 bonds); bonds protection.

2) Assembly of FEB mock-ups: bonding and gluing of the four-layer flexible board; gluing of the multilayer flexible board to the rigid base; mounting of the SMD components on the flex-mounts to the flexible-rigid board; mounting of the pitch-adapter on the flexible-rigid board; spTAB bonding of the chipcables to the chip mock-ups; mounting of the tabbed chips on the board (spTAB bonding to the board and to the pitch adapter).

3) Connection of sensor assembly to FEB: assembling of multilayer analog cables; spTAB bonding (over 4000 bonds) and gluing/protection of analog cables to FEBs and sensor assembly. The sensors are mounted (glued) on the mechanical support on dielectric microinsulators. The total number of bond joints on Demonstrator 2-a is amounts to about 20 000.

Conclusions

The successfully achieved assembly of Demonstrator 2-a, shown in Fig. 1, confirms the chosen design-technological solutions for manufacturing multi-sensor modules. The experience gained will be applied with the forthcoming manufacturing of CBM-STS modules.

A Concept for the CBM-STS Sensor Cooling

S.N. Igolkin[1], A.I. Svischev[2], Yu. A. Murin[3], J. Heuser[4], and the CBM-MPD STS Consortium
[1]St.-Petersburg State University (SPbSU), St.-Petersburg, Russia; [2]Central Construction Bureau for Machine-Building (CCBMB), St.-Petersburg, Russia; [3]Joint Inst. for Nucl. Research (JINR), Dubna, Russia; [4]GSI, Darmstadt, Germany

The sensors of the CBM Silicon Tracking System (STS) are to operate in a harsh radiation environment. To work properly, they have to be kept cooled to temperatures potentially as low as -25°C. The development of the CBM-STS cooling system comprises a technical challenge due to the requirement for the material budget minimization of the tracker, considerable maximum heat production (1.5W from a typical sample sensor with 62 by 62 mm^2 area) and due to large variation of heat produced within the tracking stations (40 mW/cm^2 for the interior sensors close to the beam pipe compared to 4 mW/cm^2 from the external ones). Above all complications mentioned, the sensors could be cooled only from one side since the other is covered by the analog cables delivering sensor signals to the read-out electronics.

To solve the problems, the cooling system could use a cooled gas fed to a "mattress" located in front of the plane of detector lines depicted in Fig. 1. The mattress is made of two 10 μm mylar films tack-welded along the axis of the ladder. One of the films is solid, the other one, facing the detector plane, is perforated. The detectors are thus cooled from one side by gas directed flow in the gap between the mattress tubes and detector planes when the cooling gas is injected into the gap through the perforations.

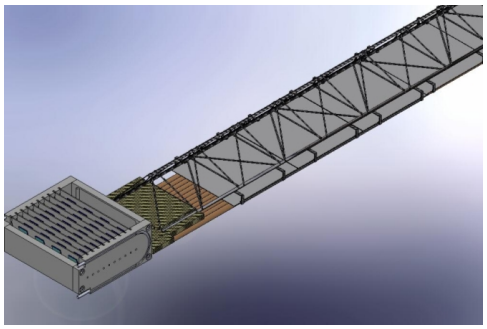

Figure 1: CBM-STS ladder with gas cooling arteries under the sensors.

A performance evaluation has been carried out and the gas consumption been calculated to remove about 1.5 W at a temperature of -25°C with an input-to-output gas temperature gradient of 1°C. The result is shown in Tab. 1.

For such sample system, the impact of the clearance value of a 8-tube "mattress" with 4.0 mm (upper numbers) and 0.5 mm (bottom numbers) perforation holes to the cooled face surface of the sensor are summarized in Tab. 2. The uniformity of the gas distribution depends on the ratio of the tube area to the sum of areas of the holes perforated in it. The calculations performed show that 32 holes of 1 mm diameter are enough for cooling the sample while for 0.5 mm holes their total number in a sample 8-mm tube should be increased to 128.

	He	H_2	N_2	Q, W	Δt, °C
G, kg/h	1.04	0.39	5.14	1.5	1.0
Q_n, m^3/h	5.9	4.3	4.1		

Table 1: Gas net (G) and volume (Qn) consumption to keep a sample sensor cooled as described in the text.

	He	H_2	N_2
V, m/s	3.0 24	2.25 18	2.1 16.8
α, W/(m^2·deg)	94 672	120 858	15 110
Δt_{gap}, °C	4.1 0.6	3.3 0.5	26.0 3.5

Table 2: Gas velocity V in the gap, heat-transfer coefficient α, and average temperature difference between the surface of the detector and the heat carrier surface Δt_{gap}.

An alternative scheme with sensors cooled from one side through free convection of the coolant gas has been also considered to show that a heat power of Q=1.5 W can be removed through free convection over a surface at the following temperatures of the ambient gas: helium -54°C, hydrogen -48°C. For nitrogen the maximum heat power removed is around 1.2 W at -190°C. The fraction of the heat power removed through radiation is around 15%. The accuracy of the temperature stabilization is better than 5°C.

Conclusion

The modeling of CBM STS sensor He gas cooling schemes with and without "mattress" are both promising for further R&D. The decision on the usage of the free convection or turbulent gas flow should be taken after additional experimental studies to be undertaken with a heat demonstrator of the CBM STS station currently under development. The R&D effort described was undertaken within the work plan of the ISTC Project # 3540.

Materials' properties of wavelength shifting films for the CBM-RICH detector - thickness dependence and efficiency *

P. Koczon[1], A. Braem[2], C. Joram[2], M. Dürr[3], and C. Höhne[1]

[1]GSI, Darmstadt, Germany; [2]CERN, PH Department, Geneva, Switzerland; [3]Hochschule Esslingen, Fakultät Angewandte Naturwissenschaften, Germany

P-terphenyl (PT) and tetraphenyl-butadiene (TPB) have been investigated as possible wavelength shifting materials for use in Ring Imaging Cherenkov (RICH) detectors. Wavelength shifting films made out of these organic molecules absorb light in the UV region and re-emit fluorescence photons at larger wavelength. Used on top of photomultiplier tubes (PMT), they therefore can enhance the quantum efficiency of the PMTs in the UV region. For an application in Cherenkov counters, gain factors for the number of measured photoelectrons for a cutoff wavelength of 200 nm ($E_{\max} = 6.2$ eV) are 1.71 ± 0.17 for PT and 1.27 ± 0.13 for TPB compared to a PMT with borosilicate windows. See [1] for a summary of these results.

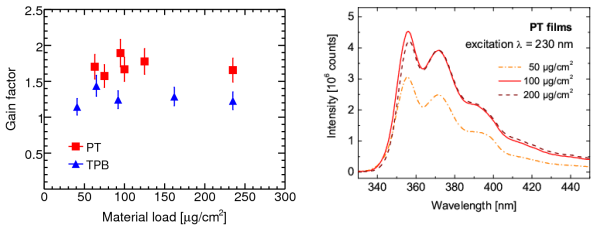

Figure 1: Left: Gain factor versus material load for a cutoff energy $E_{\max} = 6.2$ eV ($\lambda_{\max} = 200$ nm). Right: Photoluminescence spectra of PT films with different material load. See Fig. 2 for corresponding film thickness.

These investigations were continued by evaluating quantum efficiencies and gain factors for PT and PTB films of different thickness, see Fig. 1 (left). No significant dependence on the applied material load in the coating process was found in the evaluated range. This insensitivity to the material load is clearly a plus for the application in a RICH detector. With many hundreds of PMTs to be coated, there is no need for a restrictive thickness control. To better understand the thickness dependent results of the measured quantum efficiency, fluorescence measurements and scanning electron microscopy were performed with films grown on glass substrates similar to those on the PMT windows. Measurements of fluorescence intensity as a function of wavelength with excitation at 230 nm are shown in Fig. 1 (right) for PT-films of different thickness. A pronounced increase in intensity can be observed for the 100-μg/cm^2-film when compared to the 50-μg/cm^2-film, while the intensities of the 100-μg/cm^2-film and 200-μg/cm^2-film are

* We acknowledge M. v. Stenis (CERN) for coating the PMTs and test samples with PT and TPB, and Dr. J. Kraut (Esslingen) for taking the SEM images.

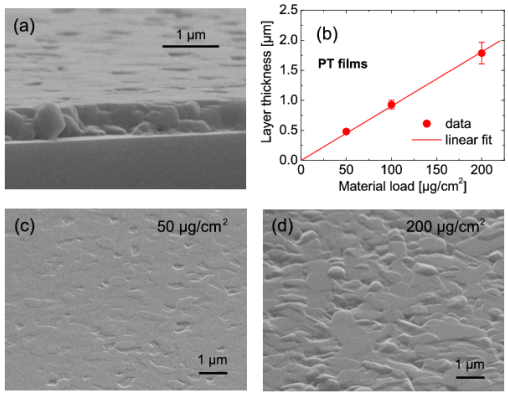

Figure 2: (a) SEM side-view of a 0.5-μm-PT-film on glass, viewing angle 80° off normal. (b) Dependence of layer thickness as measured by means of SEM as a function of material load during the evaporation process. (c) and (d) SEM bird's eye view of the layers' surface (60° off normal) for the 0.5-μm-PT-film and 2-μm-PT-film, respectively.

almost identical. Obviously, the PT-film with a thickness of 100 μg/cm^2 absorbs already almost all of the incoming photons. As a consequence, the efficiency of the PMTs is not increased with increasing film thickness. For the 50-μg/cm^2-film, however, a lower fluorescence intensity is observed. This indicates only a fraction of the available UV photons is absorbed. It suggests that for less material load than shown in Fig. 1 (left, PT) the quantum efficiency and gain factor will drop.

SEM images of PT films are shown in Fig 2. The side view in Fig. 2(a) indicates a rather smooth film growth and only minor formation of larger crystals. The measured thickness of each film is plotted against the material load applied during the evaporation process in Fig. 2(b). The thickness of the layers follows linearly the applied material load corresponding to a density of $\rho = (1.12 \pm 0.10)$ g/cm^3 which is slightly below the reported density of PT of ρ=1.23 g/cm^3. With increasing film thickness, a more pronounced formation of micro-crystals is observed which results in a higher surface roughness. However, the increased surface roughness and correlated increase in light scattering for the thickest layer shows, if any, only a small effect in the fluorescence spectrum.

References

[1] P. Koczon, C. Höhne, M. van Stenis, A. Braem, C. Joram, FAIR-EXPERIMENTS-16, GSI Scientific Report 2008.

Readout of the Hamamatsu H8500-03 MAPMT with the n-XYTER chip

P. Koczoń, C. Höhne, C. Schmidt, and W. F. J. Müller
GSI, Darmstadt, Germany

In the CBM-RICH detector, a photo-detector plane based on Hamamatsu H8500-03 MAPMTs is foreseen for Cherenkov light detection [1]. In order to cope with the high interaction rates and, consequently, the large data flow, front-end electronics with self triggered read-out chips is planned. At present, the read-out electronics is based on a first version of the n-XYTER chip [2]. This, however, has a dynamic range of 125,000 e^-, while typical photo-multipliers have a gain of order 10^6. As a temporary solution, a charge divider was developed which accomodates the MAPMT signals to the n-XYTER input (Fig. 1). A simple resistor - capacitor circuit with an attenuation factor of 50 was built and tested. This attenuator reduces the signal amplitude without strongly affecting the signal shape. The control of the n-XYTER chip as well as further data processing is performed with a Readout Controller (ROC) and the data aquisition system DABC developed for CBM [3] running on a standard Linux PC.

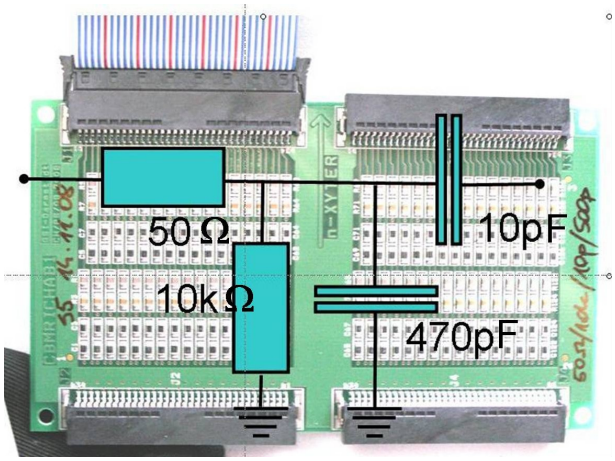

Figure 1: Charge divider

The read-out system was tested in the laboratory with a LED driven by a pulse generator. The mapping of the 8×8 pixel surface of the MAPMT to the n-XYTER channels was verified with a pinhole mask. The setup was also tested in a proton beam. It comprised a plexiglass block of dimensions (8 cm $\times$ 8 cm $\times$ 6 cm) placed directly in front of the MAPMTs, which were installed in 3 cm radial distance from the beam axis while the plexiglass extended into the beam. Protons of 3.5 GeV kinetic energy crossing the plexi-glass produced Cherenkov photons. The coincidence of two beam detectors (scintillators of 5 mm width each) located downstream of the radiator was recorded along with the MAPMT signals and used as event trigger in the offline data analysis.

A maximal event rate of $3{\cdot}10^5$ Hz could be recorded with the DABC system. This rate was limited by the bandwidth (8 MB/s) of the used Ethernet connection. It could be demonstrated that the H8500-03 MAPMT with signal attenuation and n-XYTER readout is able to register single Cherenkov photons. Figure 2 compares the ADC distribution from one selected MAPMT pixel for noise (solid line) and requiring beam coincidence (dashed line). Single photon counting is clearly demonstrated as the ADC distributions of thermal electrons and electrons from Cherenkov photons show the same shape.

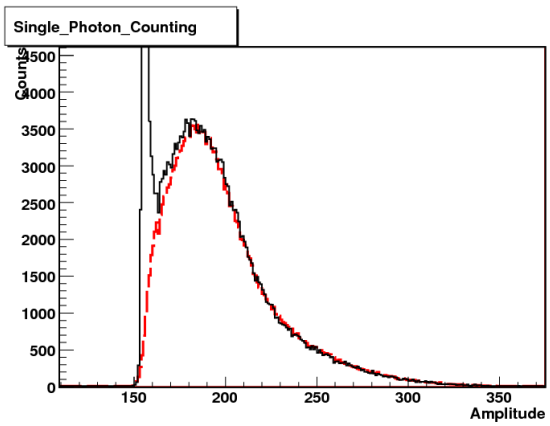

Figure 2: ADC spectrum measured with H8500-03 (data for only one pad are shown). The solid black line denotes the background from thermal electrons and noise, the dashed red line the signals from single photons. The single-photon spectrum was scaled for better comparison.

References

[1] C. Höhne *et al.*, Nucl. Instr. Meth. Phys. Res. **A 595** (2008) 187

[2] A. S. Brogna *et al.*, Nucl. Instr. Meth. Phys. Res. **A 568** (2006) 301

[3] http://cbm-wiki.gsi.de/cgi-bin/view/DAQ/WebHome, http://dabc.gsi.de/

Results from first beam tests for the development of a RICH detector for CBM

J. Eschke[1], K. Todoroki[2], and C. Höhne[1]
[1]GSI, Darmstadt, Germany; [2]University of Tokio, Tokio, Japan

A key item of the CBM physics program is the precise measurement of low-mass vector mesons and charmonium in their leptonic decay channel. In CBM, electrons will be identified using a gaseous RICH detector combined with several TRD detectors positioned behind a system of silicon tracking stations [1]. The concept of the RICH detector foresees an array of multi-anode photomultipliers (MAPMTs) as photodetector.

First beam test data for Cherenkov light detection with a 64 channel Hamamatsu H8500 MAPMT were recorded in August and September 2009 at GSI. Figure 1 shows the beam test setup. A 2 GeV proton beam was used to produce Cherenkov photons in a 8 mm thick plexiglass radiator. The signals of the MAPMT were attenuated by a factor of 40 in order to be compatible with the self-triggered readout electronics based on the nXYTER ADC chip which originally was developed for signals from Silicon sensors [2].

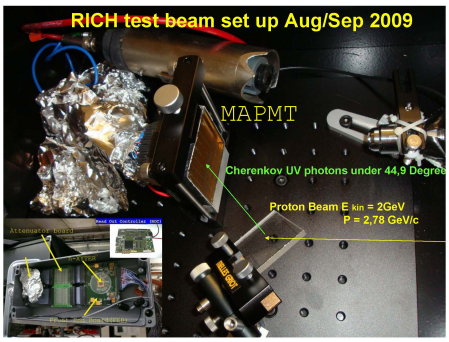

Figure 1: Test beam setup for the detection of Cherenkov photons produced by a 2 GeV proton beam in a 8 mm plexiglass radiator

A clear separation of the ADC signals from uncorrelated, low-amplitude noise events from signals of Cherenkov photons with higher amplitude was achieved by a cut on the time difference between the beam counter coincidence and the hits in the MAPMT (Fig. 2).

Figure 3 shows the event-integrated signal of the projected quarter Cherenkov ring. On average, 3.52 hits were recorded per beam event. This number agrees well with an estimate taking into account the number of produced Cherenkov photons, geometrical losses, transmission lossses and the quantum efficiency and collection efficiency of the MAPMT.

The result of this beam test demonstrates that the self-triggered nXYTER ADC chip is suited for the readout of the Hamamatsu H8500 MAPMT even with the currently needed attenuation of the primary PMT signals. It could be demonstrated that this MAPMT is able to detect single Cherenkov photons which can well be separated from noise using available timing information on the event.

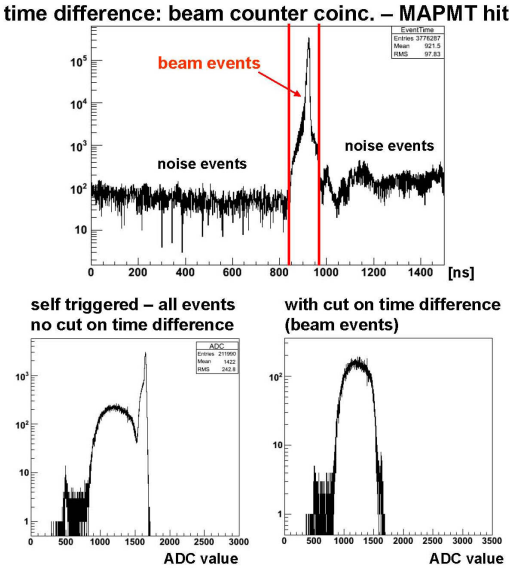

Figure 2: Time difference between beam counter coincidence and MAPMT hit (upper panel). The selection of events within the indicated lines remove uncorrelated noise events (pedestal peak) in the ADC (lower panels; note the inverted ADC scales).

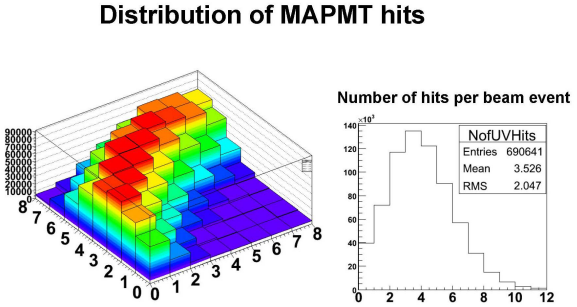

Figure 3: Quarter Cherenkov ring as detected with a 64 channel Hamamatsu H8500 multi-anode photomultiplier

References

[1] C. Höhne, *CBM-RICH layout optimization*, CBM Progress Report 2007, Darmstadt 2008, p. 17

[2] A. S. Brogna *et al.*, Nucl. Instr. Meth. Phys. Res. **A568** (2006) 301

Development of a CBM-RICH prototype in Pusan

J. Yi*, K.E. Choi, C.W. Son, K. Oh, J. Song, and I.K. Yoo
Pusan National University, Pusan, Republic of Korea

A gaseous RICH detector prototype (PNU-RICH2) of the CBM-RICH detector has been developed at Pusan National University in 2009. This is an upgrade of the mini-RICH detector [1] and has now real size dimensions in length compared to the planned CBM-RICH detector. The PNU-RICH2 includes a spherical concave CBM mirror prototype [2] and 2 types of Multi-anode PMTs from Hamamatsu (H8500, H8500C-03).

Development of the CBM-RICH prototype

In order to investigate properties of the future CBM-RICH detector, a vessel of 1.76 m radiator length was prepared following the layout proposal of the CBM-RICH detector [3]. The detector vessel is constructed with 2 mm thick anodized aluminum panels which are supported by an aluminum frame having dimensions of about $1.8\times0.6\times0.3\ m^3$. The vessel serves as a gas container as well as a dark room shielding the MAPMT from outside light. The electron beam enters through a 25 μm thick Kapton foil window of 1 mm diameter.

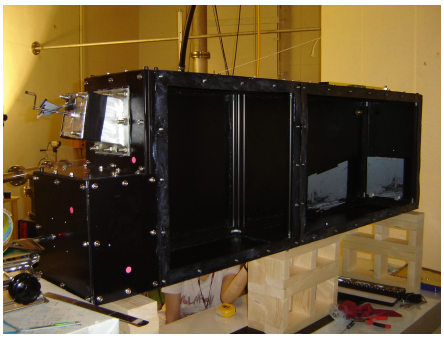

Figure 1: CBM-RICH prototype in Pusan (PNU-RICH2).

For light reflection and focusing onto the photodetector a spherical concave mirror (first CBM mirror prototype from the FLABEG company) of $20\times20\ cm^2$ size and with 3.2 m radius of curvature is positioned at a radiator length L=1.76 m in the vessel. Its alignment is precisely adjustable in 2 rotational axes with micrometer actuators. The CBM-mirror is coated with Al and MgF_2 showing efficient reflection of UV-photons [2].

Two types of Multi-anode PMTs (MAPMTs) from Hamamatsu have been implemented: one with a borosilicate window (H8500) and another with a UV extended window (H8500C-03). The latter MAPMT has $\sim$20% quantum efficiency in the UV region down to 200nm wavelength. Thus the photo detection with H8500C-03 is strongly enhanced compared to the H8500. The two 64 channel MAPMTs are installed at diagonal positions within the PMT mounting box that has space for 4 MAPMTs in total. This mounting box can be adjusted for various focal planes within a $\pm$50 mm range. This flexibility has been planned to enable the use of mirrors with different radius of curvature. A comparison of the new PNU-RICH2 and the first mini-RICH is summarized in Table 1.

Table 1: Parameters for the mini-RICH and the PNU-RICH2 detector.

	mini-RICH	PNU-RICH2
Radiator length (L[m])	0.55	1.76
No. of detected photons in one H8500	$\sim$0.8 /electron	$\sim$2.5 /electron
No. of PMT channels	64	128 (256)
Curvature of Mirror (R[m])	0.75	3.2
Mirror reflectivity	$\geq$85%, $\lambda \geq 380nm$	$\geq$80%, $\lambda \geq 200nm$
Radiator	Dry Air, N_2	N_2 (CO_2 &mixed gas)
Calculated ring diameter [mm]	17.16(N_2)	73.21(N_2), 91.91(CO_2)

Performance Test with 60MeV electrons

The PNU-RICH2 detector performance was tested with 60 MeV electrons at the Test LINAC beam line of the Pohang Accelerator Laboratory (PAL), Pohang, Korea. This test beam line delivers a high intensity electron beam of appr. 1 nA, i.e. $6.3\cdot10^9$ e^-/s in 1 μs bunches which is not easily tunable. The beam focus is very wide, about 5.5 cm $\times$ 7 cm at the exit of the dipole magnet. Beam collimation and intensity reduction are thus important considerations in the test setup. Pb blocks of 10 cm thickness with a 1 mm beam hole were placed in front of the PNU-RICH2 setup. The experimental setup is shown in Figure 2.

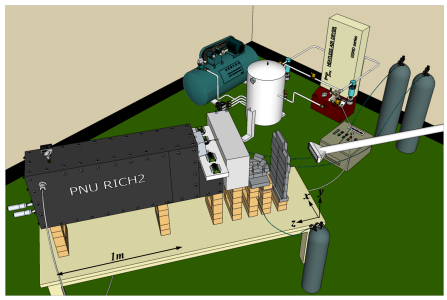

Figure 2: Experimental setup (design) with gas system at the Test LINAC, PAL.

The center of the PNU-RICH2 prototype detector was aligned to the beamline and the additional collimator in between. Two scintillation detectors are installed in front and behind the PNU-RICH2 vessel for selection of electron beamparticles. Additionally, a Multi-Wire Propor-

* fireplay@pusan.ac.kr

tional Chamber (MWPC) of 64×56 mm^2 with 32 cathode pads of 16×7 mm^2 was used for measuring the beam size at the vessel entrance.

A Programmable Logic Controller (PLC) is installed with sensors and controllers for gas control and monitoring. Mass flow controls (MFC -M3030V, Tech.co.) and electric solenoidal valves (TV2,TPC mech. co.) are used for control of the gas flow rate and to manage the flow directions. Gas flow is controlled up to 10 L/min and various gas mixtures can be selected with the MFC. Sensors are installed at the vessel to monitor gas conditions as temperature, humidity and pressure. They are monitored using a TH sensor (HTX62C, DOTECH co.) with an accuracy of ±0.3°C and ±1.8% R.H. The Pressure transmitters (TPS20,KONICS co.) work up to 5 kgf/cm^2 in the vessel and pipes with an accuracy of ±0.3% F.S.

For online monitoring and control of the gas and the High Voltage (HV) supply system, we use a control software tool, PVSSII, commonly used for LHC experiments. Its interface and a simple test are illustrated in Figure 3.

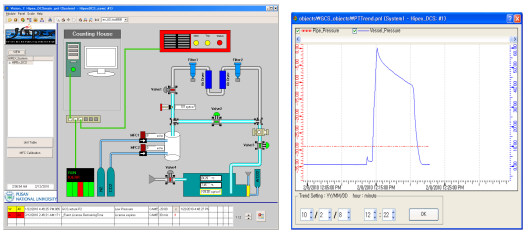

(a) DCS User Interface. (b) Pressure monitoring.

Figure 3: DCS User Interface and Monitoring test.

Results from the performance test of the PNU-RICH2 with the 60 MeV electron beam are shown in Figure 4(a) with the expected ring image for the N_2-radiator and an electron beam centered on the beamline. The presented figure shows signals integrated over all events taken. Single event display are not yet available due to restricted readout conditions of the MAPMTs and difficulties to trigger on single electrons. Since experimental data show no ring image on the photo detection plane, detailed simulations of the setup within the CbmRoot framework have been performed. Fig. 4(b) shows the result of a realistic simulation integrating 10^6 events: A 10 cm thick lead wall with a 1 mm hole is set in front of the PNU-RICH2 with a 1.76 m long N_2 gas radiator. The 60 MeV electron beam spot size and beam spread is resembled by a simulated electron beam spot of 2×2 mm^2 and 2° beam spread; electrons start 1 m in front of the PNU-RICH2.

Figure 5 presents single event displays of the simulation with the same conditions. Clear ring images are seen, however with varying positions. Simulations have shown that this position variation is caused by multiple scattering of the low momentum electron beam. It yields to the fact, that in event integrated displays the whole MAPMT surface is equally covered by hits.

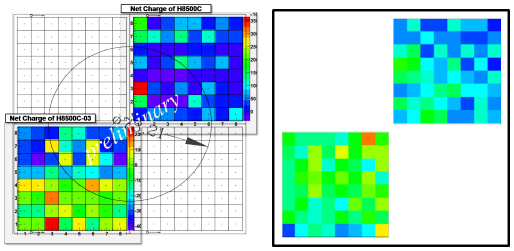

(a) (b)

Figure 4: Measured and Simulated performance. (a) Measurements with calculated ring image on the PMT plane with 2 MAPMTs with 8×8 channels each. Upper right MAPMT is H8500, and bottom left MAPMT is H8500C-03. (b) Simulation results for 10^6 events for appr. the same experimental conditions.

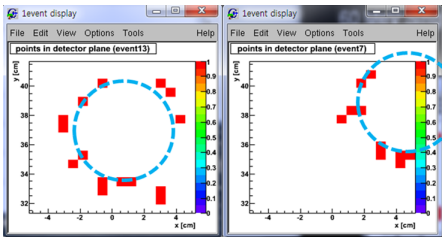

Figure 5: Single event displays in simulation.

Summary and Outlook

A CBM-RICH detector prototype has been constructed with comparable geometrical dimensions in length as foreseen for the CBM-RICH detector. This prototype will be used for performance tests in particular varying conditions of the gas radiator. A gas monitoring and control system based on PVSSII has been installed. Simulation studies for the realized setup have been performed within the CbmRoot framework.

The prototype was successfully brought into operation at the Test LINAC beam line of the Pohang Accelerator Laboratory (PAL). Due to experimental conditions, no single events could be recorded but only data samples for integrated events. Therefore no single ring images could be seen. In order to resolve single rings in future, two steps are mandatory for a successful operation of the PNU-RICH2 test setup: The electron beam intensity has to be reduced to a level which allows to trigger on single electrons. In addition, the readout of the MAPMTs has to be available on an event-by-event basis. The latter will be solved by using n-XYter chips for readout in a future testbeam.

References

[1] J.G. Yi *et al.*, CBM Progress Report 2008, p22.

[2] M. Dürr *et al.*, FAIR-EXPERIMENTS-15, GSI Scientific Report 2008; and CBM Progress Report 2008, p21.

[3] C. Höhne *et al.*, NIM A 595 (2008) 187.

Test set-up for the PMT based camera of the CBM-RICH detector*

K.-H. Becker[1], K.-H. Kampert[1], J. M. Kopfer[1], J. Pouryamout[1], and J. Rautenberg[1]
[1]Bergische Universität Wuppertal, Gaußstr.20, D-42119 Wuppertal, Germany

Introduction

The design studied so far foresees as photon detecting device of the RICH detector a camera of approx. $55\,000$ channels on a surface of $2.4\ \mathrm{m}^2$ [1]. The multi-anode PMT H8500 from Hamamatsu is a feasible solution for this requirements. A test bench has been set-up in Wuppertal to evaluate the properties of the PMT, which feed the RICH-simulations used to determine the capabilities of the detector. With the simulations in turn the requirements on the PMT-characteristics can be estimated that are needed to reach the physics goal, i.e. the electron-hadron separation.

H8500 PMT

The H8500 PMT from Hamamatsu is a multi-anode PMT with 64 channels arranged in an 8×8 matrix. The pixels are sized $5.8 \times 5.8\ \mathrm{mm}^2$ with a pitch of $6.08\ \mathrm{mm}$, resulting in a total dimension of $52 \times 52\ \mathrm{mm}^2$. It is delivered in several versions, e.g. with different glass type or higher quantum efficiency cathode. For testing purpose, we use one with the radiation harder UV-glass (transmissive down to 185 nm) and one with higher quantum efficiency.

Set-up for testing PMTs

We have installed a new dark-room lab for the tests of the PMTs. The room is sufficiently sized to hold even a RICH prototype with a mirror and camera. As shown in Fig. 1 it is equipped with everything needed to study either effects of the PMT in general, depending on the wave-length, or effects between the channels. We employ a dual deuterium (180 nm – 400 nm) and tungsten (300 nm – 2.6 μm) light source, covering a wide range in wave-length down to and below 200 nm. The monochromator provides mono-frequent light with an accuracy of 0.2 nm and a band pass of 1 nm. It is a Czerny-Turner type based monochromator on a dual-grating turret. Using the bayonet mounting flange we can plug a light-fiber to the monochromator with the other end fixed on an x-y table to scan each position on the PMT cathode. For the measurements of the quantum efficiency a pico-ampere meter and a calibrated photo-diode are installed. We can sample the 64 PMT-pulses using VME-cards based 100 MHz flash ADC's.

* supported by BMBF grant 06WU9195I

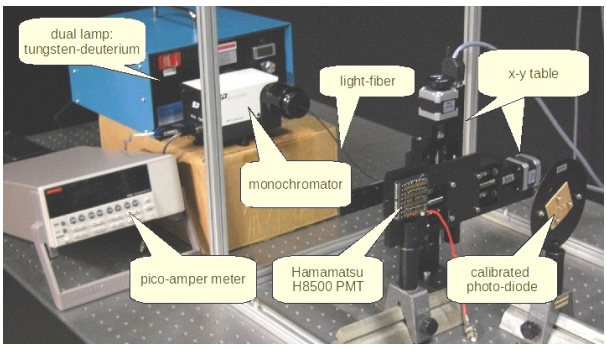

Figure 1: Set-up in the newly installed dark-room: dual light-source, monochromator, light-fiber, x-y table, PMT, pico-ampere meter, calibrated photo-diode

Test program

Besides the quantum efficiency measurement for the comparison of the different available cathode versions of the PMT, we want to quantify the possible gain in registered photons per Cerenkov-ring not only depending on the glass-type, but also considering the use of wave-length shifters [2]. Used in a film on the front of the PMT these absorb the light at smaller wave-length where the glass of the PMT is less transparent and emit light at longer wave-length. In addition, we want to study the efficiency for inclined incident angles.

With the use of the x-y table we can automatize studies like investigations on channel-inhomogeneities or on the dead-region between channels. We can also determine the channel by channel cross-talk, that might suffer from an added film like a wavelength-shifter.

Status and outlook

We have finished the major part of the set-up. After the measurements for the quantum efficiency we continue with the measurements using the full pulse-shape registered by the FADC. Later we want to use the XYTER/ROC-based read-out. Knowing precisely the detector using the alternative data-acquisition, we can estimate the effect of the designated detector read-out. A detailed design of the front-end electronics chain and layout can then be developed.

References

[1] S. Lebedev et al., CBM Progress Report 2008, p. 20

[2] P. Koczoń et al., CBM Progress Report 2008, p. 26;
P. Koczoń et al., this report.

Mechanical design for the CBM-RICH mirror mounting structure

V. Dobyrn, E. Kormin, N. Miftakhov, V. Polyakov, G. Rybakov
O. Tarasenkova, V. Tolchin, E. Vznuzdaev[1]
[1]PNPI, 188300, Gatchina, Russia

The CBM-RICH detector design currently foresees the usage of glass mirrors of (3-6) mm thickness and a radius of curvature of 3 m [1]. A rectangular form of the single mirror tiles is considered in order to allow homogenous coverage of the mirror plane. A convenient tile size would be on the order of 40×40 cm^2. Hexagonal mirror tiles are expected to show less distortions at the edges, however with the chosen comparable small radius of curvature small tiles would be necessary and irregular spacings between tiles in order to cover the mirror sphere.

In CBM, global tracking has to bridge the gap between the last STS station 1 m downstream the target and the first TRD layer appr. 4.5 m or 5 m downstream the target. The RICH design should therefore keep the material budget as low as possible in order to reduce multiple scattering of the particles. The main material budget of the RICH detector in the path of the particles will be concentrated in the mirror plane. Fortunately, as the first TRD station is placed close to the RICH mirror plane, simulations indicated that the influence of material budget is moderate [2]. Nevertheless, low material budget of the mirror wall is aimed at. Experience shows that 6 mm glass mirrors are well manageable and show good stability, however they correspond to appr. 5% radiation length. On the other hand, glass mirrors of 3 mm thickness only are expected to be at the limit for stable handling. In order to optimize the mirror thickness for CBM, R&D activities are being performed at PNPI.

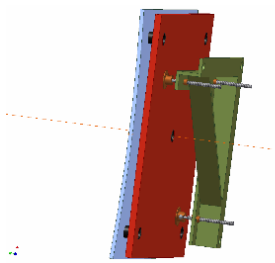

Figure 1: 3D model of the proposed mirror module for 3 mm thick glass mirrors.

A mirror module for stable mounting of thin (3 mm) mirrors of 40×40 cm^2 size was designed. It consists of a thin, rigid, low density composite sandwich panel onto which the 3 mm glass mirror would be mounted with a 5-point sphere-plane transition (Fig 1). The adjustment mechanics can then be rigidly adjusted to the sandwich not influencing the thin mirror. Finite Element Analysis (FEA) of the gravity deformation for such a mirror module was performed for several angular positions of the module. The maximum deviation of the mirror shape from a spherical shape was 2 microns only (see Fig 2).

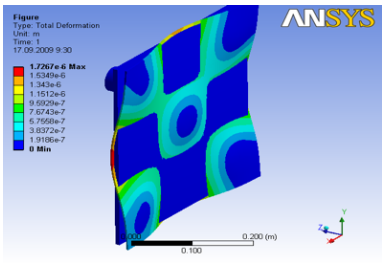

Figure 2: Mirror deformations estimated using FEA.

A test-bench for optical measurements has been developed to study the influence of the mount on the optical quality of the mirror and to determine an adjustment procedure for the mirrors (Fig 3). The following possibilities are implemented:

- horizontal ($\pm 45°$) and vertical ($+10° / -25°$) rotation of the mirrors;
- measurements of optical quality for different angle positions of the mirrors;
- time stability study for mirror mount;
- measurements of regulation dependencies for adjustment mechanics;
- study of the adjustment procedure.

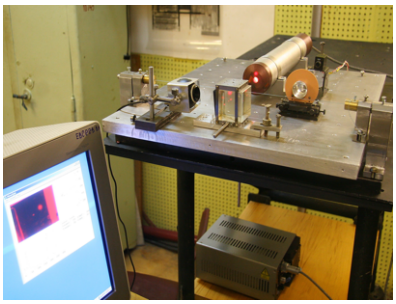

Figure 3: Test bench setup at PNPI.

Unfortunately no experimental tests could be performed in 2009 as the delivery of new CBM-RICH mirror prototypes was strongly delayed.

References

[1] C. Höhne *et al.*, NIM A 595 (2008) 187.
[2] S. Lebedev et al., CBM Progress Report 2008, page 20.

Status of MuCh software

E. Kryshen and M. Ryzhinskiy
PNPI, Gatchina, Russia

In 2009, considerable progress was made in the MuCh software development: integration of the straw tube option in the MuCh library, implementation of the manual segmentation, new features like timing and track matching algorithms, etc.

Straw tube option

The first version of the straw tube detector was implemented in a separate library by Alexandr Zinchenko (JINR, Dubna) in 2008. However, it appeared much more convenient and consistent to integrate the straw option into the MuCh library. As a first step, the parameters of the straw tube modules (position of stations, number of layers, straw diameter) were added to the MuCh geometry file, which was then used for the geometry simulation in the CbmMuch class. The general layout of the MuCh system with three straw tube stations is shown in Fig. 1 (left).

In order to include the straw detector parameters in the MuCh detector framework, the CbmMuchGeoScheme class (MuCh geometry interface) was significantly rearranged. A separate class for the digitization of MC information (CbmMuchDigitizeStraws) and the algorithm for the hit production in straw modules (CbmMuchFindHitsStraws) were developed. The CbmMuchStrawHit class was added to store information on one-dimensional straw hits. Moreover, the possibility of one-dimensional straw hit visualization was added to the MuCh visualization library (see Fig. 2).

Tracking with straw hits was successfully implemented by A. Lebedev.

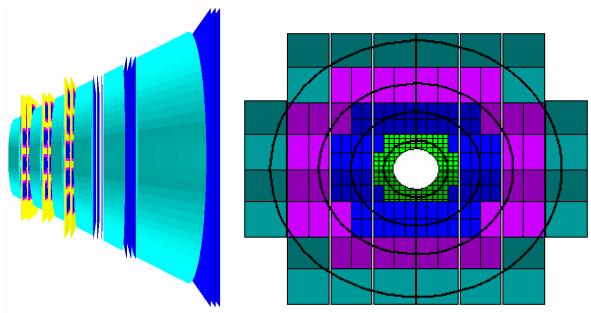

Figure 1: General layout of the MUCH system with straws (left) and example of manual segmentation for the first station (right)

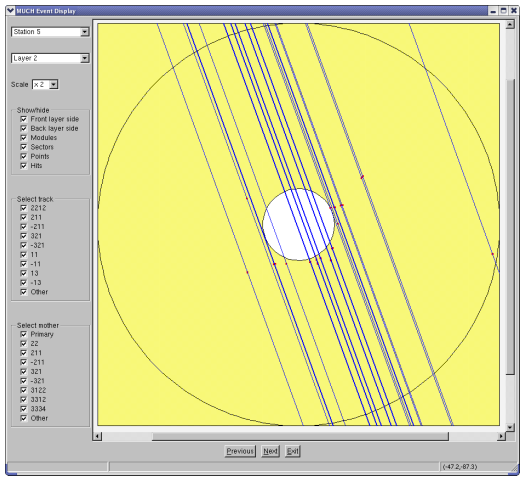

Figure 2: Visualization of straw hits

Manual segmentation algorithm

Automatic segmentation, the only option available until 2009, is based on occupancy conditions and cannot be used for the fine-tuning of segmentation parameters. A manual segmentation algorithm was developed to overcome this limitation and tune the number of channels, pad sizes, and number and radii of regions with equal pad size. The manual segmentation does not require MC simulations; the segmentation result depends only on parameters which should be defined in the segmentation input file.

The structure of the input file is the following. At first, the number of stations must be set. Then for each station the number of channels per sector and the number of regions with equal pad sizes must be specified. This general specification is followed by the parameters of the equal-pad regions, namely radii and corresponding pad sizes (width and length).

If the module dimensions do not allow to arrange an integer number of sectors, incomplete sectors will be produced on the edges of the module, having a reduced number of pads and different pad sizes compared to the settings in the input file.

In conclusion, the MuCh detector simulation, digitization, hit finding and tracking are fully functional, allowing users to tune many parameters and optimize the detector performance. Future efforts will be devoted to the improvement of hit finding procedures and parallelization of time-critical parts of the algorithms.

A possible start version of the CBM muon detector system at SIS100

A. Kiseleva[1], C. Höhne[1], E. Kryshen[2], A. Lebedev[1,3], M. Ryzhinskiy[2], and P. Senger[1]
[1]GSI, Darmstadt, Germany; [2]PNPI, Gatchina, Russia; [3]JINR-LIT, Dubna,Russia

The CBM muon detection system (MuCh) was optimized for nucleus-nucleus collisions at SIS-300 beam energies [1]. We have investigated the possibility to simplify the setup for measurements of J/ψ mesons in proton-nucleus collisions at SIS-100 beam energies. Therefore, the performance of the muon detection system has been studied as function of the number of the detector stations for J/ψ measurements in p + Au collisions at 25 GeV. The simulations are based on a segmentation of the detector layers into pads with a minimum size of 0.28×0.28 cm^2 and a maximum size of 4.48×4.48 cm^2, corresponding to a total of 560,000 channels. For full track reconstruction, the LIT global tracking package [2] is used. In order to study the sensitivity of the reconstruction algorithm on the number of the detector stations, we removed the hits in selected stations from the track finding procedure. The signal-to-background (S/B) ratio and the J/ψ meson reconstruction efficiency or the full and for the reduced systems are shown in Fig 1. Here, 1-6 means that hits of all 6 stations are used by the reconstruction procedure; 2-6 means that the hits of the first station were removed from the reconstruction; 3-6 means that the hits of the two first stations were not used in reconstruction, etc.

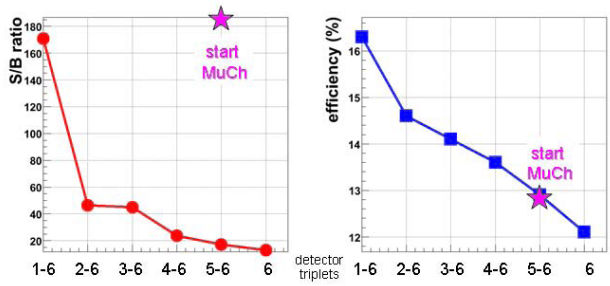

Figure 1: Signal-to-Background (S/B) ratio and reconstruction efficiency for J/ψ mesons from p + Au collisions at 25 GeV for the full (1-6) and for the reduced muon systems (for explanation see text). The stars show the results of the reconstruction for the start version of the muon system (Fig. 2).

The results of the simulations show a fast decrease of the S/B ratio (by more than a factor of 40) when removing the first station from the track finding procedure (see left panel of figure 1). This finding demonstrates that the first detector station is very important for background suppression. The reconstruction efficiency of the J/ψ mesons decreases almost linearly from 16% to 12% when decreasing the number of stations (right panel of Fig 1).

A possible start version of the CBM muon detector system to be used for proton-nucleus collisions at SIS-100 energies is shown in Fig. 2. This setup consists of 2 iron absorber layers (thickness 20 cm and 205 cm) and 2 detector stations with 3 detector layers each. The results of the track reconstruction based on this start version are depicted in Fig 1 (star symbols): the J/ψ reconstruction efficiency (right panel) is about 13% (to be compared to 16% for the full detector system with 6 stations), but the S/B ratio is as high as for the setup equipped with 6 detector stations (left panel). These results demonstrate that a start version of the muon detection system can be built with two detector stations only: a highly granulated detector triplet based on GEM technology after the first absorber, and a large-area low-granularity detector triplet after the second absorber. For the second triplet, either the first TRD station or straw-tube detectors can be used. Both options are under investigation.

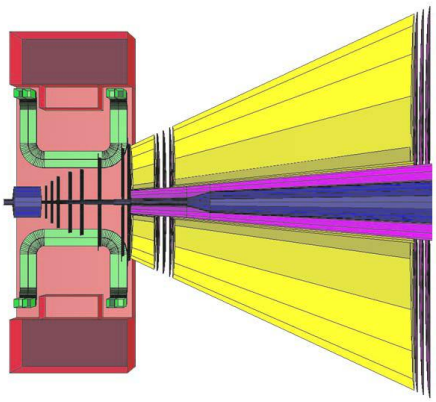

Figure 2: Reduced version of the muon system for measurements at SIS-100

References

[1] A. Kiseleva et al., *Optimization of the CBM muon detection system*, CBM Progress Report 2008, Darmstadt 2009, p. 27

[2] A. Lebedev et al., *Status of the global track reconstruction algorithm for the CBM experiment*, this report

Development of GEM chambers for MUCH

S. Chattopadhyay[1], A. K. Dubey[1], G. S. N. Murthy[1], S. Singaraju[1], J. Saini[1], Y. P. Viyogi[1], B. Bhowmick[2], and G. Ganguli[2]

[1]VECC, Kolkata, India; [2]University of Calcutta, Kolkata, India

As a part of the development of fast and high resolution detectors for MUCH, we have been working on the development of GEM chambers at VECC-Kolkata. Two chambers one with 3-GEM and other with 2-GEM configurations were tested with proton beam in september 2008 at SIS18 beamline. With GEM chamber and nXYTER readout a clear beam-spot was obtained, however a detailed measurement e.g. efficiency, position resolution and other parameters could not be obtained as the n-XYTER used for readout could be mounted only with alternate channels connected to the detector pads.

In 2009, we have made two 3-GEM chambers using 10 cm x 10 cm GEM and with two different types of pad plane. One pad plane (Chamber A) consisted of 3.5 mm x 8 mm cells and other one (Chamber B) had two types of cells, half of the pad plane was equipped with cells of 3.5 mm x 8 mm dimension and the rest half had 1.6 mm x 16 mm size. The one with finer granularity in X-direction will help to measure the position resolution in X-direction. The detector with one-type pad-size had 2.5 mm induction gap as opposed to 1.5 mm for the other detector. The enlarged induction gap was aimed at increasing the cluster size.

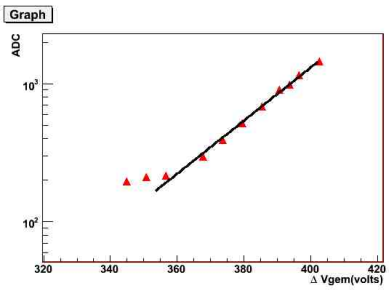

Figure 1: Variation of Fe-55 pulse height with Vgem for a 3GEM chamber

These detectors are tested with X-rays from Fe-55 source and n-XYTER readout for the first time. The variation of the Fe-55 pulse height with GEM voltage fitted with an exponential curve is shown in Fig. 1. The nXYTER ADC is subtracted from a set of dedicated baseline data taken without source for every pad.

The chambers are then tested with 2.5 GeV proton beam from SIS-18 at GSI. Charged particle response was studied at varying applied voltages. Fig. 2 shows the beam spots for two detectors.

The efficiency of the detector is measured by taking the ratio of the beam count on the prototype STS beam tracker

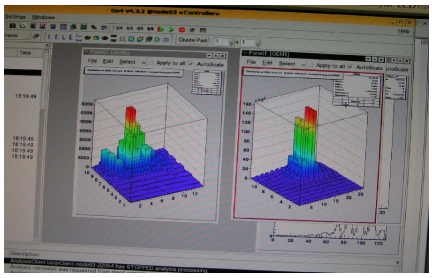

Figure 2: Beam spot as seen online

placed closest to the count on the GEM chambers. The analysis is done using the standard root based analysis setup made for CBM test-data analysis where event size is taken as $\pm$ 2000 nsec. The efficiency of the detector as a function of applied voltage for chamber B is shown in Fig. 3. The highest efficiency obtained is of the order of 80%. Investigations are ongoing to understand the observed efficiency and improve upon this number. We have made a test system with cosmic rays for obtaining the efficiency and position resolution of the detectors before they are tested with proton beam in 2010. Two types of PCB are being made with 3 mm x 3 mm and 4 mm x 4 mm cell size. These rectangular pad sizes will help to avoid the ambiguity in determining the position of the particle due to staggered geometry. These cell sizes are closer to the sizes being investigated in simulation for final use in muon chambers at CBM.

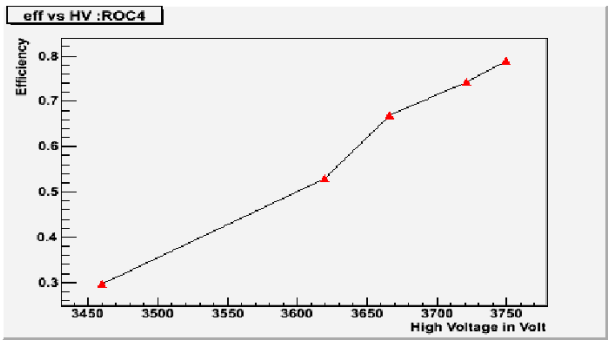

Figure 3: Variation of efficiency with applied total High Voltage (V)

Application of a granulated coordinate straw detector prototype

I. V. Boguslavskiy[1], K. Davkov[1], V. Davkov[1], G. D. Kekelidze[1], V. Lucenko[1], V. Myalkovskiy[1], L. Naumann[2], V. Peshekhonov[1], A. Savenkov[1], and A. Zinchenko[1]

[1]JINR Dubna, Russia; [2]FZ Dresden-Rossendorf, Germany

The usage of Straw Tube Trackers in the MUCH detector of CBM requires an improved straw granularity. Thin straws with a diameter of less than 4 mm cannot provide the required coefficient of granularity increase because of significant growth of difficulty to provide their homogeneity. Methods of manufacturing and installation of segmented anodes have been developed [1, 2, 3, 4].

Flat flexible cables with extremly reduced material budget have been developed. Each cable bus provides the signal and the high voltage between the anode segment over a distance of up to 2 m [5]. For checking technological opportunities of construction of these detectors in the mass production, a prototype with 360 active anode channels has been developed and tested. The prototype contains two planes of straws glued between themselves. The planes were shifted between themselves by the straw radius of 2 mm to remove the left-right ambiguity. Each plane consists of 48 straws each 400 mm long. Each straw contains fourfold-segmented anodes of 100 mm legth. The anode voltage on each segment and the information read-out were carried out via the segment contacts going through the straw wall. Fig. 1 shows the general layout of the prototype with a fragment of the straw plane with the installed flat transmission lines (TL) of about 50 cm length. Each line has 8 buses and is used for 8 segments of two neighbouring straws.

For testing of the prototype the DAQ and FEE with a threshold of about 4.5 fC has been developed. The prototype has been tested with a ^{55}Fe source at gas gains of up to 10^5. The gas mixture $ArCO_2$ (70/30) was used. The leakage current in each channel did not exceed 1 nA. We measured, that $\sim$3% of the whole number of the channels failed. In several channels ($\sim$2%) a not negligible decrease of the signal amplitudes has been observed. The homogeneity of $\sim$95% of the registration channels amounts to $\pm$9%. The main reason for non-operating channels is related to disturbed signal transmission from the segment contact wires to the amplifier inputs.

A gas leakage test of the prototype has shown that the summed up leakage rate amounts to less than $1.5{\cdot}10^{-3}\mathrm{cm}^3\mathrm{s}^{-1}$.

Measurements of the spatial resolution value of the prototype were performed on the SPS test beam H6 at CERN. The beam telescope EUDET [7] was used as track detector. Preliminary estimations have shown that the spatial resolution of the prototype amounts to 200 μm.

The radiation thickness of the straw plane without (with) installed TL amounts to 0.06%X_0 (0.15%X_0), correspondingly. The radiation thickness in the place of the spacer of 8 mm length in the prototype was almost by one order of magnitude greater. At present an opportunity of reducing this value till 0.39%X_0 has been shown.

The new development offers an opportunity of constructing coordinate detectors based on straws having the minimal granularity of 1 cm^2.

The authors express their gratitude to Ingrid Gregor and her colleagues for the given opportunity of using the telescope EUDET and help in performing the measurements.

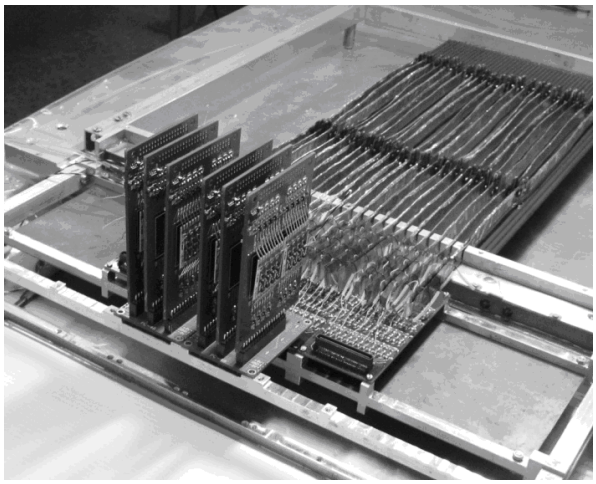

Figure 1: General layout of the straw tube tracker prototype with 96 fourfold segmented straws in two layers, the new developed very thin flat fexible cables and FEE-cards.

References

[1] K. Davkov et al., Annual Report FZ Dresden-Rossendorf 2006, FZD-461 (2007) p.34

[2] V. Peshekhonov et al., CBM Progress Report 2007, GSI Report 2008, p.42

[3] K. Davkov et al., Nucl. Instr. and Meth. A584 (2008) p.285.

[4] V. Peshekhonov et al., CBM Progress Report 2008, GSI Report 2009-03, p.35

[5] S.E. Vasilyev et al., Instr. and Exp.Technique, V. 51, No. 6 (2008) p.820

[6] Ju. Gusakov et al., submitted to Instr. and Exp.Technique

[7] URL: http://www.eudet.org

Dynamic range simulation for readout electronics for MUCH

B. Bhowmick[1], G. Gangopadhyay[1], P. Bhaduri[2], and S. Chattopadhyay[2]
[1]University of Calcutta, Kolkata, India; [2]VECC, Kolkata, India

The CBM muon detection system is designed to measure muon pairs from the decay of vector mesons and charmonia produced in heavy ion collisions. The concept is to track the particles through a hadron absorber system which is segmented in different layers with tracking detector planes placed in the gaps between those layers. The detectors proposed to be used are high-resolution gas detectors with GEM as amplifying elements. We present here a simulation study for the determination of the dynamic range (in terms of MIP) for the read-out chips associated with the detector planes.

The approach used here consists of simulating the response of single muons as minimum-ionizing particles (MIP). Their cell-wise energy deposition is compared to the energy deposition by hadrons generated by UrQMD. The dynamic range is simulated as a threshold on the energy deposition, expressed in terms of MIP, above which signals get saturated and hits are lost. The fraction of hits above the selected threshold is studied by varying the threshold. The effect of saturated cells on tracking and other properties of the MUCH response are studied.

The simulation is performed using UrQMD event generators for generating particles from A+A collisions and the Box generator to generate single muons. We use the standard MUCH geometry with 18 stations. As the segmentation of MUCH is not yet finalised, we have estimated the optimal cell size based on the fraction of multi-hit cells in different stations. We found an optimal size of 4 mm for the first 12 stations and 4 cm for the other stations.

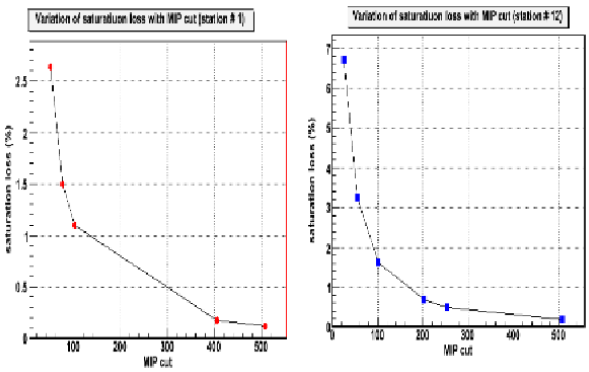

Figure 1: Percentage of lost hits as function of the applied threshold

The cell-by-cell energy deposition was obtained for both single muons and hadrons. We found an average value of 0.137 keV for muons. Different cuts on the energy deposition were applied, assuming that hits above the threshold will be lost because of saturation (Fig. 1). We find that for a threshold of 100 times the MIP value, less than 2 % of hits are lost in all stations.

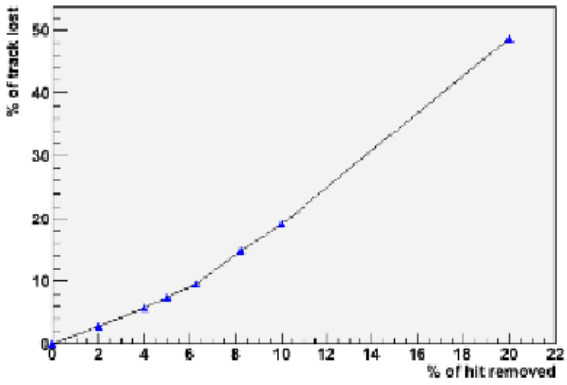

Figure 2: Percentage of track losses as function of hit inefficiency

Next, the effect of the hit loss on tracking was investigated. For this, we used 50 μ^+ and 50 μ^- embedded in central Au+Au events from UrQMD. Figure 2 shows the percentage of lost tracks as a function of the hit inefficiency. We see that about 2.8 % of tracks are lost at the obtained hit inefficiency of 2 %. In order to study the robustness of these results, we varied the number of muons embedded in the UrQMD events from 25 to 100, without observing a noticeable influence on the result.

From the results of this study, we propose that the dynamic range for the read-out system be chosen above 100 MIP in order not to significantly deteriorate the tracking efficiency.

A two-dimensional position sensitive high efficiency Transition Radiation Detector for a high counting rate environment

D. Bartoş[1], C. Bergmann[2], G. Caragheorgheopol[1], A. Herghelegiu[1], M. Klein-Bösing[2], M. Petriş[1], M. Petrovici[1], V. Simion[1], and J.P. Wessels[2]

[1]NIPNE, Bucharest, Romania; [2]University of Münster, Germany

The Transition Radiation Detector (TRD) architecture proposed by us [1] - [3] for lepton identification with the CBM experiment at the lowest polar angles is based on a double sided pad structure read-out electrode. An electron-pion discrimination efficiency better than 1% was achieved for a six layer configuration [1] with a position resolution on the order of 160 μm [3] up to an average particle rate of $2{\cdot}10^5$ particles$\cdot$cm$^{-2}\cdot$s^{-1}. In order to cope with the requirement of a reasonable geometrical efficiency, a larger size prototype, using the same architecture, but increasing the size of the rectangular pads of the central double sided read-out electrode was developed. In order to access the position information along the pad, the rectangular pads of the read-out electrode were split diagonally, each triangle being readout separately. First results on the detector performance using radioactive X-ray sources are reported here.

Typical pulse height spectra obtained in ^{55}Fe source tests for the first version of the prototype (see Fig. 1) show very good energy resolution.

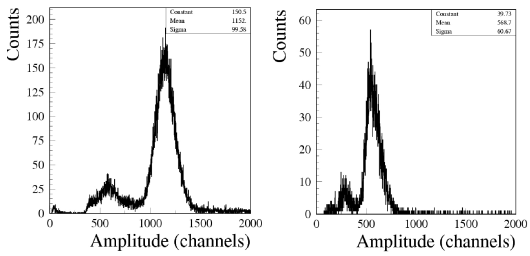

Figure 1: Pulse height spectra from ^{55}Fe source tests, anode signal (left) and pad plane signal (right).

As our ^{55}Fe source was too weak to be collimated, all tests for position resolution studies were performed using a ^{238}Pu source. The source was carefully collimated using two columns (A and B) of five collimators (2 mm diameter) each, along the pad length, column A on the center of a rectangular pad, column B at the border between two rectangular pads. The x direction is defined as being parallel with the anode wires (across the pad width), and the y direction perpendicular to the anode wires (along the pad). For those events in which at least three rectangular pads (six triangles paired two by two) were fired the position resolution in x direction could be determined (U_a = 1750 V). Results are shown in Fig. 2. The second, smaller peak seen in each distribution is due to X-rays that penetrate the thin plexiglass wall between the two rows of collimators. An average standard deviation of $\sigma_x \sim 1.34$ mm is obtained from fits to the distributions. If we subtract the contribution of the spot size on the anode plane, an intrinsic position resolution of $\sigma_x \sim 0.970$ mm is estimated. Results

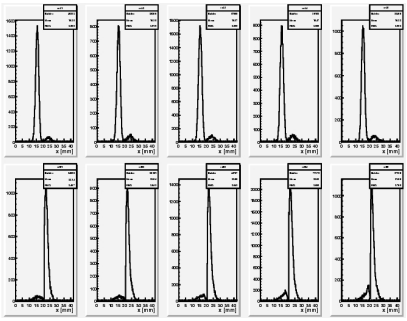

Figure 2: Position resolution in x-direction, collimator row A (upper plots), collimator row B (lower plots).

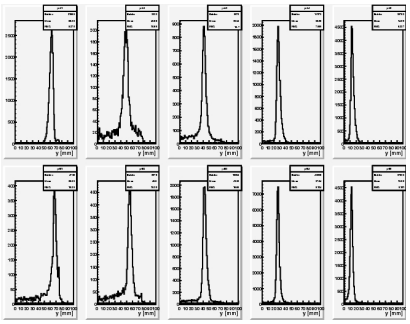

Figure 3: Position resolution in y-direction, collimator row A (upper plots), collimator row B (lower plots).

for the position resolution across the anode wires (y coordinate) are shown in Fig. 3. An average standard deviation of $\sigma_y \sim 2.49$ mm is obtained from Gauss fits of the presented distributions. Subtracting the contribution of the spot size estimated on the anode plane, an intrinsic y resolution of $\sigma_y \sim 2.31$ mm is determined. An algorithm for extracting positions along the anode wires using the information from the split pads is under development [4].

References

[1] M. Petrovici et al, NIM. A 579, (2007), 961

[2] M. Petriş et al., NIM. A 581, (2007), 406

[3] M. Klein-Bösing et al., NIM A 585(2008), 83

[4] C. Bergmann, this CBM Progress Report (2009).

Development and Test of a Real-Size Prototype for the CBM TRD

C. Bergmann[1], M. Klein-Bösing[1], D. Emschermann[1], J. P. Wessels[1], M. Petriş[2], V. Simion[2], M. Petrovici[2], and C. Höhne[3]

[1]Institut für Kernphysik, Münster, Germany; [2]NIPNE, Bucharest, Rumania; [3]GSI, Darmstadt, Germany

The CBM Transition Radiation Detector (TRD) will serve for particle tracking and electron identification. The innermost region of the TRD has to work at rates of 100 k hits/cm^2/s, special developments on fast gas detectors with sufficient TR conversion are thus ongoing.

We have constructed a TRD prototype (395.5 $\times$ 106 mm^2) based on a symmetric arrangement of two MWPCs with a common, central pad readout electrode made from kapton foil (25 μm) coated initially with 20 nm chromium and afterwards with 200 nm aluminum on both sides. The prototype is designed to feature a two-dimensional position reconstruction in one detector layer with a Position Resolution (PR) of 300-500 μm and a pion suppression factor of the order of 100 at 90% electron efficiency for the whole TRD consisting of up to 12 layers. The double-sided read-out pad plane concept with a gas volume of 12 mm thickness, an anode wire separation of 3 mm, and an anode cathode gap of 3 mm is retained from the previous small prototype [1] which has shown a good performance of electron/pion separation and PR in test beams. Two-dimensional track position reconstruction is reached by subdividing the 36 rectangular pads (each 10 $\times$ 80 mm^2) into 2 $\times$ 36 triangular pads with independent read-out channels for two pads back-to-back on opposite sides of the pad plane. The cluster position was reconstructed in two different coordinate-systems a and b by using a weighted (w) and an unweighted (uw) displacement d of the cluster position relative to the center of the pad group with maximum charge, based on the Pad Response Function (PRF) [1] for signals measured on eight adjacent pads (see Fig. 1). The second coordinate system b is shifted by

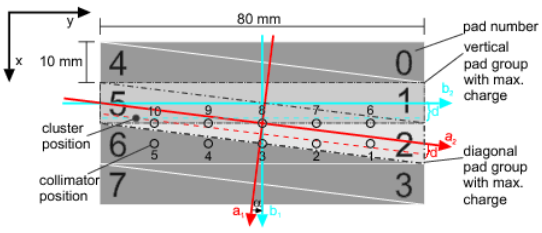

Figure 1: Sketch of the eight used pads, collimator positions 1 - 10 and wire positions

half a pad width and rotated by α relative to a. The PR and the energy resolution (FWHM/Energy) has been examined using a collimated ^{238}Pu (20.2 keV photons) and an ^{55}Fe (5.9 keV photons) source at 10 collimator positions. The energy resolution of the prototype is 26.5 $\pm$ 4.9% for the ^{55}Fe source and 21.7 $\pm$ 5.5% for the ^{238}Pu source. The position resolution of the real-size prototype cannot be determined by a source measurement of one single prototype due to the unknown absolute position of the initial photon. The PR is correlated with the deviation of the reconstructed coordinate from the collimator coordinate and the deviation of the measured collimator diameter from the reconstructed diameter. The increasing deviation for collimator position

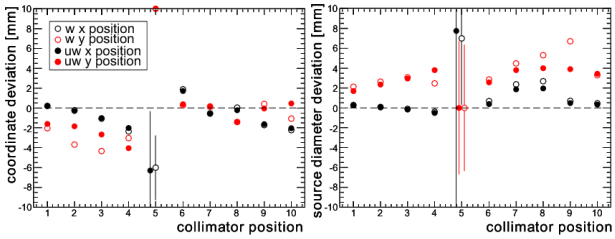

Figure 2: Reconstructed position spectra are fitted to a Gaussian distribution to determine collimator position (left) and diameter (right).

3, 4, and 5 is due to the small number of pads used for this measurement. Therefore, data efficiency (ratio of reconstructed events to all measured events) decreases and only events inducing maximum charge on pad two or five can be reconstructed. The reconstructed x-coordinates and collimator diameter show a good agreement with the expected values for all reconstruction methods (see Fig. 2). The reconstructed y-coordinates and collimator diameter deviate from the theoretical values because of the diagonal shift generated by the non-gaussian shape of the PRF and the accumulation of reconstructed clusters next to the wire positions due to the electric field characteristic perpendicular to the wire direction. The absolute PR will be measured at a cosmics or test beam run using a silicon tracking detector, scheduled for 2010. The PR in y-direction of the real-size prototype is given by the wire distance divided by $\sqrt{12}$ because the measured clusters are located in the avalanche region volume surrounding the anode wires. Thus, other pad and chamber geometry options have to be checked.

References

[1] M. Klein-Bösing et al., "Position resolution of a high efficiency transition radiation detector for high counting rate environments", Nucl. Instr. Meth. Phys. Res. A 585 (2008) 83-87

TR-Efficiency Studies for the CBM Transition Radiation Detector

P. Reichelt*[1], H. Appelshäuser[1], and M. Hartig[1]
[1]Institut für Kernphysik, Goethe-Universtität, Frankfurt am Main, Germany

In the CBM experiment at FAIR, a Transition Radiation Detector (TRD) is foreseen for tracking and electron/pion discrimination. A thin gas volume without drift region is considered in order to have sufficiently fast readout for the intended high collision rates. This however compromises the TR-photon absorption efficiency, which is essential for electron identification. In this report, we discuss an approach of increasing the yield of TR-photons by selecting suitable materials for the readout pads of the detector, from which photons can be re-emitted.

Measurement of TR-photons

When electrons pass through the radiator of a TRD, transition radiation photons can be produced and emitted in forward direction, thus entering the gas volume of the detector. The probability of such photons being absorbed depends on the mass attenuation coefficient of the corresponding material and its density and thickness. The remaining photons reach the readout structure of the detector, which is typically coated with copper. During tests with ALICE-TRD chambers [1] it was found that a portion of these photons causes ionization of the copper. The subsequent emission of a secondary photon into the gas volume contributes to the TR-signal. In this work we tried to optimize this effect in order to enhance the measured TR energy.

Figure 1 shows the simulated energy distribution of detected photons using Xenon gas[1] and a 5 μm copper coating. The energy of directly absorbed photons is $\mathrm{E_{direct}} = 38.8\ \%$ of the total produced TR-spectrum and the energy from secondary photons is $\mathrm{E_{pads}} = 3.3\ \%$. To compare the portion of $\mathrm{E_{pads}}$ for different materials, thicknesses close to a radiation length of $10^{-3}X_0$ have been used in the simulation, see Table 1. The last columns show the results for two different TR-spectra as produced by electrons with 2 and 10 GeV/c. In both cases copper is best. Heavier elements seem to be more efficient for higher electron momenta. Elements with significantly different Z do not have their K-lines in the energy range of the TR-spectrum and therefore have not been considered.

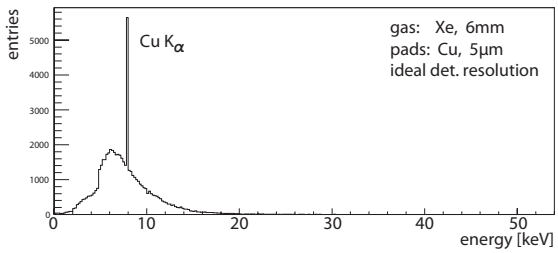

Figure 1: Simulation of a TR-spectrum as measured with a TRD using copper readout pads.

Element	Thickness	$\mathrm{E_{pads}}$ (2 Gev/c)	$\mathrm{E_{pads}}$ (10 Gev/c)
Cr ($Z = 24$)	22 μm	3.4 %	2.3 %
Fe ($Z = 26$)	18 μm	4.3 %	3.3 %
Cu ($Z = 29$)	15 μm	4.4 %	4.0 %
Ga ($Z = 31$)	25 μm	4.0 %	3.9 %
Rb ($Z = 37$)	90 μm	1.8 %	2.3 %

Table 1: Contribution of secondary photons for different materials and electron momenta.

The photon yield can still be improved by increasing the thickness of copper and we found that it saturates at $\mathrm{E_{pads}} = 4.7\ \%$ when implementing a 20 μm layer.

Multiple layers

Another way to enhance the number of secondary photons is to arrange layers of the above materials such that the K-line energies and mass attenuation coefficients reduce the transmission of photons into deeper layers. Figure 2 shows the resulting photon yield of such an arrangement which is higher than the exponential distribution of a single material. However, the photons from iron and chromium are less energetic and reduce the benefit so that practically a single copper layer proves to be the most efficient coating.

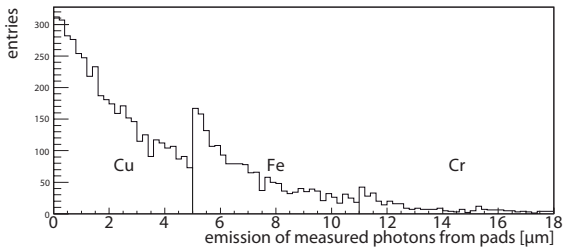

Figure 2: Origin of secondary photons (0 = pad surface).

References

[1] P. Reichelt: *Bestimmung der Gasverstärkung der ALICE-TRD-Auslesekammern*. Bachelor Thesis Goethe-Universität Frankfurt (2008).

* preichelt@ikf.uni-frankfurt.de
[1]Data reported here are based on a thickness of 6 mm for the gas layer.

Research and development of fast position sensitive gas detectors for CBM

S. Chernenko[1], G. Cheremukhina[1], S. Chepurnov[1], S. Razin[1], Yu. Zanevsky[1], and V. Zryuev[1]
[1]JINR, Dubna, Russia

R&D for fast position sensitive gas detectors is being performed at JINR for the CBM project. Several MWPC and GEM detectors with a sensitive area of appr. $10 \times 10\ cm^2$ were constructed and tested at laboratory conditions and with beam in order to study rate capability, position resolution and operational stability.

Two identical MWPC chambers were tested in collaboration with GSI, JINR, NIPNE and Münster University in a testbeam at SIS-18 [2, 3]. These MWPCs had a small enough drift gap in order to reach rates of up to several hundreds kHz per cm^2. They were of 9 mm thickness (3 mm drift gap and 3 mm anode-cathode distance), with anode wires of 20 μm diameter and a pitch of 2 mm. For an efficient absorption of TR-photons a counting gas mixture of $Xe - CO_2(85 : 15)$ was used. The signals induced on 2 rows of 16 pads of $5 \times 20\ mm^2$ were amplified with a 16-channel ASIC preamplifier/shaper [1] and sampled with a 25 MHz ADC.

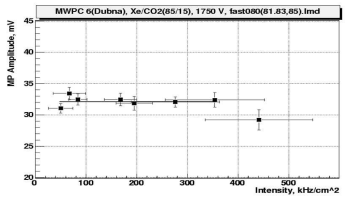

Figure 1: Rate dependence of the average signal (MWPC).

Fig.1 clearly shows that this MWPC experiences practically no degradation of the signal amplitudes up to $\sim 400\ kHz/cm^2$. The amplification factor of the MWPC was $< 10^4$. Taking into account the high rate capability, high spatial resolution and good operational stability we can consider this detector as candidate for the TRD CBM even in the innermost high rate region.

Furthermore, a 3-stage GEM detector with 2D readout was constructed and tested at laboratory conditions at JINR (Fig.2, left).

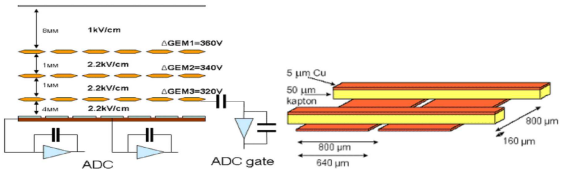

Figure 2: Schematic view of a 3-stage GEM detector (left) with 2D readout PCB (right) [4].

The detector has been tested with a gas mixture of $Ar/CH_4(85 : 15)$. A 2D PCB with strips and an active area of $10 \times 10\ cm^2$ was used for readout (Fig.2, right).

Connectors for FEE were placed on the back side of the PCB. The total number of FEE channels using the ASIC described in Ref. [1] for readout were 256. X-ray tests were performed using a collimated Fe^{55} source. Fig.3 (left) presents the measured energy resolution of the detector of $7,6\%$. The amplification factor was about 10^4.

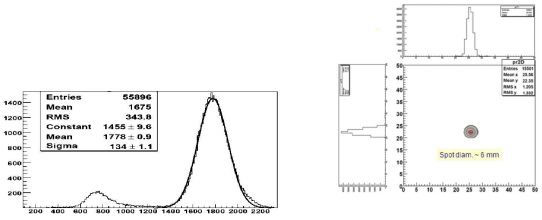

Figure 3: Energy resolution of the 3 stage GEM detector (left). Two dimensional plot of the Fe^{55} spot obtained with the 3 stage GEM detector (right).

An image of the Fe^{55} spot obtained with this detector is shown in Fig.3, right [5].

The described GEM detector was also tested with FEE based on the n-XYTER chip (PCB RevC). The obtained spatial resolution is shown in Fig.4 and corresponds to $\sim 140\ \mu$m(X) and $\sim 120\ \mu$m (Y).

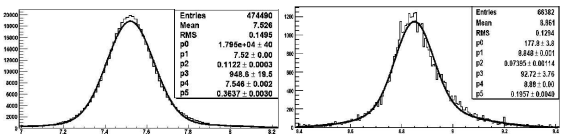

Figure 4: Spatial resolution of X (left) and Y (right) coordinates of the GEM detector, n-XYter readout.

We would like to express our gratitude for help to A. Andronic, V. Babkin, P. Braun- Munzinger, C. Garabatos, V. Golovatyuk, M. Petrovici, M. Petris, C. Schmidt, P. Senger, F.Uhlig, H. Wessels.

References

[1] H.K. Soltveit et al., GSI Annual Report 2005, p72.

[2] A. Andronic et al., INSTRUMENTS-METHODS 37, GSI Annual Report, 2006.

[3] M. Petrovici et al., FAIR-EXPERIMENTS 13, GSI Annual Report 2006.

[4] V. Zryuev, CBM-Russia Meeting, Dubna May 2009.

[5] Yu. Zanevsky, CBM Collaboration Meeting, GSI March 2009.

Development of an improved TRD layout with detailed pad design

D. Emschermann[1], E. Belolaptikova[2], C. Bergmann[1], C. Höhne[3], and F. Uhlig[3]
[1]IKP, Münster, Germany; [2]IKF, Frankfurt am Main, Germany; [3]GSI, Darmstadt, Germany

The geometry of the Transition Radiation Detector (TRD) was updated in CbmRoot, the CBM Simulation and Analysis Framework. It is based on the previous Jul09 geometry and therefore keeps the detector dimensions and outline. The TRD in CbmRoot consists of 3 detector stations, see Figure 3, each composed of 4 layers. The geometry update implements a realistic number of channels introducing a variable pad size across the different detector chambers. A total of 1256832 channels add up to 1100m^2 detector surface [1]. 81194 16-channel ASICs are required to readout the TRD.

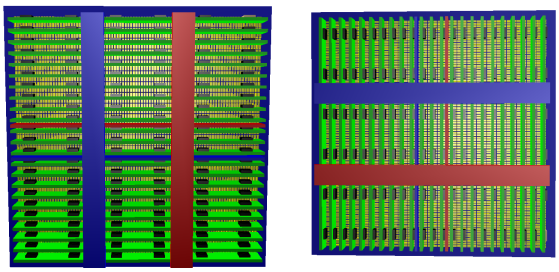

Figure 1: A TRD chamber in layer 1 (left) and rotated by 90 degree in layer 2 (right).

The detector surface is covered by Multi Wire Proportional Chambers (MWPCs) with a quadratic footprint. The cathode pad plane of each chamber features rectangular pads, providing a sufficient position resolution along one dimension. In a given TRD layer, all pads in the detector chambers share a common orientation, the long axis of the pad is positioned either vertically or horizontally for odd or even layers respectively. The change of pad orientation is achieved by simple rotation of the detector chambers by 90 degrees around the center of the chamber, see Figure 1. The combination of the orthogonal coordinates determined in two adjacent detector layers allows to determine the charged particle track position in the detector plane.

The size of the rectangular pads is increasing with growing radial distance from the beam pipe. It is scaled in such way to not exceed a maximum hit rate of roughly 100 kHz per pad, see Figure 3. Due to space constraints on the detectors with the highest channel density, the front-end boards on the chamber backside will have to be mounted in upright orientation, see Figure 2.

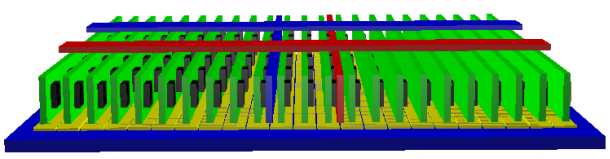

Figure 2: Front-end boards arranged on the backside of the TRD chamber with highest channel density.

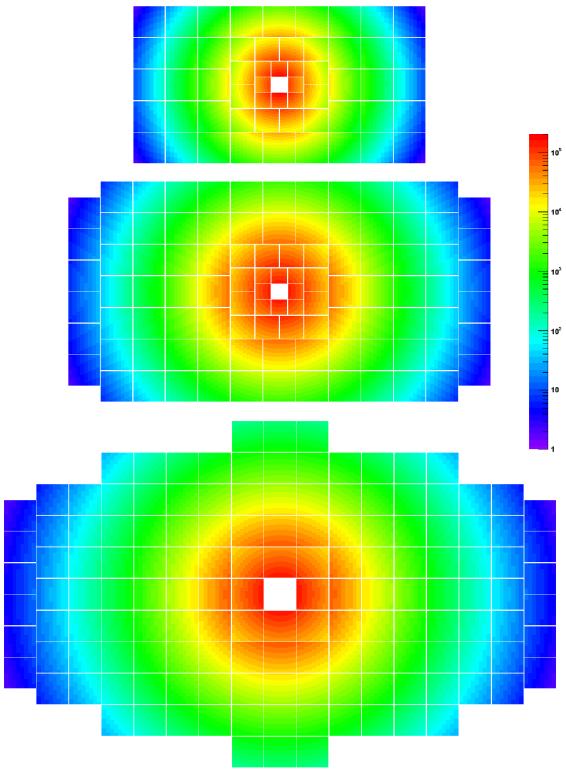

Figure 3: Hit distribution per pad and second for TRD stations 1,2 and 3 (from top to bottom), chambers with horizontal orientation of pads.

The next iteration of the TRD geometry will include the following improvements: A fixed pad with of 5mm in all chambers resulting in a fixed chip-to-chip distance on the front-end boards. The pad size will then be scaled by variation of the pad length. In addition the aggregation of readout uplinks to chambers will be optimised.

References

[1] D. Emschermann, "TRD geometry in CbmRoot", CBM Wiki, 2009, http://cbm-wiki.gsi.de/cgi-bin/viewauth/CbmRoot/CbmRootTrdGeometry.

Development of ceramics RPC for high rate capability timing detector application

L. Naumann[1], R. Kotte[1], D. Stach[1], and J. Wüstenfeld[1]
[1]FZ Dresden-Rossendorf, Germany

For the most forward kinematic region of the CBM experiment the usage of timing Resitive Plate Chambers (RPCs) with high rate capability is required. Prototype timing RPCs have been developed at Forschungszentrum Dresden-Rossendorf (FZD). Electrodes with a volume resistivity of about $10^9\,\Omega$cm are preferred for high rate capability purposes. Special ceramics composites have been developed and processed. A prototype with dimensions of the ceramics electrodes of $10\times10\,\mathrm{cm}^2$ has been exposed at the electron accelerator ELBE at FZD with 32 MeV single-electron beam pulses. The flux of the primary beam is tunable from few electrons/s to 10^7 electrons/s. The exposed region amounts to about $10\,\mathrm{cm}^2$. A careful analysis of the results allows a continuous improvement of the ceramics RPC properties. During an exposition in September 2009 it appeared that the ceramics RPC shows an all-time high rate capability for resistive plate counters. The working characteristics for the new ceramics RPC is plotted in fig. 1. The efficiency of the four-gap device with 300μm gas gap width amounts to 95 % for fluxes up to $5{\cdot}10^5\ \mathrm{s}^{-1}\mathrm{cm}^{-2}$ and has been compared in fig. 2 with float glass [1] as well as semiconductive glass RPCs [2]. Fig. 3 shows that the time resolution is independent for fluxes up to $10^5\ \mathrm{s}^{-1}\mathrm{cm}^{-2}$ and amounts to about 100 ps.

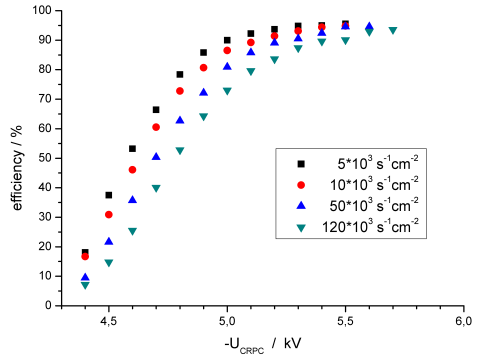

Figure 1: Working characterisics fot the ceramics RPC in dependence on the electron flux.

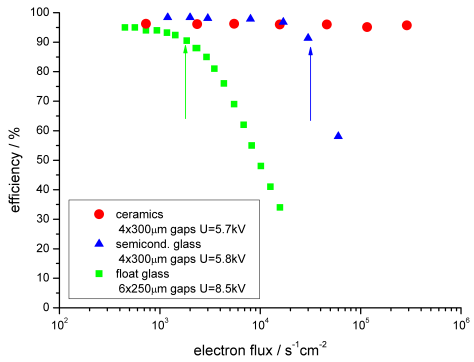

Figure 2: Efficiency of RPCs with float glass, semiconductive glass and ceramics composite electrodes in dependence on the electron flux. The rate cabability for the ceramics exceeds the float glas by more than two orders of magnitude.

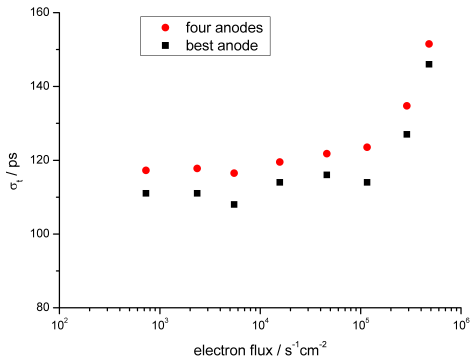

Figure 3: Time resolution of the ceramics RPC in dependence on the electron flux.

References

[1] R. Kotte et al., Nucl. Instr. and Meth. A564 (2006) 155.

[2] V. Ammosov et al., Nucl. Instr. and Meth. A576 (2007) 331.

A prototype of high rate MRPC for CBM-TOF

Y. Wang[1], J. Wang[1], X. Zhu[1], Y. Li[1], J. Cheng[1], N. Herrmann[2], I. Deppner[2], Y. Zhang[2], P. Loizeau[2], P. Senger[3], and D. Gonzalez-Diaz[3]

[1]Tsinghua University, China; [2]University of Heidelberg, Germany; [3]GSI Darmstadt, Germany

Multi-gap Resistive Plate Chambers (MRPCs) are planar gaseous detectors made with resistive electrodes. Such detectors have a good time resolution, a high efficiency and a relatively low cost. These excellent characteristics make MRPCs favorite detectors for high-granularity large-area time of flight (TOF) systems in modern nuclear and particle physics experiments, such as STAR, ALICE, FOPI, HADES and HARP [1]. The TOF wall of CBM, used for hadron identification, is proposed to be assembled with MRPCs [2, 3]. However, new materials should be investigated in order to adapt MRPCs to the high-rate environment foreseen, with fluxes up to 20 kHz/cm2. The use of electrodes made of low resistivity glass is an inspiring way of improving the MRPC rate capability. A kind of low resistive glass (with bulk resistivity of about 10^{10} Ωcm) has been developed to assemble a high rate MRPC prototype. Presently, the glass biggest dimension is 30cm*30cm, with 0.7mm thickness. 50cm*50cm glass is being developed to fit to the outer part of the wall.

Fig. 1 shows the structure of the high rate MRPC. It is mirrored and consists of 10 gaps. The gap width is 0.22mm. The beam test was performed with 2.5 GeV protons at GSI-Darmstadt. The prototype shows a promising performance: efficiencies above 90 % and time resolutions below 90 ps were obtained for a particle flux up to 25 kHz/cm^2, as is shown in Figs 2 and 3. When the particle flux increases every 5 kHz/cm2, the efficiency decreases by 1 % and the time resolution deteriorates by 4 ps. All of these performances can meet the requirement of CBM-TOF.

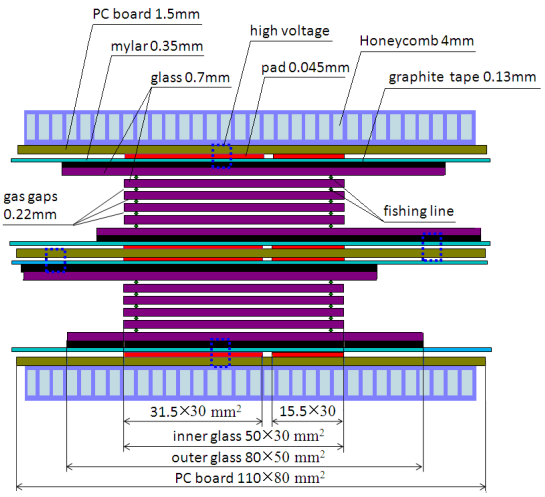

Figure 1: Structure of high rate pad readout MRPC

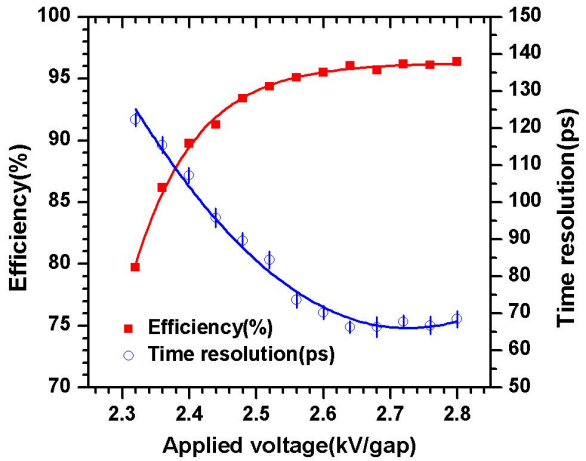

Figure 2: Efficiency and time resolution as a function of high voltage at a rate of about 3 kHz/cm3

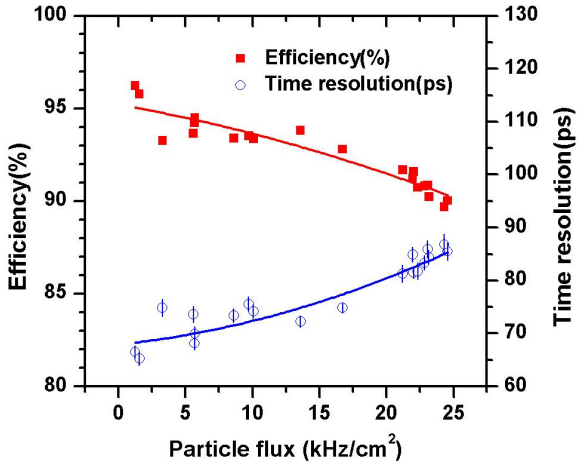

Figure 3: Efficiency and time resolution as a function of particle flux at an applied voltage of 2.6 kV/gap

References

[1] A. Akindikov *et al.*, Nucl. Instr. Meth. Phys. Res. **A 602** (2009) 709

[2] L. Lopes et al., Nucl. Instr. Meth. Phys. Res. **A 533** (2004) 69

[3] CBM collaboration. Compressed Baryonic Matter Experiment-Technical status report. January 2005

Performance of Long-strip MRPC for CBM-TOF

Y. Sun[1], C. Li[1], Z. Tang[1], and L. Xu[1]
[1]USTC, Hefei, China

The CBM-TOF wall will be used for Hadron identification with accurate Time-of-Flight measurement and large area coverage. Multi-gap Resistive Plate Chamber (MRPC), which has excellent performance and relatively low cost per channel, is a good candidate for CBM-TOF. Concerning the outer part of the TOF wall, long-strip pattern (with 25 cm, 50 cm and 100 cm strip length, respectively) is enough to satisfy the experimental multiplicity requirement.

In the long-strip design of MRPC, the cross-talk is critical to the detector performance. A test was carried out between August and September 2009 at GSI to test the performance of Long-strip MRPC prototypes.

The MRPC module has ten gas gaps of 250 μm, arranged in two stacks. Normal floating glass of 700 μm thickness is used as resistive plate. The High-Voltage (HV) electrodes, on the outer surface of each glass stack, are made by Licron spray with surface resistivity of ~40 MΩ/□. The readout structure of the prototype is schematically shown in Figure 1. The readout strips are 50 cm long, 2.5 cm wide and with 0.6cm gaps between them. The signals are read out from both ends of each strip.

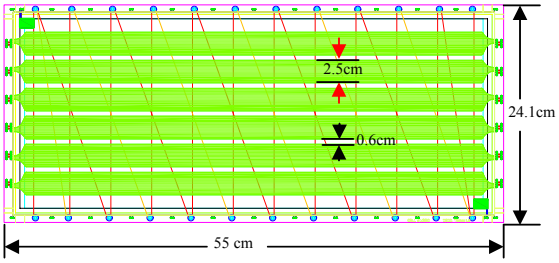

Figure 1: Readout structure of the Long-strip MRPC.

The test was performed at GSI in Cave-B behind the FOPI experiment, using the secondaries of a 3.5 GeV/*c* proton beam interacting with a lead target. The trigger area of 4 cm × 2 cm (along and across the MRPC strips, respectively) is defined by two scintillators, which are read out from both ends by 4 PMTs offering the reference time with ~63 ps σ time resolution.

The efficiency and time resolution of the MRPC at different HV is shown in Figure 2. At working voltage of around ±7 kV, a time resolution of 60 ps σ can be achieved with a detection efficiency over 97%.

In the cross-strip scanning test, the efficiency of each strip is shown in Figure 3. The gentle incline at the strip edge mainly comes from the 2 cm wide trigger width. When triggered on the centre of a strip (strip 4 in this case), the efficiency of nearby strip is mainly from cross-talk contribution. The test result of 3% gives the upper limit of the cross-talk probability. The real cross-talk should be less than this value because 1/3 of these signals have a valid charge recorded, indicating that they possibly come from charge sharing with the neighbour strip or double-hits within the same primary collision.

At the same time, the efficiency drop between strips is observed to be less than 1%.

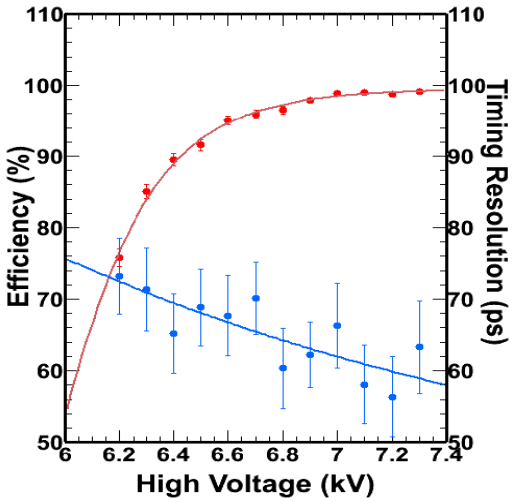

Figure 2: The efficiency and time resolution vs. the HV.

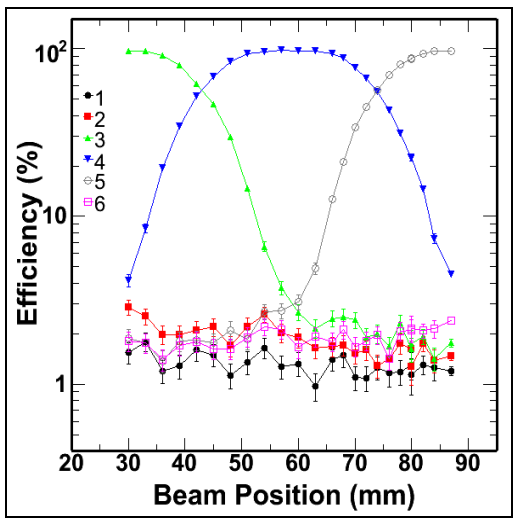

Figure 3: The efficiency of each strip at different trigger positions.

The data will be further analysed with the silicon tracking system which is available at the late stage of the test in order to reconstruct the intrinsic strip-profile.

Toward a high granularity, high counting rate, differential readout timing RPC

M. Petrovici[1], V. Simion[1], M. Petriş[1], D. Bartoş[1], G. Caragheorgheopol[1], I. Deppner[2], N. Herrmann[2], M. Kiss[2], P. Loizeau[2], Y. Zhang[2], and M.C.S. Williams[3]

[1]NIPNE, Bucharest, Romania; [2]Physikalisches Institut der Universitaet Heidelberg; [3]CERN, Geneva

The CBM experiment will be confronted with the selection of rare probes in a high multiplicity environment with up to 1000 produced charged particles, at collision rates up to 10^7 events/s. Hadron identification in such a limiting environment is a real challenge and requires intensive R&D activity for developing high resolution and high granularity timing detectors at affordable cost. The inner part of the TOF covers 50-100 mrad around the beam axis with an estimated flux densities of charged particles up to 20 kHz/cm^2. Therefore, a high counting rate and high granularity detector is required for this particular region of the TOF wall. The differential strip readout resistive plate counter (RPC) architecture proposed by us [1, 2], based on a low resistivity glass ($\sim 10^{10}$ Ωcm) showed a very good behaviour of the time resolution as a function of counting rate up to 16 kHz/cm^2.

A new differential configuration based on a high granularity strip structure readout electrodes is reported here. The counter has a symmetrical structure of 2 x 5 gaps of 140 μm size each, with the resistive electrodes made from commercial float glass of 0.5 mm thickness ($\sim 10^{12}$ Ωcm resistivity). The readout electrodes have a strip structure (2.5 mm pitch, 1.1 mm width) with a strip length of 46 mm. The high voltage electrodes have the same strip structure as the readout. The active area is 46 x 180 mm^2 and is read out with 72 strips. The whole structure is housed in a gas tight rectangular aluminum box.

The counter was tested first with a ^{60}Co source using a high voltage of 1.98 kV/gap and a gas mixture (85% $C_2F_4H_2$, 10% SF_6 and 5% C_4H_{10} (isobutane)) flushed at normal pressure. Typical signals recorded without any amplification at both ends of a measured strip (anode - negative signal, cathode - positive signal) are presented in Fig.1. A good syncronization of the positive and negative signals at the two ends of the strip can be observed.

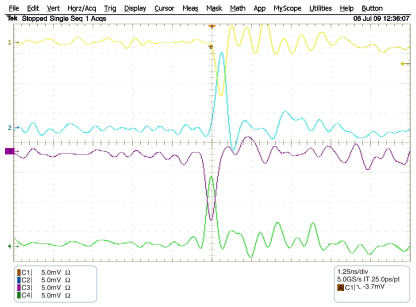

Figure 1:

A differential front-end electronics based on NINO ASIC chip [3], provided both the time and time-over-threshold information. The walk corrected data were used to calculate the RPC time performance. With a narrow condition of 3 cm in position along the strip, a cut out of the small amplitudes in the reference plastic scintilator and selecting large signals in RPC (large time over threshold) a time resolution of σ = 96 ps was obtained after subtracting quadratically the contribution of the reference counter measured in separate runs using 2 identical scintillators and phototubes.

The in-beam test has been performed at the SIS accelerator of GSI - Darmstadt in a joint measurement campaign of the CBM-TOF Collaboration using secondary particles produced by proton beam of 3.1 GeV/c on a Pb target. The number of strips fired in an event, respectively the cluster size, at 1.9 kV/gap applied high voltage, can be followed in Fig.2-left panel for one of the measured counters. The mean value of the distribution is 1.14. This very small

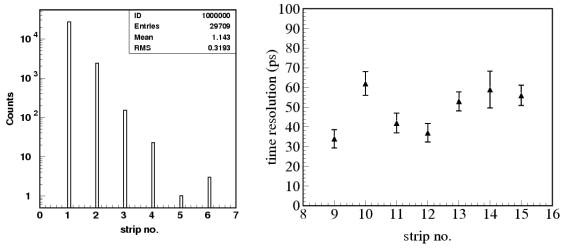

Figure 2:

value of the cluster size is a consequence of the gap size and the strip structure of the high voltage electrodes. The single counter time resolution for the measured strips can be seen in Fig.2 -right panel. The results open the perspective to built large area time-of-flight detectors with very good time resolution and a high granularity for high multiplicity environment. Detailed studies on efficiency and multi-hit performance are on the way.

References

[1] D. Bartoş et al. 2008 NSS/MIC, Vols. 1-9 Book Series: IEEE Nuclear Science Symposium - Conf. Rec. Pg: 1933-1935

[2] D. Bartoş et al., CBM Progress Report 2008(2009), 43

[3] F. Anghinolfi et al., Nucl. Instr. And Meth. A 533(2004), 183

Design and performance of a fully differential Multigap RPC

I. Deppner*[1], N. Herrmann[1], M. Ciobanu[2], D. Gonzales-Diaz[2], K.D. Hildenbrand[2], M. Kis[2], Y. Leifels[2], P.-A. Loizeau[1], and Y. Zhang[1]

[1]Physikalische Institut Uni. Heidelberg, Heidelberg, Germany; [2]GSI, Darmstadt, Germany

In the current design of the CBM experiment, hadron identification is based on the Time-of-Flight measurement provided by a wall of Multi-gap Resistive Plate Chambers (MRPC). Due to a lower rate the outer most part can be covered with float glass MRPCs in a multi-strip configuration.
In order to study a possible configuration of such systems, a prototype of a Multi-strip MRPC with fully differential readout was developed (see Fig.1). The active area of the

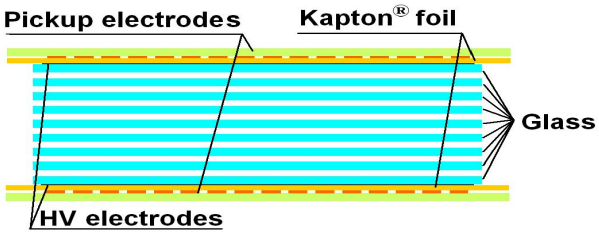

Figure 1: MRPC layout

prototype is 28 x 16.5 cm^2. Its active volume is subdivided by nine 0.55 mm thick float glass plates. The space between the glass plates is ensured by 220 μm thick fishing lines. The bottom and top plates are covered by conductive layers (surface resistivity 100 MΩ/cm^2) to form electrodes to which HV in the order of 11 $\pm$ 1 kV is applied, resulting in an electric field for operating conditions ranging from 120 - 130 kV/cm. The two outermost plates (PCB 4mm) serve as support for the MRPC and contain also the readout strips which have a width of 7 mm. The distance between the strips is with 3 mm relatively large and leads to an reduced cross talk. This strip configuration together with the total number of gaps was simulated to have an impedance of 100 Ω. A good impedance matching with the front-end electronics [1] is necessary to reduce signal reflections in the counter. Measurements with an reflectometer show a real impedance of about 80 Ω. Another advantage of the proposed strip configuration is that the strip width is comparable with the cluster size of an avalanche, which was shown to be approximately 7 mm at a field of 108 kV/cm [2]. Therefore charge sharing can only happen between two strips. Due to the totally symmetric layout of the counter the signal is fully differential which minimizes the common mode pickup noise in the preamplifier. For signal amplification and discrimination we use the so called PADI 2 [1] with time-over-threshold function. The LVDS timing output signals from PADI are fed into an expansion card for the high timing resolution system (TACQUILA) [3], which allows time over threshold functionality for TACQUILA.
The described setup was tested in August 2009 with a 3 GeV proton beam in cave B. Using the tracking information from silicon detectors the efficiency for different strips and different positions perpendicular to the strip (y-position) could be determined with accuracy of 1 mm (see fig. 2). The efficiency of each individual strip shows a plateau of 6 mm in the overlap region of the strip in the order of 95%. It drops slightly towards the side of the strip, but in the middle of the gap between the strips it still amounts to be about 80%. The total efficiency of the RPC is over all about 95%. In addition the average cluster size, i.e.

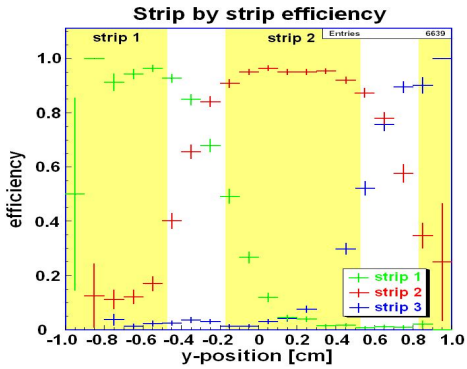

Figure 2: Strip by strip efficiency: the yellow area depict the position of the strips.

the number of neighboring strips that fire simultaneously, was determined. At 11 kV the cluster size was found to be 1.2 strips which means, $\sim$ 83% of all hits are single strip events. Three strip events were found with a probability of about 2% allowing to estimate the total cross talk in this configuration to below 3%.

References

[1] M. Ciobanu, N. Herrmann, K.D. Hildenbrand, M. Kis, A. Schüttauf, " PADI, a fast Preamplifier - Discriminator for Time-of-Flight measurements", IEEE NSS, Dresden, (2008), 2018-2024

[2] I. Deppner, N. Herrmann, R. Averbeck, C. Ciobanu1, K.D. Hildenbrand, T.I. Kang, M. Kis, Y. Leifels, K. Piasecki, A. Schüttauf, D. Gonzalez Diaz, and the FOPI Collaboration " Characterisation of FOPI narrow strip RPCs", CBM Progress Report 2008

[3] K. Koch, E. Badura, " High resolution double-hit timing and time over threshold measurement feasibility for the TACQUILA system", IEEE NSS,Honolulu, HI, (2007), Volume: 1, 320-321

* deppner@physi.uni-heidelberg.de

Progress in the simulation of Multi-strip RPCs

D. Gonzalez-Diaz[1], G. Kornakov[2] for the CBM-TOF group
[1]GSI, Darmstadt, Germany; [2]USC-LabCaF, Santiago, Spain.

Timing Resistive Plate Chambers in multi-strip configuration, pioneered by the FOPI experiment [1], are planned for covering the low-granularity part of the CBM-TOF wall. A recent experiment at GSI cave-B has shown that, with an adequate optimization of the strip-layout and readout, the multi-strip concept is sound in terms of timing and efficiency, and well suited for a multi-hit environment. The progress since previous discouraging attempts [2] has been made possible through a combined effort of detector design in conjunction with sophisticated simulations [3].

The newly developed RPC-simulation package is by now based on a (1+1+1) factorization of the original 3D problem. Signal formation (across the gas gap) is treated first; signal induction (across the strip) is calculated in a second step by using weighting field techniques. Finally, the propagation along the strip up to the amplifier is calculated by resorting to the HF-solver APLAC [4].

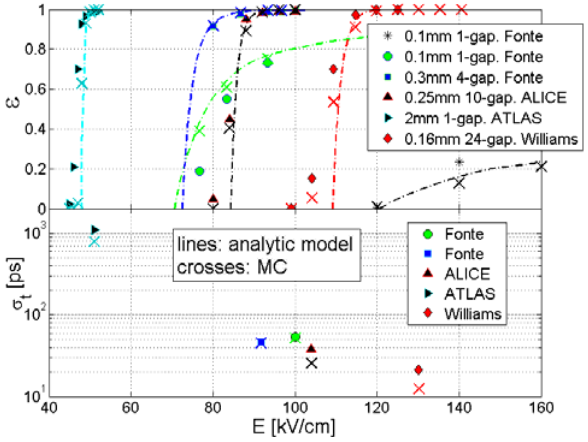

Figure 1: Efficiency and resolution for various RPCs.

We have made substantial progress in the first part of the problem (signal formation) during the last months: the simulation is based on a microscopic image of the avalanche, parameterized through a computationally-inexpensive algorithm and driven by recent measurements of the parameters of the electron swarm [5]. The results for efficiency and resolution are shown in Fig. 1 for wide-strips/pads of various remarkable world-wide efforts. Results from the simulation are shown (crosses) together with analytical formulas (dot-dashed lines), when available. The simulation relies at present on only one free parameter, a sort of shape-independent equivalent charge-threshold Q_{th}=10-100fC, not always known or available. This single quantity is used by detector developers to characterize the complex amplifier+discriminator response. This assumption seems to work, according to our simulations, with remarkable accuracy, despite Q_{th} being an 'effective' value.

With the signal generation under control it is possible to explore the multi-strip response by including the signal induction and propagation. Fig. 2 shows the most characteristic observable, the efficiency as a function of the transverse coordinate for a previous attempt [2] (left) and preliminary results from the recently developed prototypes in [6]. Although in both cases the transverse profile is dominated by a rather large width of the trigger system (2 cm), the shear cross-talk shows up as a flat background independent from the transverse coordinate, visible once the trigger position is far away from the strip under study: previously observed cross-talk at the level of 80-90% has been now reduced to much more respectable 1-3% levels.

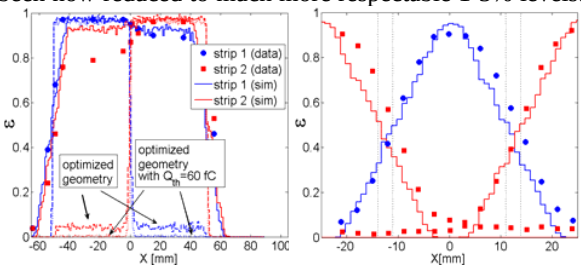

Figure 2: Efficiency vs trigger position across the strips for [2] (left) and for an optimized structure from [6] (right). Lines are the results from simulation.

Much progress has been done in the analytical understanding of cross-talk,, that is shown to be reducible to a 2-strip situation in many typical cases, characterized by 2 dominant modes (or propagation velocities) as:

$$I_{tr}(t)=\frac{T}{2}\frac{I_{v1}(t)+I_{v2}(t)}{2}+\frac{Z_m R_{in}}{(Z_c+R_{in})^2}\frac{I_{v2}(t)-I_{v1}(t)}{2}$$

$$I_{ct}(t)=\frac{Z_m R_{in}}{(Z_c+R_{in})^2}\frac{I_{v1}(t)+I_{v2}(t)}{2}+\frac{T}{2}\frac{I_{v2}(t)-I_{v1}(t)}{2}$$

References

[1] A. Schuettauf et al., NIM A 3(2009)679.
[2] A. Blanco et al., NIM A 485(2002)328.
[3] A. Berezutskiy et al, GSI report 2008, FAIR-EXP-23.
[4] http://web.awrcorp.com/Usa/Products/APLAC/
[5] E. Basurto et al., Proc. to 28th ICPIG, Prague, 2007.
[6] Y. Sun et al., also on this book.

e/π separation with calorimeter system

M. Prokudin[1], I. Korolko[1], and Yu. Zaitsev[1]
[1]ITEP, Moscow, Russia

Introduction

Initial estimation of hadron rejection factor for the CBM calorimeter system was performed using Monte-Carlo information from tracking system, ECAL and preshower. With this note we describe the developed algorithms and present our current results.

Method

The identification procedure for all reconstructed tracks starts from an attempt to find a local maximum of energy deposition in a 3×3 area around the hit cell. The track is considered as charged hadron if the distance between the track entry point and closest local maximum is greater than 1 calorimeter cell. Then we construct a 3×3 cluster around found local maximum and select the 2×2 subcluster with maximum energy deposition to minimise the energy contributions from neighbour particles.

The energy deposited in the 2×2 subcluster after calibration is called E_{calo}. The energy deposition for electrons (positrons) should be roughly equal to their momenta measured by tracking system (P_{track}), while for charged hadrons the ratio E_{calo}/P_{track} is less than unity (see Figure 1). We tune the cut value on this ratio to have 95% efficiency for electrons. The separation power of the cut is shown in Table 1. The cut is sensitive to the momentum of incoming particle due to the finite calorimeter resolution. Therefore we plan to upgrade the identification procedure with energy dependent cut on E_{calo}/P_{track}.

The electron identification with preshower is highly dependent on tracking precision. The deviation of particle impact point true position from the prediction of tracking system is ~ 2 cm. This is compatible with the size of smallest calorimeter cell (3 cm). The error in determination of cell hit by the track leads to a dramatic decrease in identification efficiency. Therefore we propose to use the maximum of two energy depositions: in preshower cell hit by the track and preshower cell on top of the calorimeter cell with maximum energy deposition. The procedure ensures better electron identification efficiency with only slight decrease in hadron descrimination. The rejection power of the cut on preshower energy deposition (tunned to have 95% efficiency for electrons) is shown in Table 1.

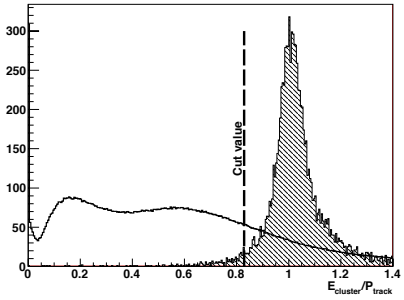

Figure 1: E_{calo}/P_{track} for electrons (hatched histogram) and pions (black line)

Finally we define shower shape as a ratio of energy deposited in the 2×2 subcluster to the energy deposition in a 3×3 cluster. The hadron showers are wider and this ratio could be used for electron identification. We use different cuts for each calorimeter section tuning the cut value to have 95% efficiency for electrons. The separation power of the cut together with all previous cuts is shown in Table 1. The cut on shower shape is highly sensitive to the calorimeter occupancy. In future we plan to tune the exact cut values separately for different colliding ions because of the high sensitivity to the energy contributions from neighbor tracks.

Results and conclusions

As is shown Table 1 the separation power of calorimeter system is highly dependent on the occupancy. It is as large as couple of hundreds for light colliding ions and drops down to dozens for Au ions while the efficiency for electrons is maintained at constant level of 86%. The described procedure still could be improved. The energy dependent cut on E_{calo}/P_{track} ratio will significantly increase the hadron rejection as well as individual tuning of shower shape cut for different colliding ions.

Table 1: Pion rejection factor

Cut name	Colliding system and calorimeter region					
	pC 30 GeV			AuAu 25 GeV		
	Inner	Middle	Outer	Inner	Middle	Outer
E_{calo}/P_{track}	43.7	20.4	10.6	6.7	4.2	2.9
E_{PS}	282.3	116.6	62.7	19.6	14.0	8.7
Shower shape	386.2	187.6	104.8	31.0	22.8	13.6

The superconducting dipole magnet for CBM

E.A. Matyushevskiy, P.G. Akishin, A.V. Alfeev, V.S. Alfeev, V.V. Borisov, V.V. Ivanov,
E.I. Litvinenko, A.I. Malakhov.
JINR, Dubna, Russia

The superconducting (SC) dipole magnet is an essential constituent of the planned CBM experiment. The magnet should host the target, the Micro-Vertex Detector (MVD), and the Silicon Tracking System (STS). It is located in the immediate proximity to the RICH detector. The magnetic fringe field in the volume of the RICH detector should not exceed a value of 250 Gs. A field integral of about 1.0 Tm is required over a distance of about 1 m. The angular acceptance of the magnet should cover 50° in vertical and 60° in horizontal direction. The magnet gap has to be large enough to permit the installation and maintenance of the STS (not less than 1.3x1.3 m²).

The conceptual design of the dipole magnet is presented in Fig. 1. The magnet is supplied with a yoke of magnetically soft iron with low carbon content. The top and bottom beams form the poles of the magnet.

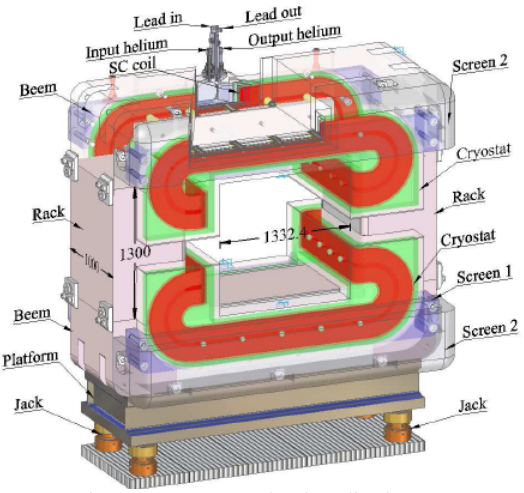

Figure 1: Superconducting dipole magnet

The "Cossack saddle" shape of the SC coils allows for minimization of the magnet length along the beam direction. The coils are covered with magnetic field clamps which reduce the field in the volume of the RICH photodetectors. The coils are produced from a cable with SC strings. The cross-section ratio of superconductor to copper is 1:6. The large copper content of the SC cable allows for overheating the cable up to 30 K during the evacuation of the energy stored in the magnet if the SC cable becomes normal conducting. The cryostat of the excitation coils (see fig. 2) includes a helium vessel, a nitric screen and a vacuum casing. The helium vessel is fastened in the vacuum casing on supports produced of fibrous and plastic materials. It is cooled by liquid helium.

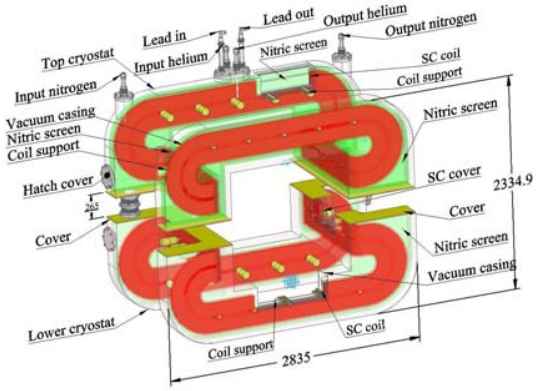

Figure 2: Cryostat of the excitation coils.

The thermal flow through the supports (36 pieces) amounts to 3.8 W, and the thermal losses through radiation account for 0.22 W. The nitric screen is cooled down to temperatures below 70K. The nitric screen is fixed on the helium volume's supports. The thermal losses by radiation are 35 W. Inspection plates and hatches of the vacuum casing provide access to the equipment inside. The evacuation of the casing is provided by oil-free vacuum pumps.

The upper cryostat is equipped with a feeder with two current leads (1.5 кА each) for input-output of the excitation current. The feeder has ports for incoming and outgoing liquid and gaseous helium. The pipelines and the elements of communications going to the helium vessel create thermal losses at the level of 1.8 W .

The calculation of the field has been performed with the computer codes RADIA and TOSCA demonstrating that a current of 1.0 kA is sufficient to create a field of 1.15 T. The field distribution along the Z-axis is presented in fig. 3. The field does not exceed 350 Gs in the photo-detectors plane of the RICH.

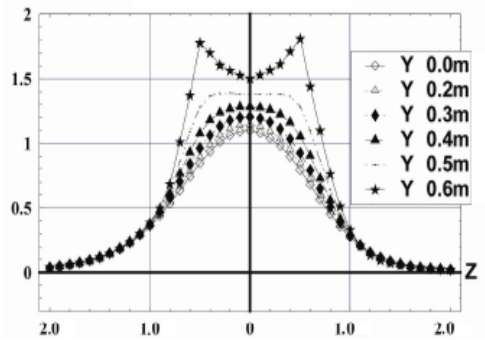

Figure 3: Magnetic field distribution calculated by RADIA.

Prototype readout ASIC for silicon strip detectors readout using Time-Over-Threshold method.

K. Kasinski and R. Szczygiel
AGH University of Science and Technology, Krakow, Poland

Abstract: The Time-Over-Threshold scheme is proposed for the CBM STS silicon strip detectors readout. A prototype ToT readout chip was designed in the CMOS UMC 180 nm technology. This report summerizes the architecture of the chip and first measurement results.

ASIC architecture

The ASIC contains 30 channels (+ one test channel), each comprising charge sensitive amplifier with two switchable linear discharge feedbacks [1] for two detector polarities, comparator and trimming DAC for comparator offset voltage correction. The outputs of the channels are multiplexed into a single output buffer. Simplified scheme of a single channel is presented in Fig. 1. Additionally the

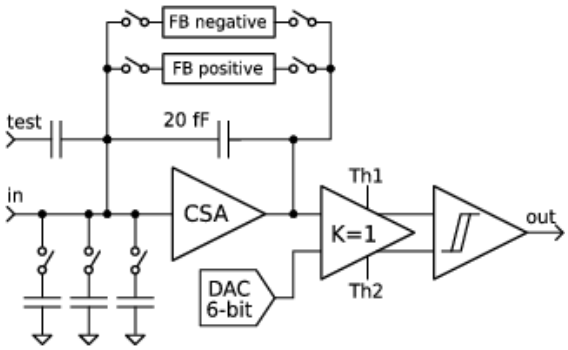

Figure 1: Simplified single channel scheme.

chip includes test pulse injection circuits and test capacitors for simulating the detector capacitance. The ASIC size is 1.52 x 3.24 mm^2. The photo of the ASIC is presented in Fig. 2.

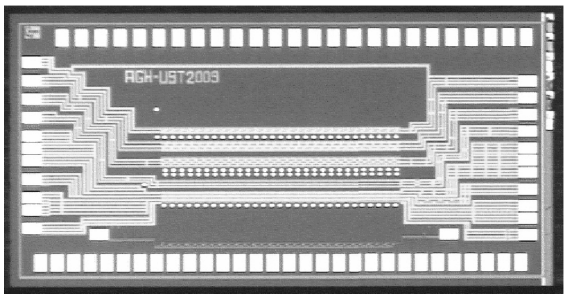

Figure 2: Photo of the ASIC.

Test setup and first measurement results

The test board was designed based on Xilinx Spartan 3 FPGA. The board was controlled via NI SBRIO FPGA + Real Time Card and NI USB-6259 DAQ card. The setup allows reading the output data with 20 ns resolution. The tests were performed using external pulse generator. Initial tests with the ASIC connected to a 2 cm AC-coupled p-type detector and Mo X-ray source are in progress. Fig. 3 presents the signals probed at the output of the CSA for different input pulse amplitudes. Fig. 4 shows an example of output pulse width vs input charge characteristics for a single channel.

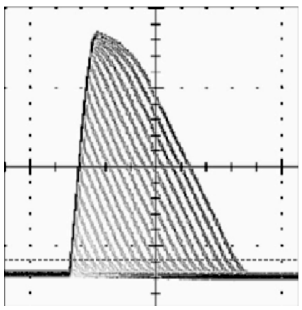

Figure 3: CSA output for different input signals amplitudes.

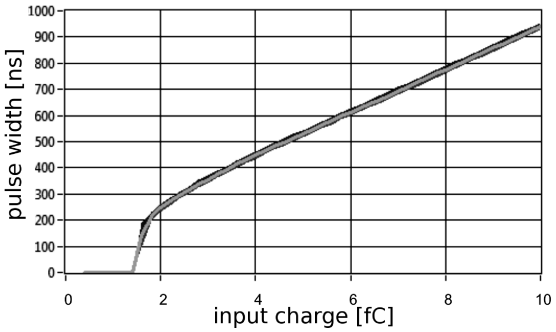

Figure 4: Example of time-over-threshold characteristics of a single channel.

References

[1] Nucl. Instr. and Meth. A 359 (3) (1997) 313

Development of the derandomizing architecture for CBM-STS

E. Atkin, Yu. Bocharov, V. Butuzov, A. Klyuev, D.Osipov, D.Semenov, and A. Simakov
National Research Nuclear University "MEPhI", Moscow, Russia

Currently MEPhI is engaged in developing a derandomizing readout electronics for the CBM-STS. The core of this detector electronics is expected to be formed by a 128-channel mixed-signal ASIC, implemented by the UMC CMOS 0.18μm technology. Its structure is based on using a data-driven high-speed analog signal switching circuit, the validity of which was confirmed earlier by the prototype solution 4 to 2 [see CBM Progress report 2006, p. 52.].

The basic task of 2009 was to develop building blocks for the second prototype version of the ASIC, wherein it is planned to implement a high-speed analog switching circuit of the 128 to 16 structure, having a more sophisticated arbitration logic and supplemented by both an input analog part and an output ADC. The principal points of the new version specification are the presence of a 9-bit signal digitalization at output and low power consumption within 2 mW/channel at a maximum average channel hit-rate not less then 150 kHz.

The analog part includes a DC CSA with a detector leakage current compensation circuit and a CR-RC shaper (100 ns peaking time), both designed according the STS specs. The derandomizing part consists of asymmetrical analog switch array and arbitration logic. The basic goals were to reduce the total power consumption and minimize the area, occupied on chip. That is achieved by splitting the channel in two parts: analog read-out chain and processing mixed-signal one. The processing chains, as distinct from the read-out ones, are essentially more power consuming. This is acceptable since the number of processing chains (16) is far less than that of the read-out ones (128).

Taking into account the incomplete input channel occupancy, the use of an analog derandomizer permits to minimize the number of data processing channels. The quantitative characteristic in this case is being the derandomization factor D = M / N, where M number of data read-out channels, N number of data processing channels. From the viewpoint of reducing the number of architecture blocks and using an on-line data processing, the system is designed as an unbuffered one. The derandomization factor is therefore chosen such as to make the signal loss not exceed the specified error probability at a known maximal average hit-rate of the read-out channel.

The technique of choosing the derandomization factor may be based on analyzing the probability of a simultaneous occupation of a number of processing channels, taking into account the maximum average hit-rate. Fig. 1 presents the results of analysis for maximum average hit-rate (f) in a channel from 150 to 1200 kHz at 128 read-out channels (P probability of a simultaneous occupation of N channels).

A developed low-power ADC block has a resolution of

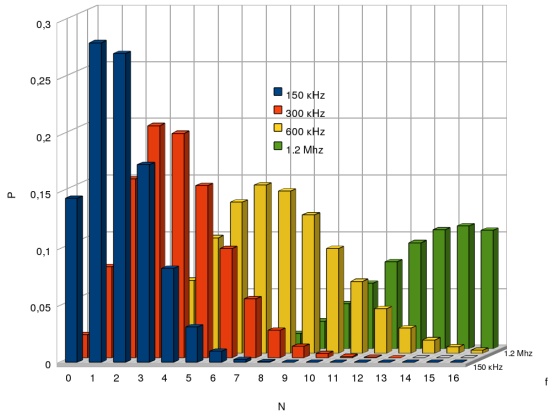

Figure 1: Probability of a simultaneous occupation of N channels

9 bit and a sample rate of 20 MSPS. It is based on a conventional pipelined architecture, but with the use of special techniques of reducing power consumption. The dramatic decrease of power dissipation was achieved by sharing the amplifiers and comparators by the adjacent stages of ADC. By using this method, the number of amplifiers has been reduced from eight to four, and the number of comparators from 17 to 11, compared with the classical pipelined architecture. In addition, all of the comparators have a dynamic structure. Pipelined architecture allows additional reduction of consumption by reducing the resolution and stage scaling.

Simulation results in ADC power dissipation of 9 mW at a 1.8 V supply and 20 MSPS. For the 400 KHz input signal ENOB is 7.9. ADC area is 0.55 sq. mm (Fig.2).

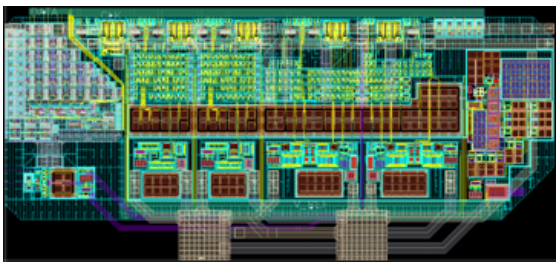

Figure 2: ADC layout

At the prototyping stage the number of readout chains was reduced down to 24 and the number of the output ADC down to 1. That provides a cost-effective approach in the technological run. The latter is planned to be in the "double mini@sic" form (chip dimensions 3240x1525 sq. μm) during the first half of 2010.

A Self-triggered Amplifier/Digitizer Chip for CBM

T. Armbruster*, P. Fischer†, and I. Peric
University of Heidelberg, Germany

Introduction

Different approaches for the readout of the various subdetectors in CBM are currently under investigation. For the charge readout of the 1.2 million TRD channels a self-triggered mixed-signal ASIC is being designed in a CMOS 180 nm technology. The chip, having 32-64 channels, will amplify, digitize and digitally process the incoming charge pulses with hit rates up to 100 kHz per pad. For each hit, a complete digital snap-shot of the internally produced pulse, together with a 12 bit time-stamp, will be sent out, producing data rates of about 1 Gbit/s per chip. An additional feature will be an on-chip ion tail cancellation and baseline correction filter, especially needed due to the wire chamber characteristics.

This report summarizes the status of the TRD readout electronic by describing the planned chip architecture and the measurement results so far achieved with the latest test-chip iteration.

Chip Architecture

In Fig. 1 the preliminary chip architecture is sketched. The analog part (blue) mainly consists of a preamplifier, a second order shaper and a pipeline ADC. The digital processing chain (yellow) begins with an IIR filter and ends at a FIFO buffer. In between some hit detection and event building logic will generate the digital hit packages containing the pulse data and some meta information. A data extraction unit could optionally also be integrated into the data chain, as it is shown in the diagram. To interconnect the channels and the output serializer (not shown), a token ring network will act as a balanced arbiter.

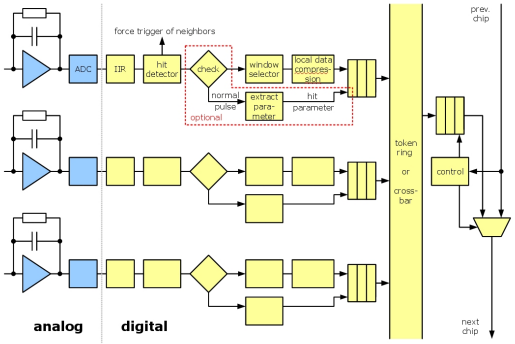

Figure 1: Preliminary block diagram

Prototype Results

The latest test-chip [1] has 26 analog preamplifier/shaper channels (each including a discriminator for test purpose) and, moreover, 8 current-mode pipeline ADCs that are connected to some of the amplifier channels. Threshold scans have shown the preamplifiers having only 800 e ENC for 30 pF detector capacitances at pulse peaking-times of 100 ns while consuming 3.6 mW. The pipeline ADCs have been successfully tested up to sample rates of 24 MSamples/s and show an effective resolution of 7.5 bit. The power consumption per ADC is only 4.6 mW.

The whole system from preamp to ADC, including some digital on-chip data encoding, has also shown good results. By connecting a shaper output to an ADC, analog hit pulses could be recorded. For Fig. 2 1000 digitized pulses were read out, proving the proper function of the complete mixed-signal channel including the synthesized on-chip control and decoding logic.

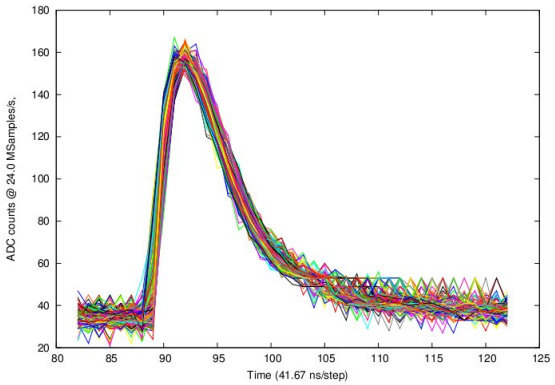

Figure 2: 1000 digitized hit pulses

Future Work

Since most of the analog part - up to the ADC - has reached a proper development status, the main focus of investigation is now on the digital chain and on the inter-channel and -chip connection methodology. First simulations of the IIR ion tail cancellation filter have delivered promising results. Nevertheless, another analog test-chip iteration has been submitted in November 2009 for testing several improvements in design and layout. Measurement results will probably be presented at the 15th CBM collaboration meeting.

References

[1] T. Armbruster, P. Fischer and I. Peric, "A Self Triggered Amplifier/Digitizer Chip for CBM", TWEPP'09 Proceedings, 16 November 2009, Paris, p. 457, CERN-2009-006.

* tim.armbruster@ziti.uni-heidelberg.de
† peter.fischer@ziti.uni-heidelberg.de

Front End Electronics for High Counting Rate TRD Using a Prototype ASIC

V.Catanescu[1], D.Bartos[1], and Gh. Caragheorgheopol[1]
[1]National Institute for Physics and Nuclear Engineering, Bucharest, Romania

A dedicated ASIC for a high counting rate transition radiation detector (HCR-TRD) [1], developed at NIPNE, was tested stand alone and using signals delivered by a TRD prototype.

ASIC specifications

The ASIC chip was designed in AMS CMOS 0.35 µm N-well technology. It has 8 identical analog channels, each with two outputs: one fast semi-Gaussian output and the other a peak-sense output. All channels have a self trigger capability with variable threshold. For an easy interconnection with an acquisition system, the chip implements an Input/Output interface working on a request/grant basis. There are also some specific features for high counting requirements: fast recovery from overload, good response to double pulse and high rate pulses, base line restoration due to leakage current and/or high counting rate. For testing purposes a test pulse generator was implemented at the chip level [2,3].

Analog Channel main specifications

Average pulse rate over 300kcps; charge input range 0.15fC...165fC, input type: single ended; channel gain 6.2mV/fC; shaping time 20ns or 40ns; output pulse FWHM 62ns or 110ns; output voltage swing 0...1V; output DC voltage level 0.2...1V; channel ENC (detector capacitance Cd=25pF) <980e (shaping time=40ns) and <1170e (shaping time=20ns); integral nonlinearity <0.21% (shaping time=40ns) and <0.91% (shaping time=20ns); overshoot(undershoot) <0.4%; peak-sense output settling time to 0.1% of final value <450ns; peak-sense output decay < 25µV/µs; channel variable threshold 0...165fC; power consumption about 11mW/channel.

Fast and pulse peak-sense output signals

A typical response of an analog channel (fast output and peak-sense output) to different current delta pulses and to a garfield signal is shown in Fig1.

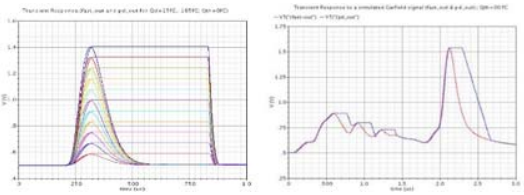

Fig1. Response to delta and garfield current signals

FEE specifications

The FEE is built on a PCB motherboard having two connectors for coupling with a small PCB on which the ASIC is bonded. FEE acts like a local interface between ASIC and an acquisition unit. It accepts the analog or digital signals generated by the ASIC or by the acquisition unit and realises coherent data and control exchanges according to the request/grant protocol.

Digital signals like "event", "request", "ready", "reset" are processed by the FEE unit.

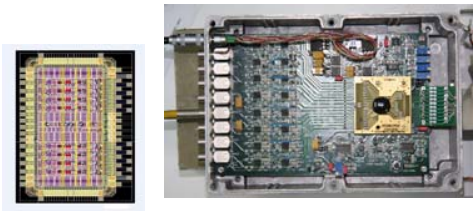

Fig2. ASIC layout and FEE prototype for HCR-TRD

Test results

The FEE (ASIC+ motherboard) was tested with a pulse generator and real signals delivered by a HCR-TRD prototype using Fe^{55} and Pu^{238} X ray radioactive sources.

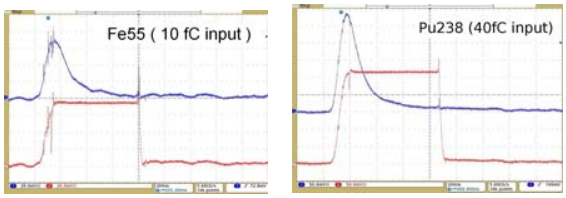

Fig3. Signals delivered by a HCR-TRD prototype and processed with the FEE described in the text

The exhaustive tests of the FEE and HCR-TRD are on the way.

Reference

[1] CBM Collaboration, "CBM Technical Status Report" January 2005
[2] V.Catanescu, "Specific requirements for analog electronics for a high counting rate TRD", CBM 10th Collaboration Meeting, Sept.25-28, 2007, Dresden
[3] V.Catanescu, D.Bartos, GH.Caragheorgheopol, "Analog FEE for High Counting Rate Transition Radiation Detector", DPG, Bochum, March 18, 2009

A Wide Applicable TDC with Event-Driven Readout

H. Deppe[1] and H. Flemming[1]
[1]GSI, Experiment Electronics, Darmstadt, Germany

Introduction

2009 the GSI ASIC desgin group presented the first prototype of the event-driven TDC ASIC GET4. This ASIC was originally designed for the CBM Time of Flight subdetector system but its excellent time resolution and the triggerless operation make this chip to a good TDC candidate for other detectors especially in the FAIR environment.

TDC Overview

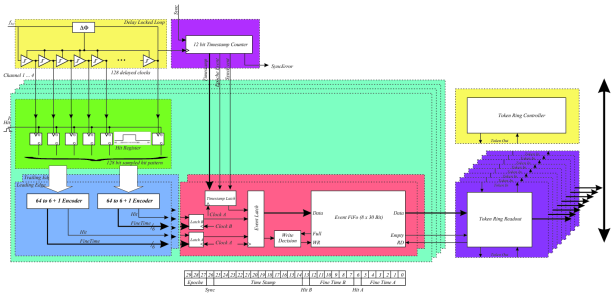

Figure 1: Block diagram of the GET4 TDC ASIC.

Figure 1 shows a block diagram of the GET4 ASIC. Main part of the time measurement system is the time core with an 128 stage Delay Locked Loop (DLL). Each of the four channels has an 128 bit hit register which is clocked by the timing signals of the DLL, four data encoders and two derandomization units. The readout of the data is done by a token ring based readout logic.

The time resolution of the TDC is given by the delay of one DLL delay element. The theoretical value is

$$\sigma_{th} = \frac{1}{\sqrt{12}} \frac{1}{128} T_{cyc} \qquad (1)$$

With a design clock frequency of 156.25 MHz the theoretical limit is $\sigma_{th} = 14.4$ ps. The splitting of the 128 bit hit register into two parts with separate data encoders makes GET4 able to cope with a burst hit rate of 312.5 MHz. The GET4 detects leading and trailing edges for time over threshold calculation.

Test Results

Figure 2 shows time measurements between channel 0 and channel 2 of the GET4 TDC. The measured correlated time resolution is 34.3 ps which leads into an uncorrelated time resolution of 24.2 ps. The histogram also shows that

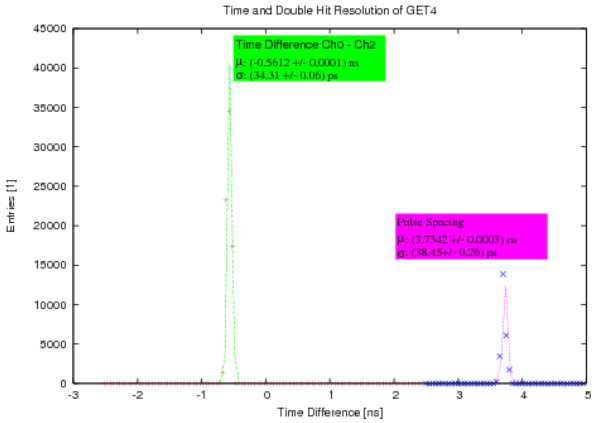

Figure 2: Histogram for time resolution and double pulse resolution determination.

the TDC can resolve double hits with ≤ 3.7 ns puls spacing. Beyond that it could be shown that GET4 is able to measure puls widths below 1 ns.

Evaluation board FEET-TDC

For detector and FEE developments an evaluation board with two GET4 ASICs on board was designed. This board with the two ASICs on the left side is shown in figure 3.

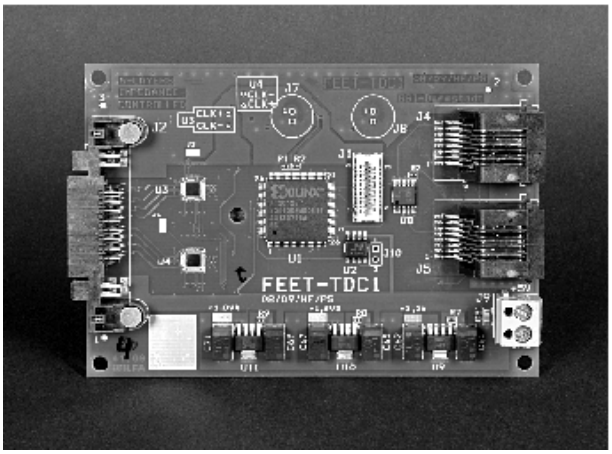

Figure 3: Picture of the FEET TDC pc-board (courtesy of G. Otto).

References

[1] H. Deppe and H. Flemming, The GSI Event-driven TDC with four Channels GET4, Nuclear Science Symposium Conference Record, 2009 IEEE

Single Event Effect Studies on the 180 nm UMC process with the GSI Heavy Ion Microprobe

S. Löchner*[1], B.E. Fischer[2], B. Merk[2], and K.-O. Voss[2]
[1]GSI Darmstadt, Experiment Electronics; [2]GSI Darmstadt, Material Research

Introduction

For the future experiments at the new FAIR accelerator facility radiation damages to electronic components are an important issue. In this regard, the ASIC design group of the GSI Experiment Electronics department has launched a research project for the characterisation of Single Event Effects (SEE) on the 180 nm UMC process, including the development of an ASIC called *GRISU*[1].

SEE is the term for effects in semiconductor devices triggered by a single ionising particle in contrast to effects triggered by a damage accumulated by many particles. A good choice to test these effects is the irradiation with heavy ions. Several irradiation tests with different heavy ions were performed at the X6 testing site. The beam was widened so that the entire *GRISU* chip has been irradiated at the same time[1].

First results showed that some digital storage cells were more sensitive to SEU than expected from simulation. To clarify and understand this unexpected high sensitivity the *GRISU* chip was irradiated with the sub-micron resolution beam of the heavy ion microprobe at the X0 testing site.

Single Event Effect Studies with a Single Heavy Ion Hit Microprobe

Briefly, the microbeam is situated at the end of the GSI heavy ion linear accelerator. The ions entering the microbeam line through object slits are focused down to a focal spot of about 500 nm in diameter by means of magnetic quadrupole lenses. Deflecting magnets, situated in front of the focusing lenses, are used to move the beam spot in the focal plane[2].

In May 2009 a *GRISU* chip was irradiated with a carbon microbeam with an energy of 4.8 MeV/u. This corresponds to a Linear Energy Transfer (LET) of approximately 2.25 MeV cm^2 mg^{-1}. In total five different test structure areas were irradiated. The ASIC has been scanned over $80 \times 80\,\mu\mathrm{m}^2$ for the first three SEE tests and $20 \times 20\,\mu\mathrm{m}^2$ for the last two tests.

As an example of these test results an inverter chain of different transistor sizes is depicted. The layout overlay picture of the irradiated area and the observed Single Event Transient (SET) events are shown in Fig. 1. Each red circle represents a SET event. The circle centre points to the measured origin by the microbeam DAQ system whereas the radius represents the 3σ position accuracy of 612 nm. For inverter chain no. 4 and 5 SET events were measured

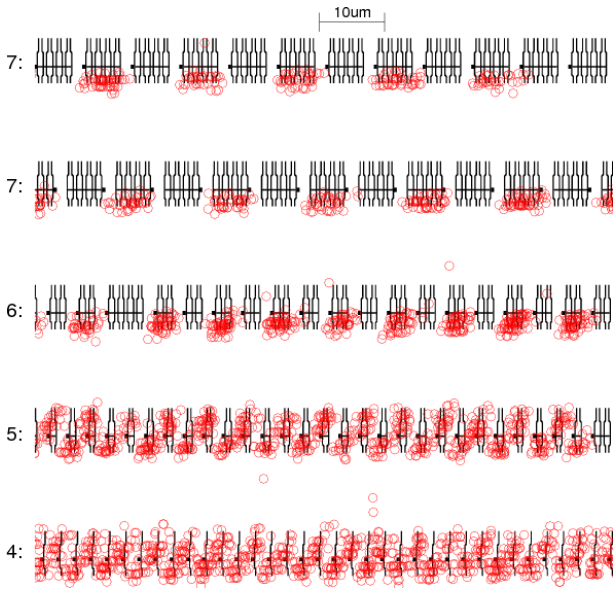

Figure 1: Overlay of inverter chain test structure layout and position of SET events. The radius of the circle is equivalent to 3σ position accuracy or approx. 600 nm.

for NMOS transistors (lower layout part in each row) as well as for PMOS transistors (upper layout part). However for inverter chain no. 6 and 7 SET hits were only measured for NMOS transistors. The explanation for this is that the node capacitances of these PMOS transistors are larger compared to the smaller NMOS.

Results

The first measurement showed that the microbeam setup is a powerful tool for spatially resolving SEE investigations. However the number of events for a closer statistical analysis as well as the resolution must be increased for closer investigations of the 180 nm process, especially for the study of some special memory structures on the *GRISU* chip.

References

[1] S. Löchner, "Radiation Studies on the UMC 180 nm CMOS Process", GSI Scientific Report 2009

[2] B.E. Fischer, "The Scanning Heavy Ion Microscope at GSI", Nuclear Instruments and Methods in Physics Research, Section B, 10-11, 693-696 (1985)

* s.loechner@gsi.de

Characterization of the n-XYTER chip and preparations for the engineering run

C.J. Schmidt[1], M. Höhl[1], V. Kleipa[1], W. Müller[1], H.K. Soltveit[2], and A. Lymanets[3]
[1]GSI, Darmstadt, Germany; [2]Phys. Inst. Univ. Heidelberg, Germany; [3]Univ. Frankfurt, Germany

The n-XYTER ASIC, developed and prototyped by the EU-FP6 NMI3 DETNI collaboration in 2006, has undergone extensive testing and evaluation during the past years at GSI. This 128 channel ASIC [1] realizes a self triggering front-end readout architecture that will as such uniquely serve the CBM collaboration to prototype a purely data driven detector readout chain. CBM intends to employ this readout chain early on in detector prototyping and system development and study the implications of such change in readout paradigm.

During 2009 the mixed signal chip underwent detailed investigations on the chips performance and various mechanical, electronic and software integration aspects. In parallel it was integrated into the novel, dedicated data driven CBM readout chain and DAQ under development. Chip performance became for the first time experimentally accessible in all depth with the successful smooth realization of the entire chain, in which every single link was new and marginally tested.

With the data chain operative and versatile test and control software available, finally pulse hight spectra could be taken. To this end the chip was connected to a small dc-coupled strip detector of 300 μm wide and 10 mm long strips. The strips, wide compared to the 50.7 μm strips of the CBM prototypes, would reduce the probability of events sharing charge among neighboring channels. With this setup, an enclosed ^{241}Am gamma source was employed to generate signals in the sensor. This source provides several predominant gamma lines that generate below one MIP equivalent charge signals with reasonable detection efficiency in the 300 μm thick sensor. This source thus almost perfectly matches the needs for this chips evaluation. Using the 26.3 keV (7.2 ke in Si) together with the 59.5 keV gamma line (16.3 ke in Si) for gain calibration, 460 ENC could experimentally be confirmed on the latter line, which is in agreement with simulation considering a detector capacitance on the order of 6 pF but unprecisely known.

Chip testing was particularly intensified and extended to the study of the multi-channel spread of analogue parameters among the 128 input channels. These activities were performed in view of a larger production run for this ASIC targeted to improve the chips availability for neutron scattering detector applications on one hand and on the other hand for detector prototyping within CBM and eventually beyond within FAIR. In this production run and with the preparatory engineering work realized at Physikalisches Institut Heidelberg, the most severe drawbacks encountered in the current realization are being addressed and will be

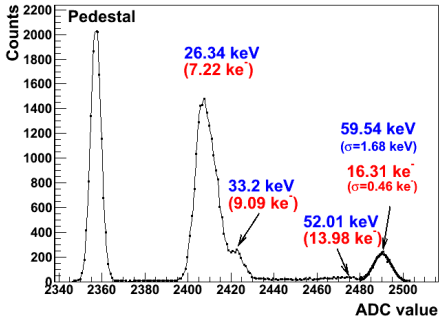

Figure 1: ^{241}Am gamma spectrum measured with the n-XYTER chip in self triggered mode on a 300 μm Si-strip detector. Several characteristic lines are seen, the rightmost one corresponding to 59.5 keV. The fit of a gausian to it reveals a resolution of 460 ENC. The pedestal was additionally added through a random trigger in the n-XYTER test trigger mode, which may be employed for an alternative, triggered operation of the chip.

corrected. These are:

- extermination of an observed severe temperature coefficient of up to 4%/K in the analogue baseline.
- annihilation of several layout related deficiencies potentially causing powering problems and consequently an observed and undesired channel to channel base line shift across the chip.
- reduction of the observed channel to channel base line spread that effectively reduces the dynamic range.
- improvement of in-channel as well as inter channel cross talk.
- implementation of an optional reduction in gain by about a factor of 4 in order to enhance the dynamic range.

A more in depth report on these submission preparations is published in the GSI Scientific Report [2]. We expect to have the n-XYTER available in sufficiently large numbers in spring this year. Automated extensive per chip characterization and tests are planned for this production batch.

References

[1] NIM A, 568 (2006) 301-308
[2] H.-K. Soltveit, GSI Scientific Report 2009.

CLOSY: A very Precise Clock Generation for Timing Measurements and Synchronization of the CBM ToF Wall

K. Koch
GSI, EE-Department, Darmstadt, Germany.

***Abstract*–A new electronics for precise clock generation and distribution has been designed for the CBM ToF-wall. The main card (CBM-CLOCK-SYTEM) is based on a frequency synthesizer chip to create two independent output frequencies that are phase coupled. An additionally downstream fast CPLD creates a synchronization signal, which is needed as a periodically epoch marker for the system.**

Introduction

In the concept of the CBM-Time of Flight (ToF) detector readout two phase coupled high-performance frequencies are needed [1]. One is directly used for time measurements with an event driven TDC (FEET-board, GET4 TDC chip) [2, 3], the other for synchronous data transportation reasons (Read Out Controller board, ROC) [4]. The front-end boards with the GET4 TDC chip have a clock requirement of about 160 MHz with very low jitter, less than 5 ps sigma. The ROC board has a need for a 250 MHz clock, but with less strict demands due to jitter.

Circuitry

Based on a programmable any-rate XO (Silicon Laboratories, Si570) a low jitter synthesizer and jitter cleaner (Texas Instruments, CDCL6010) and a fast CPLD (Xilinx, XC2C32A) an impedance controlled six layer board has been developed that delivers two phase coupled signals (250 MHz and 156.25 MHz) and an additional synchronization signal (SYNC) (see Fig. 1).

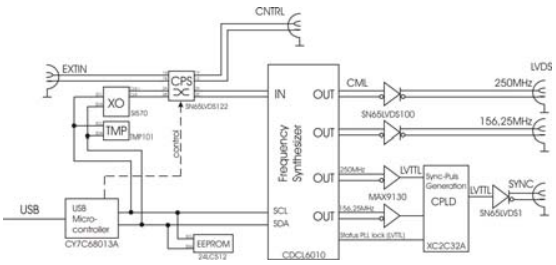

Figure 1: Simplified schematic of CLOSY2 (CPS: cross-point switch, TMP: temperature sensor).

Inside of the frequency synthesizer an integrated jitter cleaner with the option of a narrow external PLL loop filter also offers the opportunity of using a non optimal external clock source relating to incoming jitter.

To define the suitable output frequency, a rational fraction of 5/8 from 250 MHz (156.25 MHz) would be a good choice to get a fixed frequency relation concerning to the requirement of the TDC chip and the ROC board.

Results

Best results will be obtained with an oscillator clock frequency of 312.50 MHz (Jitter measurement at CNTRL output: σ_{TIE} ~ 2.7 ps, σ_{Period} ~ 3.7 ps).

The outputs then show much better results than the above-mentioned requirements (see Table 1).

output freq.	method	@CLOSY2	20 m distance
156.25 MHz	TIE	3.2 ps	4.2 ps
	Period	2.3 ps	3.1 ps
250.00 MHz	TIE	4.0 ps	6.0 ps
	Period	4.2 ps	5.4 ps

Table 1: Sigma values of timing jitter (TIE: time interval error, output signal at CLOSY2 and 2 times cascading over 20 m distance, XO frequency = 312.50 MHz).

Conclusion

The clock system is ready to be used in the CBM ToF environment with very good parameters exceeding the requirements. The essential control parameters are easy configurable via USB or over a boot sequence stored in an EEPROM on board. The CPLD is also reprogrammable in the case of other frequency ratios or delaying the SYNC signal.

Above all, CLOSY could be deployed in other physics experiments as well as laboratory equipment with the need of precise phase coupled clocks.

References

[1] W.F.J.Müller, V.Friese: CBM Progress Report 2008, GSI Report , Darmstadt, Germany, 2009, (http://www.gsi.de/documents/DOC-2009-Feb-233-1.pdf)

[2] H.Deppe, H.Flemming: Development of High Resolution ASICs for CBM-ToF, GSI Scientific Report 2007, p.250 (http://www.gsi.de/informationen/wti/library/scientificreport2007/PAPERS/INSTRUMENTS-METHODS-44.pdf) (1997) 56.

[3] H.Flemming, H.Deppe: Development of High Resolution TDC ASICs at GSI, Nuclear Science Symposium Conference Record, 2007 IEEE.

[4] S.Manz: Status of the Read Out Controller for the FEET Boards, 13. CBM Collaboration Meeting, March 9-13, 2009, GSI Darmstadt (http://www.gsi.de/documents/DOC-2009-Mar-97-1.pdf).

Design and Implementation of the Read Out Controller for the GET4 TDC of the CBM ToF Wall Prototype

S. Manz[1] and U. Kebschull[1]

[1]Kirchhoff Institute for Physics, Heidelberg University, Heidelberg, Germany

Introduction

The Time of Flight detector of the CBM experiment will assemble about 12 500 GET4 ASICs [1]. Those chips give a very precise timestamp (resolution better than 25 ps) to detected hits and then deliver the data (24 bits/hit) via a serial LVDS link to the Read Out Controller (ROC). At the moment, the FPGA of one ROC interfaces up to 14 GET4 chips. However, the current hardware allows up to 28 GET4 chips and even more should be possible with the new generation of ROCs. In addition to the combination and synchronization of the data from all GET4 chips into one data stream, the ROC has to provide a control interface for all the chips.

Modular Design

The GET4 readout chain is one of several readout chains needed for the experiment, all with similar requirements. Therefore we implemented a modular system which separates the readout logic from the transport logic. Much functionality can be reused and only the interface to the frontend electronics needs to be exchanged. In addition, this modular approach allows an efficient development of the firmware by more than one designer. The GET4-ROC is developed as a readout logic module in the "Universal ROC" design. More details concerning the "Universal ROC" design can be found in [2].

Readout Logic

Until now a basic readout module for the GET4 chips has been developed. Figure 1 shows an overview of the ROC. First the serial data is sampled and deserialized. Then the decoded data is combined into a single data stream. At the moment a simple round robin algorithm is implemented. This stage also performs very basic message building. For future versions a slightly more complex token ring readout in combination with improved message building is planned. The sampling on the data ports can be switched off by a configurable mask register (e.g. to avoid ghost data from unconnected ports).

The ROC also needs to provide a control interface to the GET4 chips and to the ROC itself. Single commands can be send via transport logic to the ROC. In case of a command for the GET4 chips, this command is passed to the GET4-boards (the so called FEET boards) via a serializer. On default, the command is sent to every connected FEET board. To address only specific boards the control path implements a configurable mask register as well.

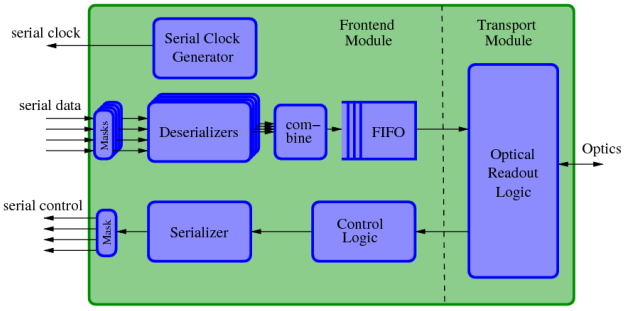

Figure 1: Block diagram of the ROC's functionality.

Transport Logic

At the moment there are two transport logic modules available to connect the ROC to a DAQ-PC, Ethernet and optics (see [3] for details concerning the optics). While Ethernet is better tested and a convenient solution for small setups, some features only come with the optics module. Those features are a high bandwidth (current hardware: ca. 230 MB/s) for the data readout and deterministic latency messages for synchronisation. However the optical readout chain requires an additional PCIe card, the ABB [4].

Future Prospects

The current version of the GET4 readout module provides a basic interface. The module is usable, however it is not feature complete. Besides the improvement of many smaller details, the features that will be developed in 2010 are a proper synchronization technique and simple data processing tasks.

References

[1] H. Flemming and H. Deppe, "GET4 TDC ASIC", GSI internal report, March 2009

[2] N. Abel, S. Manz and U. Kebschull, "Design and Implementation of an Universal Read Out Controller" GSI Scientific Report 2009, Darmstadt, Germany

[3] F. Lemke et. al, "A Unified Interconnection Network with Precise Time Synchronization for the CBM DAQ System", IEEE NPSS Real Time Conference, 2009, Beijing, China

[4] W. Gao et. al, "Improved Active Buffer Board of CBM", GSI Scientific Report 2008, Darmstadt, Germany

Design and Implementation of an Universal Read Out Controller

N. Abel[1], S. Manz[1], and U. Kebschull[1]
[1]Kirchhoff Institute of Physics, Heidelberg University, Heidelberg, Germany

Introduction

Since 2007 our contribution focused on the Silicon Tracker's FEE (Front End Electronic), consisting of the nXYTER, an ADC (Analog Digital Converter) and a ROC (Read Out Controller) [1]. The implementation of the nXYTER specific ROC has been done very successfully, as the beam tests in September 2008 [3] and September 2009 [2, 4] proved. Our first ROC setup consisted of the nXYTER readout logic and a PPC based Ethernet transport logic. This setup is called the nXYTER Starter Kit, which turned out to be very helpful in small laboratory setups, where physicists need quick access to the nXYTER and its measured data. The Ethernet interface keeps the communication effort as simple as possible, since every common PC supports it.
However, in the final experiment thousands of ROCs will be used. In this setup Ethernet will not be an option any longer. This is primarily caused by the galvanic isolation coming with fiber optics and by the fact that the certain ROCs are synchronized via Deterministic Latency Messages (DLMs), which by definition depend on optical fiber [5]. Thus, a second transport logic, the Optical Transport, has been implemented. In our first concept, the Optical Transport was planned to fully replace the Ethernet transport. Due to the usefulness of the Starter Kit this plan has been altered. Today, we fully support both, Ethernet and Optical Fiber, as two equal solutions.

The Universal ROC

While our first setup solely focused on the nXYTER, today we are also designing and implementing readout logic for the FEET chip [8] and the TRD chip *(in planning stage)*. To keep the re-usability as high as possible, we did split the ROC into two fully independent modules: the readout logic (RL) and the transport logic (TL). Both are connected to each other via a standard bus for slow control and via a FIFO for the hit data transport (see figure 1). This internal interface is common for all transport modules and all readout modules. Therefore the development of the modules can be done independently.
The strict separation of the chip into RL and TL also influences the software on the PC. At this, RL and TL can be seen as two different layers. A change from Ethernet to Optic causes the change of the whole communication setup. Of course fiber cables instead of Ethernet cables have to be used. But more important, there is no fiber port on the PC. Therefore the ABB board (which in short acts as an adapter from fiber to PCIe [6]) has to be used. This leads to the utilization of completely different drivers. However, the overlying DABC software [7], which implements slow control and data taking, has not to be changed at all. Using encapsulation, it does not even have to notice the change from Ethernet to Optic. On the other hand a change of the RL from nXYTER to FEET only influences the control software and does not require any changes on the driver software.
In conclusion the modularization of the Read Out Controller and the consequential separation of the control software into different layers, enables us to provide an Universal ROC, which offers quick access to a long-run tested transport logic. This leads to a significant increase of stability and reliability compared to a development from the scratch. Beyond that, the modularization concept allows us to easily add a new readout logic for further FEE setups.

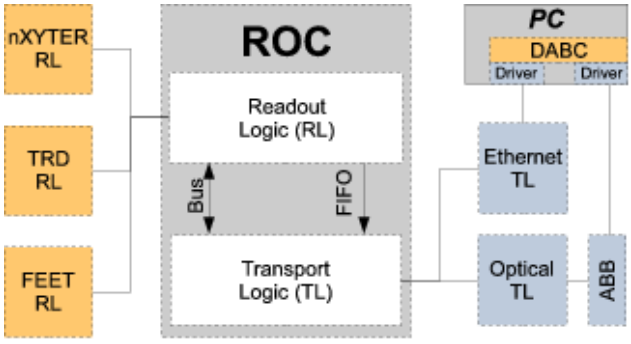

Figure 1: The unitized layout of the Universal ROC

References

[1] N. Abel et. al, "Development of the Read Out Controller for the nXYTER Front End Board", GSI Progress Report 2007, Darmstadt, Germany

[2] B. Bozsogi, "Test of CBM Silicon Tracking Detectors in a proton beam at GSI", Student Report, 2009, Budapest, Hungary

[3] cbm-wiki.gsi.de/cgi-bin/view/Beamtime/BeamTimeGsiSep2008

[4] cbm-wiki.gsi.de/cgi-bin/view/Beamtime/BeamTimeGsiAug2009

[5] F. Lemke et. al, "A Unified Interconnection Network with Precise Time Synchronization for the CBM DAQ System", IEEE NPSS Real Time Conference, 2009, Beijing, China

[6] W. Gao et. al, "Improved Active Buffer Board of CBM", GSI Scientific Report 2008, Darmstadt, Germany

[7] Linev et. al, "Software development for CBM readout controller board", GSI Progress Report 2008, Darmstadt, Germany

[8] Sebastian Manz, "GET4 readout chain", CBM Collaboration Meeting, 2009, Split, Croatia

Prototype Results of an Optical Communication Network for the CBM DAQ-System

F. Lemke, S.Schenk, and U. Bruening[1]
[1]University of Heidelberg, Mannheim, Germany

Introduction

For the CBM Data Acquisition (DAQ) System a specific protocol has been developed considering the special demands of limited area for hardware, radiation tolerance, support for different types of network traffic and the need of synchronization mechanisms. Within the CBM network only a single bidirectional fiber link is used for the three network traffic classes: Data Transport Messages (DTM), Detector Control Messages (DCM), and Deterministic Latency Messages (DLM). DTMs are optimized for data transfer from the detector frontend to the backend computing cluster. The DCM class provides a higher fault tolerance level to guarantee the delivery of control messages. DLMs are used for precise time synchronization. The CBM DAQ protocol fulfills all requirements mentioned before and was implemented for the usage within the Field Programmable Gate Arrays (FPGA) of all developed readout chain boards. The chain, developed by several groups, consists of Read-Out-Controller (ROC) boards interfacing and initializing the front-end electronics and building link-packets, Data-Combiner-Boards (DCB) combining data streams from multiple ROCs, and finally Active-Buffer-Boards (ABB) for receiving, buffering and reorganizing the data. The ABB also writes the data via PCI express to the memory of the back-end node.

Prototype Setup and Measurements

All presented measurements and results in [1] and within this section are prototype build-ups consisting of DCBs V1.3 shown in Fig. 1, also known as the HTX-Board, the Avnet ADSAES-XLX-V5LXT as ABBs and ROC boards, which are also called SysCore Board V2. The preferred combinations for conducted tests were ABB - 2ROCs and ABB - DCB - 2ROCs, because they are sufficient to prove the concepts and to declare them as suitable for a final build. Due to given data rates, the ROC-DCB-ABB chain is currently running with 2.5 Gbps optical links. This link speed can be increased with feasible design changes by at least a factor of two, if necessary. During the first tests with the prototype systems test pattern generators were used to create random sized data and control packets. Data streams included periodically embedded DLMs. After successful tests with different setups, the optical protocol was combined with logic of the ROC and ABB development groups. In the next step a complete readout chain was tested under real usage conditions. It was possible to use control messages to read and write registers within the ROC and to control initializations required by ROC logic. Also a data stream of a detector readout was activated and written into main memory of the computing node for further processing. The theoretical peak bandwidth utilization of the protocol for each link is over 240 MB/s, which is more than 95 percent of the maximum possible bandwidth of 250 MB/s considering 8b/10b coding on a 2.5Gb/s link. Measurements for data bandwidth utilization show that we can reach more than 220 MB/s, which is over 90 percent of the possible protocol bandwidth. The message based precise time distribution requires deterministic latency within the DAQ system. Besides special synchronization mechanisms implemented in hardware, a recovered receive clock has to be used for sending messages. The clock's jitter must be less than 40 ps peak-to-peak to guarantee correct transceiver operation. Therefore a jitter cleaner device presented in Fig. 2 was developed. Deterministic latency has been proven in multiple long-term lab tests and DLMs were successfully sent.

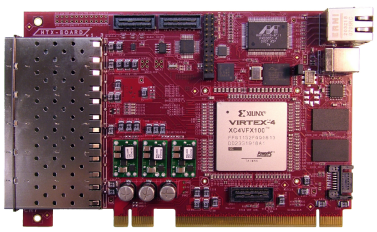

Figure 1: Data Combiner Board V1.3

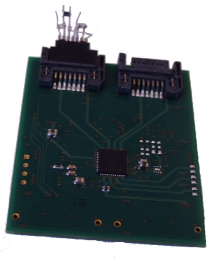

Figure 2: Jitter Cleaner Extension Board V1.0

References

[1] Frank Lemke, David Slogsnat, Niels Burkhardt, Ulrich Bruening, "A Unified Interconnection Network with Precise Time Synchronization for the CBM DAQ-System", 16th IEEE NPSS Real Time Conference 2009 (RT 09), May 10-15, Beijing, China.

Optical Communication Tests with Active Buffer Board

W. Gao*[1], A. Kugel[1], A. Wurz[1], G. Marcus[1], M. Stapelberg[1], and R. Männer[1]
[1]Department of Computer Science V, ZITI, University of Heidelberg, Mannheim, Germany

Introduction

The Active Buffer Board (ABB) is the transfer unit in the CBM DAQ sub-system. It receives CBM events, performs local buffering and formatting and forwards them to the host PC via the PCIe channel. Based on the development of the ABB-v1 (with Virtex 4 FPGA), the ABB-v2 (AVNET Virtex 5 board) is successfully equipped with optical link functions. Also, 3 traffic classes, DAQ (data acquisition), CTL (control) and DLM (deterministic latency message) are defined. To access these traffic classes, a software interface is built. A multi-threaded higher level software supports the interleaved data and control accesses. As shown in figure 1, the ABB communicates with the DCB (data combining board) or the ROC (read-out controller) over fibre. Commissioning DAQ chain tests show good channel performance. [1]

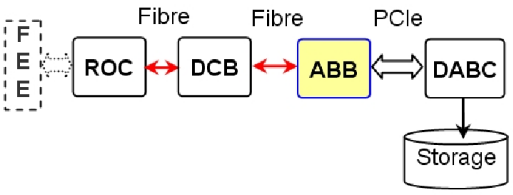

Figure 1: ABB in DAQ test chain

Firmware

To the ABB-v2 board, HDL development on the Virtex 5 FPGA (XCV5LXT110) involves the DMA engine and the link protocol module, as well as the new traffic classes processing. An efficient transfer of data from the FEE (front-end electronics) to the host over optical links is possible in this way.

A FIFO structure has been carefully designed, where the incoming DAQ packets are buffered. We have two options for this buffer, one is a 128KB internal Block RAM FIFO, the other is a 256MB external DDR SDRAM FIFO. The buffer is written and read asynchronously, which demands special treatment for the data count, especially for the larger DDR FIFO version. Otherwise the software would run into a time-out DMA status or even crash. CTL messages are important in coordinating the data flow between the front-end and the back-end. New logic design reserves buffers both for outgoing and incoming CTL messages, because in the link protocol, CTL messages can be delayed for some cycles, which is different from DLM messages. Control/Status register pairs are set to the PCIe DMA logic related to the optical link and the traffic class buffers. They enable the software to access the new firmware components.

A link protocol module has been developed by CAG Group, Uni. Heidelberg. It manages the high-speed transfer over optical channels and multiplexes the traffic classes on a single link after arbitration. [2]

A data generator inside the ABB board is implemented to emulate the link behaviour in the ABB stand-alone (internal loop-back) test. It helps also to source the pseudo-DAQ data packets in the performance test.

Software

The new software development aims at a continuous data transfer under multiple traffic classes.

Functions for CTL message sending and receiving are built into a new software component, the ABB Daemon, which enables the ABB board to communicate with the FEEs via DCB or ROC over optical links. Multiple CTL messages can be merged. The command carried in the CTL message can be successfully acknowledged by the receiver. The DMA targeted to the FIFO-structure data source was upgraded and verified. The PCI driver has been updated with functions corresponding to the new traffic patterns. The ABB Daemon provides a serialization of CTL and DAQ packets from the ABB while allowing concurrent access from multiples threads/applications.

Tests of traffic classes

All new features of the ABB-v2 have been proven reliable. CTL message tests have been well proceeded because they are the management for almost all DAQ activities. Application-level tests for CTL message latencies result in 0.138 ms for write-read and 0.053 ms for read. The basic functionality of the DLM messages has been tested, the full integration into the software stack is in work. When 2 ROCs are connected, DMA performance in transferring DAQ packets is about 300 MB/s.

References

[1] W. Gao, et al. Active Buffer for DAQ in CBM Experiment. IEEE-RT'09 Conference Record. 2009.

[2] F. Lemke, et al. A Unified Interconnection Network with Precise Time Synchronization for the CBM DAQ-System. IEEE-RT'09 Conference Paper. 2009.

* wenxue.gao@ziti.uni-heidelberg.de

Usage of DABC in software development for CBM DAQ

S. Linev[1], J. Adamczewski-Musch[1], and H.G. Essel[1]
[1]GSI, Darmstadt, Germany

CBM readout controller

The CBM readout controller board (ROC) was developed to control nXYTER-based [1] front-end electronics and deliver data from the nXYTER to a PC via Ethernet. A first version of PC software libraries (ROClib [2]) for communication with the ROC was implemented.

Then a significant redesign of this software was required because new ROC firmware will support various kinds of front-end electronics and optic transport from ROC to PC. It was necessary to separate the communication (transport layer) from the device-specific controlling and configuration (application layer).

Data transport

The application layer together with communication interfaces is kept in ROClib. An abstract *roc::Board* class defines the interface for communication and data transport. The transport layer was removed from ROClib and implemented as plug-ins of the Data Acquisition Backbone Core (DABC) [3], a general purpose data acquisition framework. DABC had already been used with the previous ROClib for building DAQ applications for ROCs.

The UDP transport between ROC and PC was reimplemented with the powerfull DABC socket handling classes, allowing to handle several socket connections in one thread.

Several firmware and software components were developed at Uni Heidelberg for the optic transport from ROC to PC via a PCIe board (AVNET-board). This consists of a linux driver for the board, a user-space library (mprace) and a special daemon application. Appropriate DABC *device* and *transport* classes were implemented on top of this software.

Introducing a communication layer interface in ROClib allows to develop application software which is fully independent from the communication implementations like the DABC plug-ins.

Control interface

To control and configure different front-end electronics connected to the ROC, a control-space access interface was defined in ROClib. It consist of a single operation - *noper*, which is just a list of *put* and *get* register operations, implemented in the DABC plug-ins. Based on such interface, a number of device-specific classes were implemented in ROClib to configure ADCs, nXYTERs, I2C bus and other components.

Data format

All data taken from one kind of front-end are packed in messages of fixed length. Message format and even message size depend on the connected electronics, firmware version and the kind of the connection. To handle all possible formats a class *roc::Message* was introduced. It provides a convenient way to access the data fields for any supported message type.

User tools

The transport and control classes are used in several applications:
rocutil - command-line tool for device configuration;
rocGui - Qt4-based configuration GUI;
go4monitor - go4-based [4] program for taking and displaying data from a single ROC.

Test beamtime 2009

During September beamtime up to 6 ROCs reading data from different detectors were running in parallel. They delivered up to 30 MB/s to a single PC running the DABC data acquisition, which sorted and stored the data to list-mode data files. At the same time data was monitored online by several *go4monitor* applications, connected to the DABC application through standard GSI data channels.

Status and outlook

The developed software allows to configure and run ROCs in different environments. DABC is used as core framework for the implementation of ROClib software. A succesfull beamtime was operated with a DABC-based DAQ system in September 2009. The development of the optic transport via PCIe board is mostly finished. Information and latest news on cbm-wiki.gsi.de

References

[1] A.S. Brogna et al., “N-XYTER, a CMOS read-out ASIC for high resolution time and amplitude measurements on high rate multi-channel counting mode neutron detectors”, Nucl. Instrum. Methods A 568 (2006), pp. 301-308

[2] N. Abel et al., “Software development for CBM readout controller board”, GSI Scientific Report 2008, p. 228

[3] J. Adamczewski, H.G. Essel, N. Kurz, S. Linev, “Data Acquisition Backbone Core DABC”, Journal of Physics: Conference Series 119 (2008) 022002

[4] J. Adamczewski, M. Al-Turany, D. Bertini, H.G. Essel, S. Linev, “Go4 online monitoring”, IEEE Trans.on Nucl. Science, Vol.51, No.3, June 2004, pp 565-570

Hadron identification with CBM at SIS-100

D. Kresan , V. Friese , C. Höhne , and P. Senger
GSI, Darmstadt, Germany

The investigation of p+A collisions up to 30 GeV and A+A collisions from $4A$ to $11A$ GeV beam energies is considered as part of the CBM research program and will be performed in the first phase of FAIR with a start version of the CBM detector at the SIS-100 accelerator. This start version consists of two detector systems: the Silicon Tracking System (STS) placed in a magnetic field for the measurement of momenta and vertices, and a Time-Of-Flight (TOF) wall located 10 m downstream of the target for hadron identification. We investigated the capabilities of this start set-up for the identification of primary hadrons, assuming the standard CBM magnetic field and a TOF resolution of 80 ps.

Central (b=0 fm) Au + Au collisions at $4A$ GeV, as one of the lowest energies considered for CBM, were generated with the UrQMD model [1] and simulated in the CBM setup with the CBMROOT software package. No intermediate tracking system was used; tracks from the STS were directly extrapolated over 9 m to the TOF wall and merged with TOF hits. For details of the event reconstruction algorithm implemented in the current framework see [2]. We used the same method for hadron identification by time of flight as applied at $25A$ GeV [3].

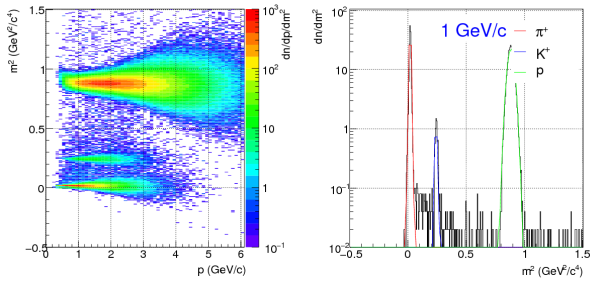

Figure 1: Left: Squared mass versus momentum distribution for reconstructed primary particles from central Au+Au collisions at $4A$ GeV beam energy. Right: Squared mass distribution for $p = 1$ GeV/c.

The distribution of the squared mass versus momentum of reconstructed primary particles is shown in Figure 1. Pions, kaons and protons are well separated; hence, a clean particle identification is possible by selecting tracks within a momentum-dependent window in m^2 around the expectation value for each particle type. The distribution of the transverse momentum at midrapidity of reconstructed and identified primary K^+ from central (b=0 fm) Au + Au collisions at $4A$ GeV beam energy is shown in Figure 2. The dotted line shows the distribution in full phase space, the solid red line kaons within the CBM acceptance and the filled region reconstructed and identified kaons.

At $4A$ GeV, the average laboratory momentum of the produced particles is considerably lower than at SIS-300 energies. This induces large acceptance losses at small transverse momenta due the in-flight decay of kaons over the distance of 10 m to the TOF detectors. As the resolution in m^2 increases rapidly with momentum, inefficiencies at larger transverse momentum occur because of the increasing overlap of the m^2 distributions of pions and kaons. We conclude an overall good performance of the primary hadron measurements with a start version of the CBM detector at SIS-100 at FAIR.

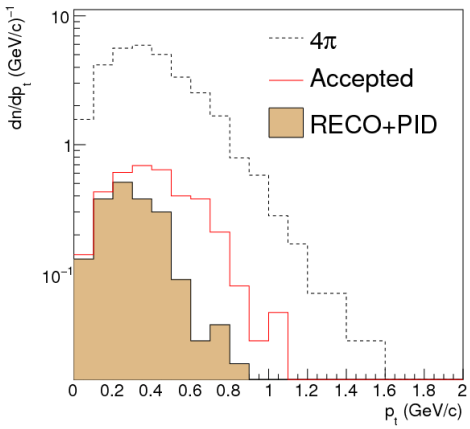

Figure 2: Transverse momentum distribution at midrapidity ($1.0 < y_{LAB} < 1.1$) for primary K^+ from central Au+Au collisions at $4A$ GeV beam energy generated with UrQMD

For this study, both STS and TOF were assumed to be unmodified with respect to the full CBM setup. In the future, the setup will be optimised to lower beam energies, such as placing the TOF wall closer to the target in order to decrease kaon decay in flight, or lowering the magnetic field to improve on the geometrical acceptance. A systematic study of the effect of the time resolution of the stop detector on the kaon/pion separation is also planned.

References

[1] S. A. Bass *et al.*, Prog. Part. Nucl. Phys. **41** (1998) 255

[2] D. Golubkov *et al.*, CBM Progress Report 2008, Darmstadt 2009, p. 76, and references therein

[3] D. Kresan and C. Höhne, CBM Progress Report 2008, Darmstadt 2009, p. 63

Study of high p_T pion production with CBM at SIS100 energies

V. P. Ladygin[1], A. I. Malakhov[1], and T. A. Vasiliev[1]
[1]LHEP JINR, Dubna, Russia

Multi-particles dynamics (jets and/or correlations) sensitive to the properties of hot and dense matter can be studied in detail with CBM because of the very large statistics expected for pion production in heavy-ion collisions. Hard probes can provide information on the coexistence phase even in the energy domain of SIS100 [1]. The first step of such investigations at CBM can be the study of high transverse momentum spectra of pions, because high-energy single partons forming the secondary particles are valuable probes of hot and dense matter [2, 3].

Simulations were performed for 10,000 central Au+Au events at 10 GeV per nucleon, generated with UrQMD, using the September 2009 trunk version of CBMROOT. The standard CBM geometry and magnetic field for the electron setup were employed. Particle momenta were reconstructed in the STS with the Kalman Filter procedure; particle identification was accomplished using the time-of-flight information from the RPCs. Pions were selected using the

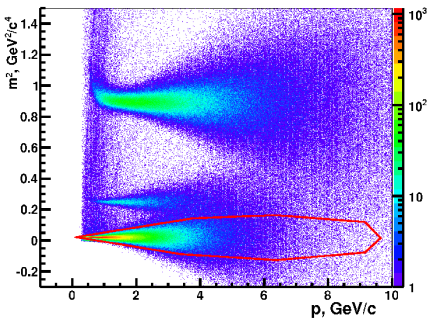

Figure 1: The $m^2 - p$ correlation for $Au + Au$ UrQMD central events at 10 GeV. The line is the graphical cut used for the pion selection.

$m^2 - p$ correlation as presented in Fig. 1. A good separation of protons and kaons from pions is visible up to $p = 8$ GeV and $p = 4$ GeV, respectively. The same graphical cut (shown by the solid line in Fig. 1) was used to select both negatively and positively charged pions.

The ratio of the numbers of π^+ and π^-, $R = N_{\pi^+}/N_{\pi^-}$, as a function of transverse momentum p_t is shown in Fig. 2. Clearly, the p_t region where strong medium effects were observed [2, 3] is accessible at SIS100, even with rather limited statistics.

The open squares in Fig. 2 represent the ratio R obtained for UrQMD events. It is below unity for SIS100 energies reflecting the n/p asymmetry of the colliding nuclei. The open triangles in Fig. 2 show R obtained for particles reconstructed in CBM, but using the true PID. A good agreement between UrQMD predictions and reconstructed

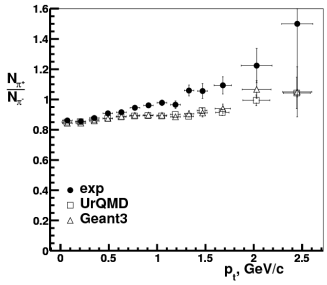

Figure 2: Ratio of the numbers of positively and negatively charged pions in central $Au + Au$ collisions at 10 AGeV as a function of transverse momentum p_t

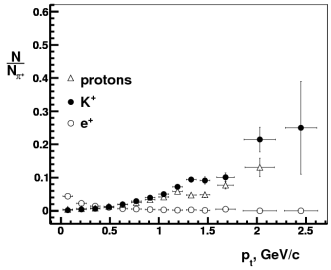

Figure 3: Ratio of p, K^+ and e^+ wrongly identified as pions to the number of π^+ as a function of p_t

events is observed. The full circles are obtained for pions selected by the $m^2 - p$ correlation (see Fig. 1). Here, the statistics for pions is about three times lower because of the TOF acceptance. The deviation of the N_{π^+}/N_{π^-} ratio from the UrQMD predictions at $p_t > 1$ GeV/c is mostly related to the admixture of protons and K^+ wrongly identified as π^+ (see Fig. 3), whereas the contribution of misidentified K^- and $\overline{p}$ to the π^- is much smaller. Therefore, a reliable measurement of R at 10A GeV is possible only up to $p \approx 1 - 1.5$ GeV/c. At higher momenta, a more sophisticated PID procedure is required to decrease the number of misidentified p and K^+.

In a next step, the energy and system size dependence of the high p_t pion spectra as well as azimuthal correlations will be studied.

References

[1] V. P. Ladygin, A. I. Malakhov and T. A. Vasiliev, 14-th CBM Collaboration Meeting, Trogir, Croatia, 6-9 Oct. 2009, https://www.gsi.de/documents/DOC-2009-Oct-233-1.pdf

[2] S. S. Adler *et al.*, Phys. Rev. **C69** (2004) 034910

[3] C. Alt *et al.*, Phys. Rev. **C77** (2008) 034906

Ξ^- on-line reconstruction in Au+Au collisions at 25A GeV with CBM

I. Vassiliev[1,2], I. Kisel[2], and M. Zyzak[2,3]

[1]Goethe-Universität, Institut für Kernphysik, Frankfurt am Main, Germany; [2]GSI, Darmstadt, Germany; [3]Taras Shevchenko National University of Kyiv, Ukraine

The main goal of the CBM experiment is to study the behaviour of nuclear matter in the conditions of high baryonic density in which the transition to a deconfined quark gluon plasma phase is expected. One of the signatures of this new state is the enhanced production of strange particles; therefore, hyperon reconstruction is essential for the understanding of the heavy-ion collision dynamics. Hyperons will be measured in CBM by their decay into charged hadrons, which are detected in the Silicon Tracking System (STS).

To study the feasibility of on-line reconstruction of hyperons in the CBM experiment, a set of 10^4 central Au+Au events at 25A GeV, generated with UrQMD, were simulated. They contain on average 0.98 Ξ^-, which decay almost exclusively into $\Lambda + \pi^-$ with a lifetime of $c\tau$ = 4.91 cm. The Λ daughters decay predominantly in the STS detector. The standard geometry with two MVD stations at z = 5 cm and z = 10 cm (thickness 500 μm) and eight STS stations of double-sided segmented strip detectors is used for tracking. No kaon or pion identification with the time-of-flight detector (TOF) is applied; however, it is important to use the TOF measurement in order to select proton tracks from the sample and reconstruct the $\Lambda \to p\pi^-$ decay.

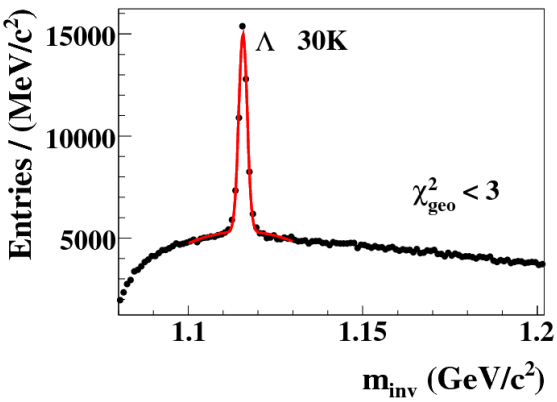

Figure 1: $p\pi^-$ invariant-mass spectrum. About three Λ per event were found.

The on-line reconstruction of Ξ^- events includes several steps. First, fast track finding and fitting in the STS is performed using the L1 reconstruction package [1, 2]. Then, off-vertex tracks ($\chi^2_{primary} > 3\sigma$) are selected for the Λ search, where protons, identified by the TOF detector, are combined with negatively charged tracks to a Λ candidate, using the KFParticle package [3]. A quality cut on the geometrical vertex ($\chi^2_{geo} < 3\sigma$) is used to suppress the combinatorial background. The obtained invariant-mass spectrum is shown in Fig. 1.

For the reconstruction of Ξ^-, only Λ candidates with invariant mass inside a 3σ = 10 MeV window around the book value are used. Primary Λ are rejected by an impact parameter cut ($\chi^2_{primary} > 5\sigma$) and a cut on the Λ decay vertex position ($z_{vertex} > 4$ cm). The remaining candidates are combined with secondary, negatively charged tracks ($\chi^2_{primary} > 3\sigma$). These Ξ^- candidates are accepted if having a good quality geometrical and topological detached vertex ($\chi^2_{geo} < 6\sigma$, $\chi^2_{topo} < 5\sigma$) and $z_{vertex} > 3$ cm. Fig. 2 shows the resulting $\Lambda\pi^-$ invariant-mass spectrum. The signal reconstruction efficiency is about 1.07%. The reconstructed mass value of (1.321 $\pm$ 0.003) GeV/c^2 is in a good agreement with the simulated one (1.321 GeV/c^2). The invariant-mass resolution is found to be 2.3 MeV/c^2.

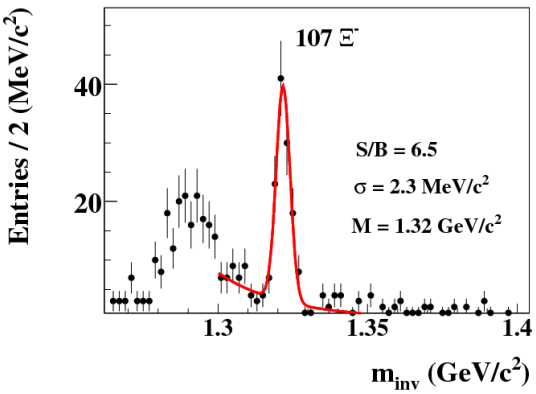

Figure 2: Reconstructed invariant-mass distribution of $\Lambda\pi^-$ candidates. 107 Ξ^- were reconstructed in 10^4 events. The S/B ratio is 6.5; the reconstructed mass value is 1.321 GeV/c^2.

References

[1] I. Kisel, Nucl. Instr. Meth. Phys. Res. **A566** (2006) 85

[2] S. Gorbunov *et al.*, Comp. Phys. Comm. **178** (2008) 374

[3] S. Gorbunov and I Kisel, CBM-SOFT-note-2007-003, http://www.gsi.de/documents/DOC-2007-May-14.html

$(\Xi^0\Lambda)_b$-dibaryon detectability study in the CBM experiment

I. Vassiliev[2,1], I. Kisel[2], and D. Malakhov[3]

[1]Goethe-Universität, Institut für Kernphysik, Frankfurt am Main, Germany; [2]GSI, Darmstadt, Germany; [3]Taras Shevchenko National University of Kyiv, Ukraine

The recent experimental evidence [1] for the existence of the H-dibaryon ($uuddss$, $I = J = 0$) provides the motivation for further experimental searches. The CBM setup gives an opportunity to detect H-dibaryons via their decay into the the $\Lambda\Lambda$ channel using the predicted decay length of $c\tau \approx$ 1-5 cm [2]. The Λ decay length of 7.89 cm allows to reconstruct the event topology and thus to efficiently distinguish the signal from the background.

To study the feasibility of H-dibaryon detection in the CBM experiment, a set of 10^4 central Au+Au events at 25A GeV, generated with UrQMD, was simulated. One $(\Xi^0\Lambda)_b$ decay ($c\tau$ = 3 cm) into $\Lambda\Lambda$ was added to each event in order to simulate the signal in the environment of background hadrons.

The main part of the background is created by the 32 primary Λ particles produced per central UrQMD event, out of which abought eight are reconstructed in the STS detector acceptance. A realistic geometry with two MVD stations at z = 5 cm and z = 10 cm (thickness 500 μm) and eight STS stations of double-sided segmented strip detectors were used for tracking. No kaon or pion identification with TOF is applied; however, it is important to use the time-of-flight measurements in order to select proton tracks from the sample for the reconstruction of the $\Lambda \to p\pi^-$ decays. A typical signal event $H \to \Lambda\Lambda \to p\pi^- p\pi^-$ is shown in Fig. 1.

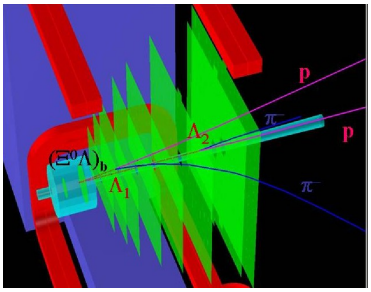

Figure 1: Event display with a H-dibaryon decay into $\Lambda\Lambda$

The H-dibaryon decay point is typically located about 5-15 cm downstream of the target. Λ decays were reconstructed as described in [3]. An impact parameter cut ($\chi^2_{primary} > 3\sigma$) provided rejection of primary Λ. The remaining daughter candidates were combined to form a H-dibaryon candidate using the KFParticle package [4], requiring good geometrical ($\chi^2_{geo} < 3\sigma$) and topological ($\chi^2_{topo} < 3\sigma$) vertices. The shape of the background invariant-mass spectrum was obtained using the event mixing technique. Its main part originates from the combination of direct Λ pairs, while the purely combinatorial contribution is one order of magnitude smaller.

The resulting signal and background invariant-mass spectra are shown in Fig. 2. For the normalisation, we assume a H-dibaryon multiplicity of $7 \cdot 10^{-3}$ as suggested by the statistical model [5] and a branching ratio of 2 % [2]. The signal reconstruction efficiency is about 0.37%. The reconstructed mass value of (2.32 ± 0.03) GeV/c^2 is in a good agreement with the simulated one (2.318 GeV/c^2). We obtain an invariant-mass resolution of 3 MeV/c^2.

Comparing with an earlier study [6], we see a drastic improvement of the invariant-mass resolution and, consequently, of the signal detection efficiency by the usage of the newly developed KFParticle software for the reconstruction of decay vertices.

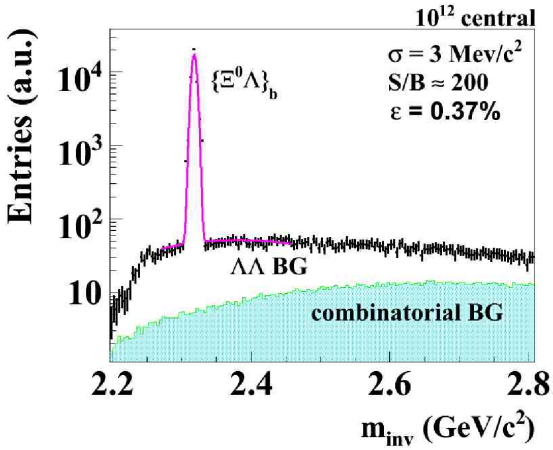

Figure 2: Reconstructed invariant-mass distribution of $\Lambda\Lambda$ candidates

References

[1] C. J. Yoon *et al.*, Phys. Rev. **C 75** (2007) 022201(R)

[2] J. Schaffner-Bielich, R. Mattielo and H. Sorge, Phys. Rev. Lett. **B 84** (2000) 4305

[3] I. Vassiliev, I. Kisel and M. Zyzak, Ξ^- *on-line reconstruction in Au+Au collisions at 25A GeV with CBM* (2010), this report

[4] S. Gorbunov and I Kisel, CBM-SOFT-note-2007-003, http://www.gsi.de/documents/DOC-2007-May-14.html

[5] J. Steinheimer, priv. comm. (2009)

[6] I. Vassiliev and I. Kisel, CBM Progress Report 2008, Darmstadt 2009, p. 62

Study of the capabilities of the CBM detector for open charm elliptic flow measurements

S. Seddiki[1,2] and F. Rami[2]
[1]IKF, Frankfurt, Germany; [2]IPHC, Strasbourg, France

Open charm will be one of the key observables of the future CBM experiment, as it is a penetrating probe of the early dense phase of the collision. In particular, its elliptic flow should be sensitive to the degrees of freedom of the medium at the early stage. In a purely hadronic scenario, open charm has a moderate interaction rate and should develop a small elliptic flow compared to lighter hadrons. The observation of a strong elliptic flow for open charm at FAIR would indicate the creation of a partonic medium [1]. The elliptic flow of open charm particles is also of particular importance for the issue of thermalization.

The present study aimed at investigating the capabilities of the CBM detector in measuring the elliptic flow of open charm. The latter will be measured using a Micro-Vertex Detector (MVD) based on MAPS-pixels. Previous studies [2] demonstrated that the experiment will allow to reconstruct a few 10^4 D-mesons per year. The measurement of their elliptic flow requires the determination of the collision reaction plane, which in CBM will be performed by a forward hadron calorimeter, the Projectile Spectator Detector (PSD).

In a first step, we evaluated the perfomance of the PSD detector for the reaction plane reconstruction. This was done for Au+Au collisions at 25 AGeV using the UrQMD event generator and the CBM simulation framework with GEANT as transport engine. The generated events were transported through a set-up including the MVD, the Silicon Tracking System (STS), located in a magnetic dipole field of 1 Tesla, and the PSD. Using the energy deposited in the PSD by spectator particles, the reaction plane of each event has been reconstructed using standard methods [3]. The results show that a very good proton/neutron separation is mandatory, since the protons are deflected by the magnetic field and spoil the azimuthal correlation of the particles with the reaction plane. The expected resolution on the reaction plane σ_{Φ_R}, assuming an ideal proton/neutron discrimination, is plotted in Figure 1 as a function of the collision centrality. A quite good accuracy can be achieved, in particular for mid-central collisions ($3fm \leq b \leq 9fm$).

The elliptic flow signal was simulated for D^+ mesons by introducing an azimuthal anisotropy with respect to the reaction plane. For each event, the reaction plane resolution was accounted for by smearing the azimutal angle of the particles according to a Gaussian distribution with σ = 40 degrees (Figure 1). The v_2 parameter was reconstructed using the Fourier analysis of the simulated azimutal distributions [3]. After applying a correction factor to account for the reaction plane resolution, the reconstructed v_2 was found to be very close to the input value within statistical errors. Figure 2 shows the expected statistical error on the integrated v_2 as a function of its magnitude using the statistics of D^+ particles corresponding to a typical CBM runtime (10^{12} events). The results indicate that, within this period, small D^+ azimuthal anisotropies could be measured only with large statistical uncertainties, while for larger v_2 values the experiment will be able to achieve good statistical accuracy (less than 15% for $v_2 \geq 0.1$). Further studies will take into account the effect of the combinatorial background contamination (not considered in the present work). The feasibility of p_t-differential elliptic flow measurements of D-mesons will be also investigated.

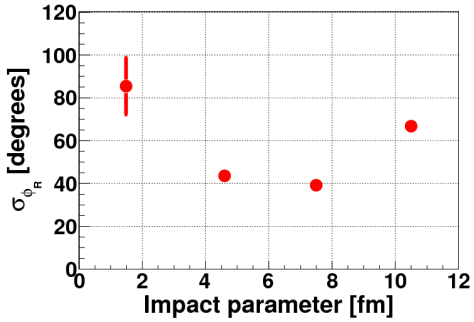

Figure 1: Reaction plane resolution as a function of the collision impact parameter (see text for details)

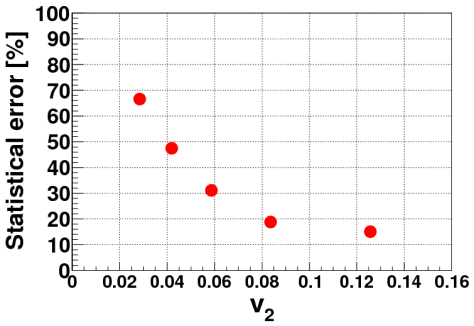

Figure 2: Statistical error on v_2 versus the magnitude of v_2 for the statistics of D^+ particles corresponding to a typical CBM runtime

References

[1] O. Linnyk *et al.*, Int. J. Mod. Phys. **E 17** (2008) 1367

[2] I. Vassiliev and I. Kisel, CBM Progress Report 2008, Darmstadt 2009, p. 60

[3] P. Danielewicz and G. Odyniec, Phys. Lett. **B 157** (1985) 146

Study of electron reconstruction in CBM at SIS100

E. Belolaptikova[1], T. Galatyuk[1], C. Höhne[2], and J. Stroth[1]
[1]Goethe-Universität, Frankfurt, Germany; [2]GSI, Darmstadt, Germany

The CBM experiment is being designed to measure hadronic, leptonic and photonic observables. The core of the experiment will be a silicon tracking and vertex detection system installed in a large-acceptance dipole magnet. Electron identification in CBM is provided by the RICH and TRD detectors. In addition, the Time-of-Flight (TOF) detector can also be used for electron identification at low momenta ($p < 1$ GeV/c). Moreover, mismatches of proton and kaon tracks to electron rings can be eliminated using TOF information. Three TRD stations have to provide sufficient identification capability for high-energy electrons and positrons and additional pion suppression for momenta large than 1.5 GeV/c. However, at 8 GeV/u kinetic beam energy, the momentum distributions of signal and background (leptonic and hadronic) sources change towards smaller values with respect to collisions at higher energies at SIS-300. Therefore, RICH and TOF information alone may be sufficient for electron identification at SIS-100.

Simulations were performed for central (b = 0 fm) Au+Au collisions at a beam energy of 8 GeV/u. The final state phase space distributions of hadrons were generated using the relativistic transport code UrQMD. Five electrons and five positrons were generated uniformly distributed in p, θ and ϕ and embedded into each UrQMD event. After event reconstruction and electron identification, each of the identified tracks is associated to its Monte Carlo information to assess the quality of the electron identification, expressed in terms of

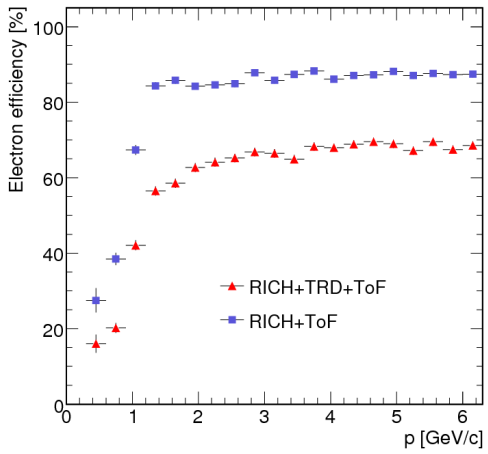

Figure 1: Electron identification efficiency as function of momentum for central Au+Au collisions at 8 GeV/u beam energy. The red triangles were obtained using RICH, TRD and TOF, the blue squares by the combination of RICH and TOF information only. The ANN cut value is -0.5.

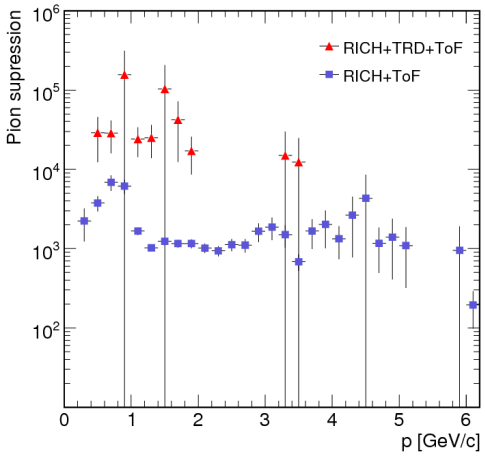

Figure 2: Pion suppression factor as function of momentum for central Au+Au collisions at 8 GeV/u beam energy. The red triangles were obtained using RICH, TRD and ToF, the blue squares by the combination of RICH and TOF information only. The ANN cut value is -0.5.

$$\text{electron efficiency} = \frac{\text{truly identified electrons}}{\text{electrons in the RICH acceptance}} \quad (1)$$

and

$$\text{pion suppression} = \frac{\text{pions identified as electrons}}{\text{pions in the RICH acceptance}}. \quad (2)$$

Two different methods were used for electron identification: 2-dimensional cuts and an Artificial Neural Network (ANN). The (preferrable) trained neural network gives continuous output values between -1 and 1, where -1 resembles wrong and $+1$ true electron candidates. Figures 1 and 2 show the electron efficiency and the pion suppression factor, respectively, obtained with an ANN cut at -0.5. A pion suppression above 10^3, as required for the study of low-mass vector mesons, at electron efficiencies above 80 % for $p > 1$ GeV can be obtained by using RICH and TOF information alone. These values are still subject to further optimization. Adding information from the TRD results in an even better pion rejection, but on a severe expense of electron efficiency.

Di-electron reconstruction with CBM

T. Galatyuk[1], C. Höhne[2], and J. Stroth[1]
[1]Goethe-Universität Frankfurt am Main; [2]GSI Helmholtzzentrum für Schwerionenforschung GmbH, Darmstadt

A strong excess of dilepton pairs over the yield expected from neutral meson decays was observed by hitherto existing high energy heavy-ion dilepton experiments (CERES, NA60, PHENIX). It is expected that electromagnetic radiation from the dense phase of the collision appears at low transverse momentum: pion-pion fusion, being the dominant process for populating ρ-like states in a hot pion gas, will favor ρ mesons located at low invariant mass and low transverse momentum. Special care should thus be taken by the CBM experiment to cover this range experimentally.

The NA60 and CERES experiments have difficulties to access low pair p_t and low masses at the same time. The NA60 experiment measures low-mass vector mesons via their electromagnetic decay to muons using the muon absorber technique. This technique works perfectly well for high-momentum muons; the major difficulty for NA60 lies in the identification of low-momentum muons. The acceptance of muons with $p_t < 0.2$ GeV/c drops by almost 2 orders of magnitude if compared to muons with $p_t > 0.5$ GeV/c [2]. A measurement of dilepton pairs with muons is naturally restricted to the invariant mass region above the 2-muon threshold of 2 times 210 MeV/c^2. The CERES experiment, on the other hand, has to apply a transverse momentum cut of 0.2 GeV/c on single electron tracks in order to suppress a huge combinatorial background from Dalitz decays of neutral pions.

In Fig. 1, the p_t-mass distribution within the CBM detector acceptance excluding any transverse momentum cut is presented. The acceptance is extended up to very low transverse momenta and very low masses. This shows that in CBM it will be possible to access the lowest invariant masses in a wide range of transverse momentum. Of course, the S/B ratio in particular in the enhancement region would increase if including a transverse momentum cut. Figure 2 shows the resulting e^+e^- invariant-mass distribution without transverse momentum cut for pairs with $0.2 < p_t/(\mathrm{GeV}/c) < 0.4$. The S/B ratio in the omega mass region is unchanged compared to the pt-integrated spectrum (S/B = 0.4) with single-electron p_t cut > 0.2 GeV/c. In the region where an enhanced dielectron yield is expected, i. e. from 0.2 to 0.6 GeV/c^2, the S/B ratio drops from 1/27 to 1/50 for the same comparison.

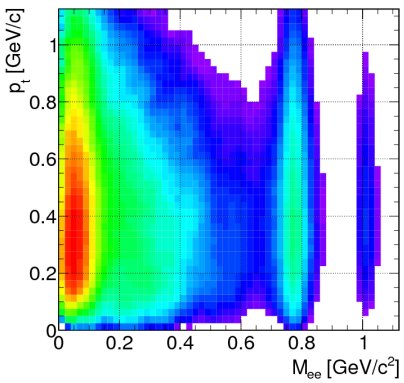

Figure 1: Distribution of accepted signal e^+e^- pairs in the transverse momentum and invariant mass plane after all cuts excluding any p_t cut. The data shown correspond to $2 \cdot 10^5$ simulated central Au+Aucollisions at 25 GeV/u. Event reconstruction was performed using the compact RICH geometry [1].

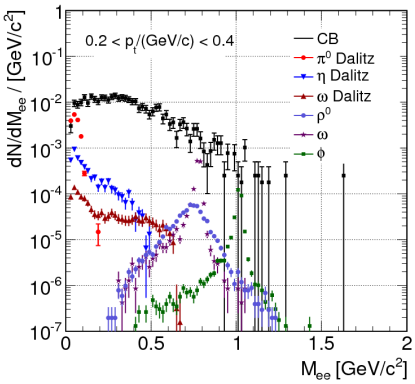

Figure 2: Invariant mass distribution for transverse momentum of the pairs = $0.2 < p_t/(\mathrm{GeV}/c) < 0.4$ after all cuts excluding any p_t cut. The data shown correspond to 10^6 simulated central Au+Au collisions at 25 GeV/u.

In this contribution we have shown with simulations including realistic detector descriptions to our current knowledge that CBM will be able to measure low-mass electron pairs in central Au+Au collisions at 25 GeV/u beam energy. The expected performance in terms of S/B ratio is well comparable to existing dilepton experiments [3]. A strong benefit of the CBM experiment will be that because of large availability of beam time and high reaction rates large statistics will be collected. This will allow a multi-differential and systematic analysis of interesting observables.

References

[1] S. Lebedev *et al.*, CBM Progress Report 2008, Darmstadt 2009, p. 20

[2] S. Damjanovic *et al.*, Nucl. Phys. **A 783** (2007) 327

[3] T. Galatyuk *et al.*, CBM Progress Report 2008, Darmstadt 2009, p. 64

Charmonium measurement in p + C collisions at SIS-100

A. Maevskaya[2], A. Kurepin[2], and C. Höhne[1]
[1]GSI, Darmstadt, Germany; [2]INR RAS, Moscow, Russia

Compared to elementary collisions, a suppressed charmonium production due to color screening in a deconfined medium is one of the long discussed signatures of Quark Gluon Plasma formation in high-energy heavy-ion collisions [1]. However, for the investigation of this process it is extremely important to know the reference, i. e. charmonium production in p+p as well as in p+A interactions at the same energy. Systematic investigations of the latter collisions allow to study the passage of charmonium states through cold nuclear matter. At the SPS, charmonium production in p+A collisions at 400 and 450 GeV was measured by the NA50 experiment [2]. So-called normal nuclear absorption of J/ψ production due to its passage through cold nuclear matter was observed. This suppression grows with increasing mass of the target nuclei. The extracted cross section for normal nuclear absorption of J/ψ-mesons is $\sigma_{abs} = 4.2 \pm 0.5$ mb. A weak energy dependence was assumed allowing to use this value for the investigation of J/ψ production in A+A collisions at 158A GeV. However, in recent measurement of J/ψ production in p+A collisions at 400 and 158 GeV, the NA60 experiment could demonstrate that the energy dependence of σ_{abs} is not weak but rising significantly to lower energies ($\sigma_{abs}(158GeV) = 7.6 \pm 0.7 \pm 0.6$ mb) [3]. Until then, the nuclear absorption at 158 GeV was underestimated and the J/ψ suppression effect thus overestimated. This experience clearly demonstrates that any study of J/ψ production in A+A collisions requires reference measurements in p+p and p+A collisions at the same energy. As SIS-100 will provide proton beams up to 30 GeV beam energy, these investigations can already be performed before SIS-300 comes into operation.

In this report, first feasibility studies for the measurement of J/ψ production in the dielectron decay channel will be presented for p+C collisions at 30 GeV beam energy. 50,000 J/ψ-mesons were generated by the HSD generator and mixed with 50,000 background events generated by UrQMD. For the combined spectrum, the J/ψ signal was scaled afterwards according to the multiplicity predicted by HSD ($5.06 \cdot 10^{-8}$ per event).

The simulations were performed with the complete setup of the CBM detector: a carbon target of 250 μm thickness, silicon tracking system (STS) with 8 stations placed inside a dipole magnetic field, compact ring imaging Cherenkov detector (RICH), segmented transition radiation detector (TRD), time of flight system (TOF), full electromagnetic calorimeter (ECAL). Tracks were identified as electrons by RICH, TRD and TOF using criteria as for the studies in A+A collisions at 25A GeV beam energy. Candidate J/ψ daughter tracks were required to have transverse momenta

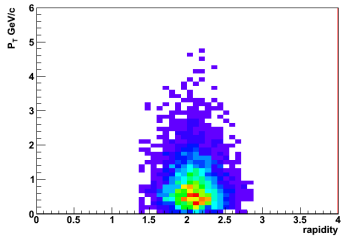

Figure 1: Distribution of reconstructed J/ψ in the p_t-y plane

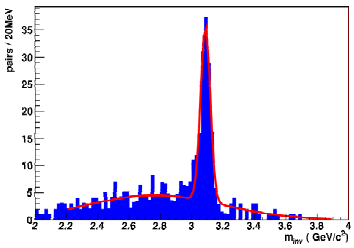

Figure 2: Invariant-mass distribution of electron-positron pairs in 10^{12} p+C interactions at 30 GeV beam energy

larger than 1.2 GeV/c. For improved electron identification, in this study also information from the ECAL was used if available. Figure 1 (left) shows the resulting phase space coverage for J/ψ reconstruction in CBM.

For the estimation of the background, 10^6 p+C collisions at 30 GeV from UrQMD were reconstructed in CBM. The background invariant-mass distribution was then reconstructed using the event mixing technique. The thus constructed background corresponds to 10^{12} events. Figure 1 (right) shows the expected invariant-mass distribution. The S/B ratio is 7.2, the significance 7.9 and the overall efficiency 7.4 %. According to the presented simulation, 330 J/ψ-mesons would be measurable for 10^{12} events. At an interaction rate of 1,5 MHz, this would correspond to eight days of data taking only. A J/ψ measurement in p+C collisions at 30 GeV beam energy is thus well feasible. Further investigations will reduce the full CBM detector used here to a start version with a RICH, TOF and only partially installed TRD and ECAL detectors.

References

[1] T. Matsui and H. Satz, Phys. Lett. B **178** (1986) 416

[2] B. Alessandro *et al.*, Phys. Lett. B **533** (2003) 167; P. Cortese *et al.*, Nucl. Phys. A **715** (2003) 679c; B. Alessandro *et al.*, Eur. Phys. J. C **33** (2004) 31

[3] R. Arnaldi and the NA60 collaboration, Nucl. Phys. A **830** (2009) 345c; E. Scomparin and the NA60 collaboration, Nucl. Phys. A **830** (2009) 239c

Muon simulations based on a realistic CBM muon detector system

A. Kiseleva[1], C. Höhne[1], E. Kryshen[2], A. Lebedev[1,3], M. Ryzhinskiy[2], and P. Senger[1]
[1]GSI, Darmstadt, Germany; [2]PNPI, Gatchina, Russia; [3]JINR-LIT, Dubna,Russia

The CBM muon detection system is designed to measure muon pairs from the decay of vector mesons ($\rho, \omega, \phi, J/\psi$) produced in heavy-ion collisions. The moderate momenta of the muons at FAIR collision energies necessitated the development of a muon detection concept with variable definition of absorber thickness according to the muon momentum. The strategy was described in [1]. In this report, we present simulations of low-mass vector meson decays into $\mu^+\mu^-$, using a realistic, modular geometrical description of the muon detectors as described in detail in [2] as well as a simple model of the detector response including cluster finding [3].

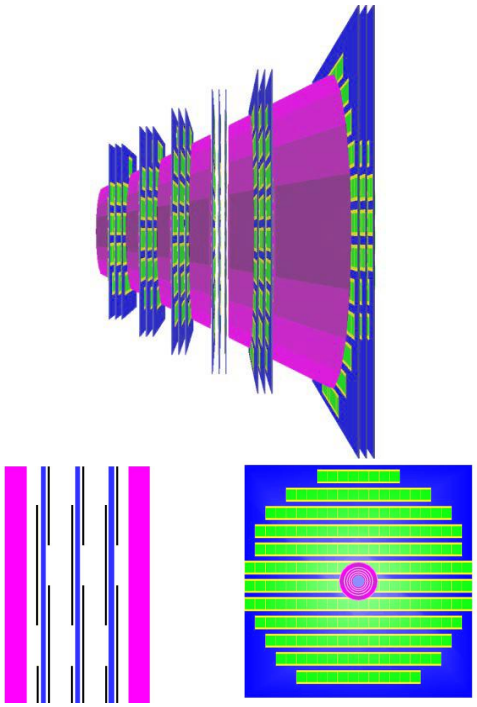

Figure 1: The modular design of the muon system. Top: total system; bottom left: side wiew of one gap between two absorbers with three detector layers; bottom right: front view of one detector layer with detector moduls.

The current design of the muon detector system foresees six hadron absorber layers (iron plates of thickness 20, 20, 20, 30, 35, 100 cm) and 15-18 gaseous tracking chambers located in triplets behind each iron slab. The geometry of this system is presented in Fig. 1, showing a side view of the full system (top), the side wiew of one gap with detector layers (bottom left), and the front view of one detector layer with detector moduls (bottom right).

In our simulations, we used a segmentation of the detector layers into pads with minimum size of $0.28 \times 0.28\,\mathrm{cm}^2$ and maximum size of $4.48 \times 4.48\,\mathrm{cm}^2$, corresponding to 560,000 channels in total. LIT tracking [4] is used for track finding in MuCh. Using the ideal detector response, we obtain a S/B ratio of 0.062 and a reconstruction efficiency of 1.8 % for the ω meson in central Au + Au collisions at 25A GeV, to be compared with S/B = 0.1 and $\epsilon = 1.9$ % obtained with a simplified, solid geometry [1]. With the realistic detector response, the efficiency deteriorates to 1.2 % because of the efficiency of the cluster finding procedure. The S/B ratio, however, is less affected (0.059). The invariant-mass spectra for both cases are shown in Fig. 2.

The next step of the muon simulations will be the implementation of a better detector response model based on the results of prototype tests.

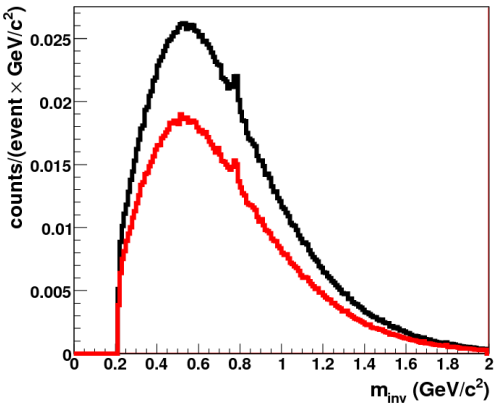

Figure 2: Invariant-mass spectra of reconstrcucted muon pairs from central Au + Au collisions at 25A GeV. The black histogram shows the result with ideal detector response, the red one that obtained with realistic response and cluster finding.

References

[1] A. Kiseleva *et al.*, CBM Progress Report 2008, Darmstadt 2009, p. 67

[2] E. Kryshen, V. Nikulin and M. Ryzhinskiy, CBM Progress Report 2008, Darmstadt 2009, p. 28

[3] E. Kryshen, V. Nikulin and M. Ryzhinskiy, CBM Progress Report 2007, Darmstadt 2008, p. 27

[4] A. Lebedev *et al.*, CBM Progress Report 2008, Darmstadt 2009, p. 81

Reconstruction of J/ψ meson p_t spectra via di-muons in CBM

A. Kiseleva[1], C. Höhne[2], E. Kryshen[3], A. Lebedev[2,4], M. Ryzhinskiy[3], and P. Senger[1]

[1]Institut für Kernphysik, Goethe-Universität Frankfurt, Germany; [2]GSI, Darmstadt, Germany; [3]PNPI, Gatchina, Russia; [4]JINR-LIT, Dubna,Russia

The reconstruction of J/ψ mesons via di-muon decays in CBM involves several detector systems: the silicon tracking stations for momentum and vertex reconstruction, the muon detection system for hadron absorption, and the time-of-flight system (TOF) for further background rejection of protons and kaons passing the absorber.

The muon detection system (MuCh) and the muon simulations are described in [1]. For the J/ψ measurements we use the first Transition Radiation Detector (TRD) station as a muon tracker station behind the last absorber (Fig. 1).

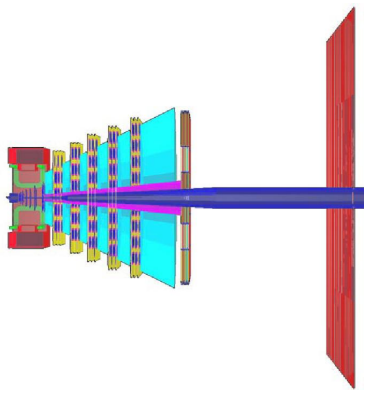

Figure 1: The CBM detector system for muon measurements. From left to right: Silicon Tracking Stations (STS), muon system (MuCh) with the first station of the Transition Radiation Detector (TRD) behind the last absorber, time-of-flight system (TOF).

The LIT global tracking package [2] is used for full track reconstruction. The resulting signal-to-background ratio for central Au + Au collisions at 25A GeV is S/B = 3 at a detection efficiency of ϵ = 14 %.

Invariant-mass spectra of the reconstructed muon pairs are shown in Fig. 2 for different p_t intervals. The background was determined using combinations of like-sign pairs, and a Gauss function was fitted to the signal peak for the determination of the reconstructed yield. This background description works well for $p_t < 1.8$ GeV/c. For larger transverse momenta, more careful background description methods have to be developed. The p_t distribution of the reconstructed J/ψ mesons (red) is shown in Fig. 3 together with the thermal input distribution generated by PLUTO (black). The red histogram corresponds to $2.7{\cdot}10^4$ reconstructed J/ψ mesons, which can be recorded within 19 hours assuming a reaction rate of 10^7 events/second.

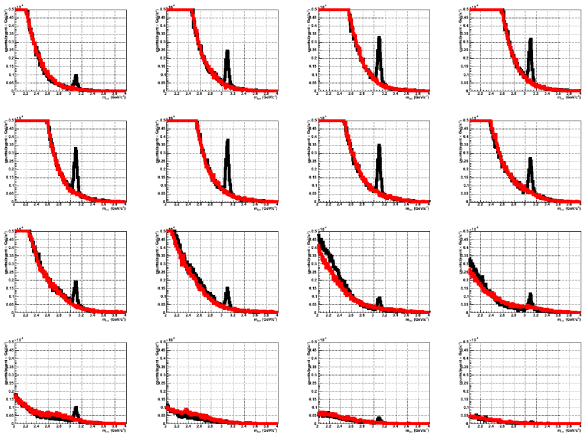

Figure 2: Invariant-mass spectra of reconstructed muon pairs from central Au + Au collisions at 25A GeV in different p_t intervals: from [0.0, 0.2] GeV/c (top left) to [3.0, 3.2] GeV/c (bottom right). The black lines shows the invariant-mass spectra of unlike-sign pairs, the red ones those of like-sign pairs.

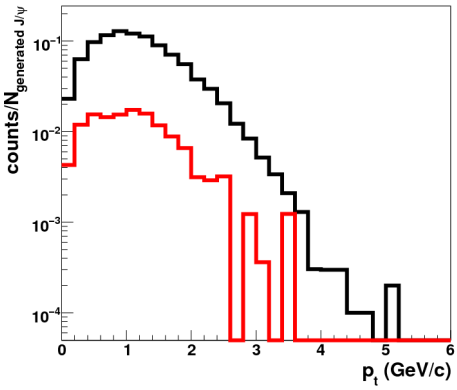

Figure 3: p_t distributions of J/ψ mesons generated by PLUTO (black line) and of reconstructed J/ψ mesons (red line), simulated for central Au + Au collisions at 25A GeV

References

[1] A. Kiseleva *et al.*, *Muon simulations based on a realistic layout of the CBM muon detector system*, this report

[2] A. Lebedev *et al.*, *Status of the global track reconstruction algorithms for the CBM experiment at FAIR*, this report

A di-muon trigger for CBM

A. Kiseleva[1], C. Höhne[1], E. Kryshen[2], A. Lebedev[1,3], M. Ryzhinskiy[2], and P. Senger[1]
[1]GSI, Darmstadt, Germany; [2]PNPI, Gatchina, Russia; [3]JINR-LIT, Dubna,Russia

The investigation of vector meson production in heavy ion collisions is one of the main goals of the CBM experiment. The experimental challenge is to perform high-statistics measurements of vector mesons via their dileptonic decays, because the branching ratios and/or the production cross sections are small. As an example, the dilepton yields per event predicted by the HSD transport code [1] for central Au + Au collisions at 25A GeV are 1.05×10^{-3} for ρ, 3.42×10^{-3} for ω, and 1.15×10^{-6} for J/ψ mesons. Therefore, a fast and efficient on-line event selection based on dilepton signatures is mandatory to reduce the data volume to the recordable rate.

The CBM muon detection system and the muon simulations are described in [2]. Previously, we presented a strategy for an on-line selection of muon pairs from J/ψ decays [3]. In this report, we outline a method to generate a trigger on muon pairs from the decay of low-mass vector mesons (LMVM) in the environment of a heavy-ion collision. Many of the muons from LMVM decays are too soft to pass the whole hadron absorber, which has a total thickness of 225 cm of iron. Therefore, we use as muon trigger stations the two detector triplets located in front of the second last and the last absorber layer, respectively (see Fig. 1). Moreover, we place a time-of-flight (TOF) detector providing a time resolution of 80 ps in the gap between the third last and the second last absorber layer.

In order to be selected as a di-muon candidate, the event has to meet the following conditions:

1. A minimum of 2 tracks should be reconstructable by the hit triplets in each station;
2. the tracks obtained by a linear fit to the hits in both detector triplets should point towards the target;
3. the velocity of the two particles should be close to the velocity of light (see Fig. 2).

If all these requirements are fulfilled, the event is recorded. We find that only one event out of 35 minimum bias Au + Au collisions at 25A GeV passes the trigger conditions. The trigger efficiency for ω mesons is 50 %.

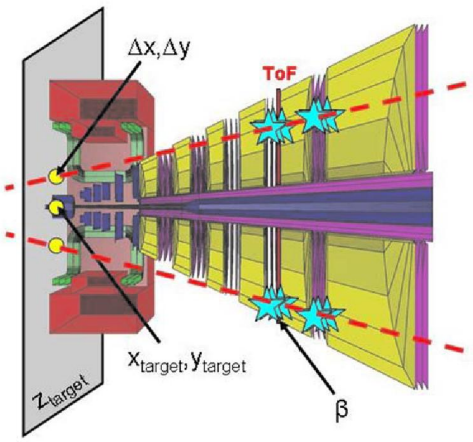

Figure 1: The CBM muon detection system. The stars correspond to hits required for the trigger. The dashed lines represent linear extrapolations of the tracks towards the target.

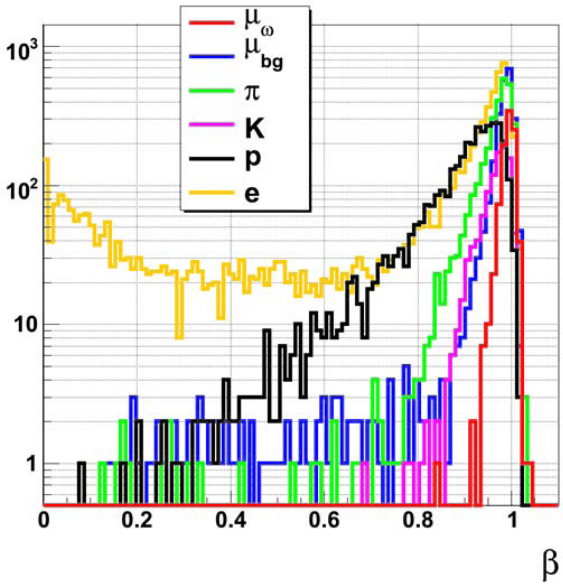

Figure 2: The velocity of the particles measured by the time-of-flight detector inside the muon system (see Fig. 1). The red histogram shows the distribution of signal muons originating from ω decays, the others those of various background sources.

References

[1] O. Linnyk *et al.*, Nucl. Phys. A **786** (2007) 183

[2] A. Kiseleva *et al.*, *Muon simulations based on a realistic layout of the CBM muon detector system*, this report

[3] A. Kiseleva *et al.*, *The di-muon trigger for CBM*, CBM Progress Report 2008, Darmstadt 2009, p. 69

Development of a trigger algorithm for the measurement of charmonia with the CBM experiment at FAIR

Partha Pratim Bhaduri[1] and Subhasis Chattopadhyay[1]
[1]Variable Energy Cyclotron Centre, 1/AF Bidhan Nagar, Kolkata-700 064, India

The Compressed Baryonic Matter (CBM) experiment [1], at the upcoming FAIR accelerator center at GSI Darmstadt, aims at the exploration of baryonic matter at high density produced in relativistic heavy-ion collisions. The proposed key observables include the measurement of charmonia, which can be measured via their decay into the dimuon channel [2]. The multiplicity of charmonium in the FAIR energy regime (E_{beam} = 10A - 40A GeV), however, is extremely small, which requires extreme interaction rates (up to 10^7 events per second) for the accumulation of sufficient signal statistics. The foreseen data acquisition system (DAQ) will be able to record events at a rate of 25 kHz. Thus, efficient on-line selection of events containing rare probes is mandatory. In this report, we describe the development of an algorithm for the on-line event selection of charmonium events and the rejection of background events baased on the information from a subset of the muon detectors only.

The aim is to select events on-line which contain muon pairs originating from charmonium decay. For faster selection, we have used hits only from the three layers of the last station which we call trigger station. Since our muon detection system is placed outside the magnetic field, high momentum muons coming from decay of J/ψ will have an approximately straight trajectory up to the last station.

The present algorithm creates triplets of all possible combinations of one hit from each layer of the trigger station. Each triplet is fitted with a straight line passing through the origin, i. e. X = m_0*Z, Y= m_1*Z. The triplet is accepted if the χ^2 of the fits in both projections satisfy $\chi^2_x < 0.2$, $\chi^2_y < 0.2$, i. e. if it can reasonably well be back-extrapolated to the target. Hits contributing to an accepted triplet are not used for the creation of other triplets. For each accepted triplet, the parameter $\alpha = \sqrt{(m_0^2 + m_1^2)}$ is calculated.

The event selection is composed of four cuts, which are applied sequentially:

1. The event must have at least one triplet.
2. The event must have at least two triplets.
3. At least one of the triplet satisfies the condition $\alpha > 0.183$, i. e. has a high transverse momentum.
4. At least two of the triplets satisfy the condition $\alpha > 0.183$.

For estimating the performance of the proposed algorithm, we have simulated 80,000 minimum bias Au+Au events at 25A GeV, generated with UrQMD, for the background and 1,000 Pluto events for signals from J/ψ decays into muon pairs. The results for the background suppression factor (BSF) and the J/ψ signal efficiency are shown in Tables 1 and 2, respectively. The signal efficiency is obtained from full track reconstruction and the measurement of the area under the invariant-mass peak.

Table 1: Background suppression factors for minimum bias Au+Au events at 25A GeV for different trigger cuts

cut	accepted events	statistical error	B.S.F
1	2624	1.95	30
2	255	6.26	314
3	91	10.4	879
4	56	13.36	1438

Table 2: J/ψ reconstruction efficiency for different trigger cuts

Cut	Reconstruction efficiency
no cut	29.3
cut 1	29.2
cut 2	24.5
cut 3	24.2
cut 4	15.3

The results demonstrate that the required event rejection of > 400 can be achieved by the proposed algorithm, using only a small fraction of the total data rate (hits from the last three layers of the MUCH system), with reasonable loss of signal efficiency. The results compare well with an earlier investigation of a di-muon trigger using a slightly different algorithm [3]. Work is ongoing to improve the signal reconstruction efficiency.

References

[1] P. Senger, J. Phys. G: Nucl. Part. Phys. **31** (2005) S1111

[2] A. Kiseleva *et al.*, CBM Progress Report 2007, Darmstadt 2008, p. 26

[3] A. Kiseleva *et al.*, CBM Progress Report 2008, Darmstadt 2009, p. 69

Reconstruction of π^0 and η with ECAL

S.M. Kiselev
ITEP, Moscow, Russia

For the study of the detection of $\pi^0 \rightarrow \gamma\gamma$ and $\eta \rightarrow \gamma\gamma$ in CBM, $2 \cdot 10^4$ central Au+Au events at 25A GeV from UrQMD, simulated and reconstructed in ECAL by M. Prokudin [1], were analyzed in the framework of the `cbmroot` package (trunk JAN09). The ECAL wall of the size X×Y=12 × 9.6 m^2 with a beam hole of 0.8 × 0.8 m^2 is located at 12 m from the target. Reconstructed photons with $p > 0.3$ GeV/c and $\chi^2_{cluster} < 3$ were used for the analysis.

The average ECAL acceptances are 50 %, 12 % and 9 % for "vertex" photons ($R_{vtx} < 1$ mm), primary $\pi^0 \rightarrow \gamma\gamma$ and primary $\eta \rightarrow \gamma\gamma$, respectively. The reconstruction efficiency is 43 %, 19 % and 27 % for "vertex" photons, π^0 and η, respectively. Figure 1 shows the invariant-mass spectra of two reconstructed photons. For the extraction of the signal, the event mixing technique was used, combining each event with the five previous events. The resulting background spectrum (B_{mix}) was normalized to the same-event one (S+B) in the region $M_{\gamma\gamma} > 0.3$ GeV, and subtracted. We find that for the π^0, the extracted signal is in a good agreement with the true one. The signal width is 15 MeV. The extraction of the η signal would require statistics of the order of 10^6 events. Table 1 gives the signal-to-background ratios and significances for π^0 and η in different p_t bins. The S/B ratio for η is about five times smaller than that obtained with ideal ECAL reconstruction [2]. More details of the analysis can be found in [3].

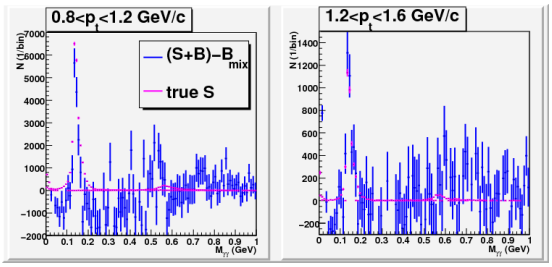

Figure 1: Extracted signal $(S+B)-B_{mix}$ (blue histogram) and true signal S (red) in the $\gamma\gamma$ invariant-mass spectrum for central Au+Au collisions at 25A GeV

p_t [MeV/c]	0.4 - 0.8	0.8 - 1.2	1.2 - 1.6
π^0	0.3 (17)	0.8 (13)	1.8 (8)
η	0.01 (1.0)	0.02 (0.7)	0.04 (4.0)

Table 1: Signal-to-background ratios in % and significances (in brackets) in the $\pm 2\sigma$ region in different p_t bins for central Au+Au collisions at 25A GeV

An analogous analysis was performed on 10^6 p+C (b=0 fm) events from UrQMD at the SIS-100 energy 30 GeV (`cbmroot` trunk MAY09, reconstructed in ECAL by M.Prokudin). Reconstructed photons with $p > 0.5$ GeV/c and $\chi^2_{cluster} < 9$ were used in the analysis. Because of the low multiplicity of secondaries, the reconstruction efficiencies in this case are close to 100 % (95 %, 93 % and 95 % for "vertex" photons, primary π^0 and primary η, respectively). The resulting invariant-mass spectra after background subtraction are shown in Fig. 2. We find a good agreement of reconstructed signal and input signal for both π^0 and η. The signal width is about a factor of two smaller than in case of Au+Au collisions (8 MeV for π^0 and 20 MeV for η). The S/B ratios and significances in different p_t bins are summarised in table 2. Details of the analysis can be found in [4].

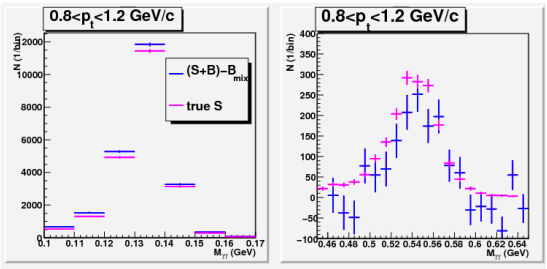

Figure 2: Extracted signal $(S+B)-B_{mix}$ (blue histogram) and true signal S (red) in the $\gamma\gamma$ invariant-mass spectrum for central p+Au collisions at 30 GeV

p_t (MeV/c)	0.4 - 0.8	0.8 - 1.2	1.2 - 1.6
π^0	1.1 (229)	3.7 (129)	8.1 (62)
η	0.05 (12)	0.1 (13)	0.3 (9)

Table 2: Signal-to-background ratios in % and significances (in brackets) in the $\pm 3\sigma$ region in different p_t bins for central p+Au collisions at 30 GeV

References

[1] M. Prokudin, *Photon reconstruction and matching*, 13th CBM collaboration meeting (2009), https://www.gsi.de/documents/DOC-2009-Mar-114-1.pdf

[2] S. M. Kiselev, CBM Progress Report 2008, Darmstadt 2009, p. 71

[3] S. M. Kiselev, *Reconstruction of π^0 and η mesons with ECAL*, 13th CBM collaboration meeting (2009), https://www.gsi.de/documents/DOC-2009-Mar-115-1.pdf

[4] S. M. Kiselev, *Reconstruction of π^0 and η mesons at SIS100*, 1st CBM-Russia-JINR Collaboration meeting (2009), http://cbm2009-may.jinr.ru/files/090520DubnaRecoPi0EtaSIS100.ppt

Reconstruction of Σ^0 in p+C collisions at 30 GeV with the ECAL

S.M. Kiselev
ITEP, Moscow, Russia

The feasibility of the reconstruction of the decay $\Sigma^0 \rightarrow \Lambda\gamma$ was studied on a sample of 10^6 p+C (b=0 fm) events from UrQMD at the SIS-100 energy 30 GeV (`cbmroot` trunk MAY09, reconstructed in ECAL by M.Prokudin). For the reconstruction of the decay $\Lambda \rightarrow p\pi^-$, the hyperon analysis package of E. Kryshen was employed [1]. Here, a Λ is accepted if each of its decay products has MC points in at least four STS stations (placed at 30, 35, 40, 50, 60, 75, 95, 100 cm from the target) and is considered reconstructed if each decay product has a correctly reconstructed track, i. e. $\geq$ 70 % of track hits belong to the same MC track. PID information is not used in the analysis. The cut strategy for hyperons includes 6 cut variables: target impact parameters for positive and negative tracks, distance of closest approach for these tracks, χ^2 and z-position of the fitted vertex, and target impact parameter of the Λ candidate. The cut values optimized for Λ in central Au+Au events at 6A GeV [1] were applied in the current analysis. The quality of the Λ signal for p+C at 30 GeV (σ_m = 1.37 MeV, S/B=39.2) is similar to that obtained for Au+Au events. The total efficiency of 5.2 %, however, is about twice lower. It can be expected that this efficiency can be improved by tuning of the cut parameters.

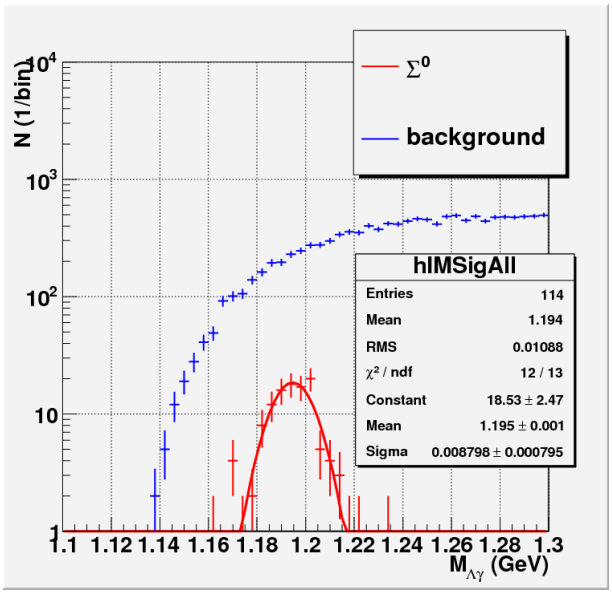

Figure 1: Invariant-mass spectra of signal and background $\Lambda\gamma$ pairs for p+C collisions at 30 GeV

Reconstructed Λ candidates within the mass range $m_\Lambda \pm 2\sigma$ and reconstructed γ with $p > 0.5$ GeV/c and $\chi^2_{cluster} < 9$ were chosen as candidates for the Σ^0 analysis. The main origin of the background are primary Λ and γ from π^0 decays ($\sim$4 γ in events with a Λ candidate). Fig. 1 shows the invariant-mass distributions of $\Lambda\gamma$ pairs. We obtain a signal-to-background ratio of about 5 %; the significance is 2.2. In order to arrive at a reasonable significance level, event statistics of the order of 10^7 is required.

The main characteristics of the analysis are summarised in Table 1. With the current statistics (114 reconstructed signal pairs), it is not possible to study the dependence of S/B on transverse momentum. The physical motivation for the study of Σ^0 and more details of the analysis can be found in [2].

statistics (events)	10^6
yield/event	0.03
acceptance	4.6 %
reconstruction efficiency	46 %
cut efficiency	14 %
total efficiency	0.3 %
σ_m	8.7 MeV
$S/B_{2\sigma}$	4.7 %
significance	2.2

Table 1: Main characteristics of the Σ^0 analysis for p+C collisions at 30 GeV

References

[1] E. Kryshen, *Feasibility of hyperon measurements at SIS 100*, 1st CBM-Russia-JINR Collaboration meeting (2009), http://cbm2009-may.jinr.ru/files/2009-05-20-dubna-sis100-hyperons.ppt

[2] S.M. Kiselev, *Reconstruction of Σ^0 in p+C at SIS100*, 14th CBM collaboration meeting (2009), https://www.gsi.de/documents/DOC-2009-Oct-235-1.pdf

Results of a Hough Tracker implementation for CBM

C. Steinle, A. Kugel, and R. Männer
Department of Computer Engineering V, University of Heidelberg, Germany

The customized Hough transform is a global method for track finding which transforms all STS detector hits into a parameter space according to the components of the track momentum (θ, $-q/p_{xz}$, m). As the direct implementation of this three-dimensional Hough space requires a huge amount of memory, this situation is avoided by the decomposition of the Hough space into several two-dimensional layers, where the number of parallelly computed ones can be adjusted to the existing hardware resources. The goal of the implementation is to process the tracking with maximum speed, which means in detail the processing of one detector hit per clock cycle. Thus the complicated calculations of the customized Hough transform according to the real detector geometry and the real magnetic field are implemented through look-up tables (LUTs), which can be calculated offline by any sufficiently precise algorithm.

Since the first approach for the application of the customized Hough transform to the CBM experiment, the usage of special parallel hardware is suggested to practically and applicably fulfill the speed requirement for a tracking decision system able to cope with 10^7 interactions per second. As such an implementation is obviously quite complicated to be build from scratch, three different levels were developed with increasing computational speed and complexity.

On the first level, a C++ software implementation package for the CBMROOT framework is designed to simulate the efficiency behaviour of the customized Hough transform. For this purpose it is clear that hardware-specific instruction sets should be avoided such that the software can run on as many computational platforms as possible. Hence substantiating the most abstract algorithm description, this is obviously the slowest implementation.

The second level of implementation is a rapid prototyping system for a conceivable multi-chip platform [1], which actually forms the third level. During the development of this second-level implementation, the Sony Playstation III with its Cell BE became also completely operational [2], because it delivers the same output data based on the same input data as the CBMROOT package.

The implementation on the third level is currently only preliminary. This means that there is no prototype, but all necessary concepts are proven to be generally operational by the HDL simulator MODELSIM, and the assumed timing behaviour is evaluated by CBMROOT framework simulations. As the parallelism level of a FPGA is exhaustive, in particular at the level of a multi-chip platform, the results of but three implementations are presented here, because they are of special interest. The first one can be characterized by using just a single chip, the second one by being the fastest possible implementation and the third one by realizing a good trade-off between timing performance and hardware requirement.

Architecture	**Time for a single event**	**Required platforms for CBM**
PC: P4@3GHz and 2GB RAM; not optimized CBMROOT simulation	4.0 s	10,000,000
Playstation III: CellBE@3.1GHz, 256MB RAM and 256kB LS; vectorized, 6SPUs	21.5 ms	53,750
1 FPGA: xc5vlx110-ff1760-3@125MHz; implementing 1 histogram layer	752.2 μs	1,881
15 FPGAs: xc5vlx110-ff1760-3@250MHz; implementing all histogram layers	62.8 μs	157
3 FPGAs: xc5vlx110-ff1760-3@250MHz; implementing 14 histogram layers	88.5 μs	222

Figure 1: Summary of the results obtained for all implementations

Figure 1 summarizes the results for all introduced implementations with regard to the time consumption for a single event and, based on this, to the number of platforms required to fulfill the CBM requirements. As the presented results are quite satisfactory with regard to the timing behaviour, the next step is obviously given by the realization of a FPGA platform prototype. In addition to this, the efficiency of the algorithm can be possibly improved by the usage of more appropriate LUTs and the application of successive decision units.

References

[1] C. Steinle, A. Kugel and R. Männer, CBM Progress Report 2007, Darmstadt 2008, p. 11

[2] C. Steinle, A. Kugel and R. Männer, CBM Progress Report 2008, Darmstadt 2009, p. 80

Optimization of the CA track finder for the STS geometry with overlapping sensors

D. Golubkov[1], I. Kisel[2], A. Kotynia[2], I. Rostovtseva[1], and Y. Zaitsev[1]
[1]ITEP, Moscow, Russia; [2]GSI, Darmstadt, Germany

Our previous work on adaptation of the Cellular Automaton (CA) track finder [1] to the realistic STS geometry with overlapping sensors allowed to recover the high tracks-finding efficiency [2] which it has had for the simplified STS description with sensors of each station arranged at the same Z position (the "same-Z" geometry).

Below we report on a detailed study of the behaviour of the track finder for the realistic STS geometry that addressed the problem of an increased number of clone and ghost tracks relative to the same-Z geometry.

In the realistic STS geometry, the sensors overlap, the hits within the same station have different Z coordinates, and also the detector contains more material. A larger number of hits (both true and fake) is produced in the sensor overlap regions giving more than one hit per track per station, additional hits also coming from the increased number of delta electrons.

To reduce the combinatorics, we optimized the X- and Y-windows used in the track candidate search based on the pull distributions (see Fig. 1).

The main component of the clones turned out to consist of short pieces of long MC tracks, broken due to hits which did not fit into the Y-window at the step of the doublet creation. These broken tracks ($\sim 4\%$) become effectively lost for analysis, since one of the pieces has low spatial accuracy, and the other has bad momentum resolution. From our studies we found that the increase in the number of clone tracks is not connected to the inhomogeneity of the magnetic field, but to the increase in the amount of multiple scattering; the main contribution to ghost tracks originates from the large hit density due to fakes (after an artificial removal of fakes, the ghost rate of about $4-5\,\%$ decreases down to $\sim 0.2\,\%$). If some hit occurs within about 5σ of the error ellipse, it is practically equivalent to the true hit for the track finder. Thus, a fake hit can be picked up instead of the true hit, which reduces the efficiency of the hit assignment.

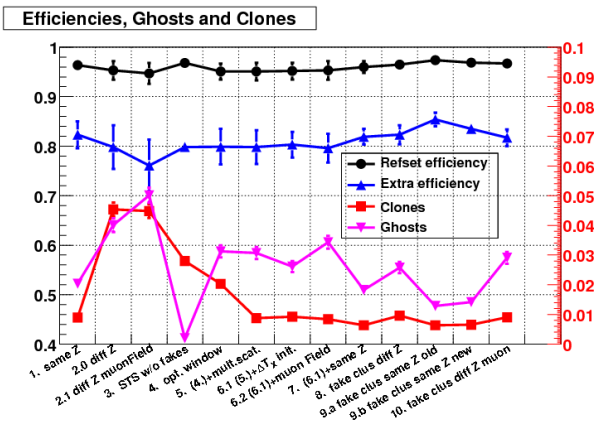

Figure 1: The track reconstruction efficiency, ghost and clone rates at the different steps of the study. The results were obtained using an MC sample of central Au+Au collisions at 25A GeV.

To improve the quality of the hit-to-track assignment, it is planned to develop a procedure similar to the outlier removal applied during the track fit. To estimate the possible increase in efficiency which can be achieved with such a procedure, we modified the track efficiency calculation by considering all hits within 5σ to belong to the track, even if the track finder picked up a fake hit in that plane. After such a "fake clusterization" procedure the number of tracks in which 100% of hits belong to the same MC track increased by $\sim 19\%$, but the relative percentage of ghosts and clones did not change significantly. This indicates that the remaining ghosts are mainly fakes (i. e. tracks consisting of a random combination of fake hits), and a cut on the fit χ^2 might be useful for their suppression. It would be also helpful to further optimize the STS geometry and reduce the combinatorics and the number of fakes, probably by re-optimization of the lengths and stereo-angles of the strips.

To summarize, the following modifications were implemented and included into `cbmroot` to decrease the number of clones and ghosts: more accurate account for multiple scattering; optimization of the X- and Y-windows for track candidate search based on pulls; optimization of the initial value of ΔT_x in singlets.

With the described modifications, the problem with clones was solved ($\sim 0.8\%$ of clones as in the same-Z geometry). The number of ghosts was reduced, too, but for further reduction more studies are necessary (track fit, outlier removal, STS geometry optimization).

References

[1] I. Kisel, Nucl. Instr. Meth. Phys. Res. A **566** (2006) 85

[2] D. Golubkov *et al.*, CBM Progress Report 2008, Darmstadt 2009, p. 76

Speed optimization of the CA based track finder in the CBM experiment

I. Kisel[1] and I. Kulakov[2,3]

[1]GSI, Darmstadt, Germany; [2]Goethe-Universität Frankfurt, Germany; [3]University of Kyiv, Ukraine

The cellular automaton (CA) based track finder (CAT) will be used both for off-line and for on-line track reconstruction in the CBM experiment [1]. Thus, a very fast and flexible realisation of the CAT algorithm is required. Therefore, the standalone CAT was modified for time optimization and execution parallelization.

First, the number of considered combinations of hits to find track segments was significantly decreased. In addition, one branching operator in the loop was removed. This resulted in a speed-up by a factor of 1.5.

Second, in order to avoid the repetition of calculations in loops, the needed values were prepared in advance. In addition, some loops were merged. These modifications led to an additional speed-up by a factor of 1.25.

Algorithm parallelization was done by reorganization in such a manner that commands of separate iterations of loops can be concurrently executed on several cores. For this purpose, iterations of main loops were reorganized, such that for each iteration the execution result of any other iteration is not required. Also, data needed for each iteration were separated in memory, such that they become independent, and the search of track segments, which takes 98 % of the time in the initial version, can be run in parallel at different stations.

For the testing of the optimized algorithm, 100 central Au+Au UrQMD events at 25A GeV were simulated. A detector geometry with 2 MAPS and 8 double-sided strip detectors was used. The efficiency and time of execution were monitored. A processor with two cores Pentium D 3.0 GHz with 2 MB L2 cache was used for the tests.

The efficiency is defined as the number of reconstructed tracks assigned to generated particles divided by the number of all reconstructable tracks. Reconstructable tracks are those having momentum greater than 0.1 GeV/c and intersecting the sensitive regions of at least four consecutive stations. A reconstructed track is assigned to a particle if at least 70 % of its hits were caused by it. If more then one track is assigned to the particle, all additionally reconstructed tracks are regarded as clones. A reconstructed track is called ghost if it is not assigned to any particle.

The reconstruction efficiency of the optimized algorithm (Fig. 1) is similar to that obtained with the initial version. The levels of clones and ghost tracks are about 3.5 %.

Timing results are shown in Table 1. For a comprehensive analysis of the package, both CPU and real times were measured. The CPU time is the sum of working times of all cores. The real time is the time spent by CAT on the track finding execution. In order to separate the gain factors due to optimization and parallelization, CAT was run both on one core and on two cores. Parallelization, using the Intel Threading Building Blocks (TBB) [2] gives a speed-up factor of 1.2 only, while on the two-core processor, a speed-up factor of 2 is expected. This can be explained by the dependence at data level of the tasks executed in parallel. Also the additional overhead for the parallelization control could give a certain influence on the speed of CAT. This overhead can be estimated to be 15 %. The algorithm optimization gives an additional speed-up by a factor of 2 (see Table 1).

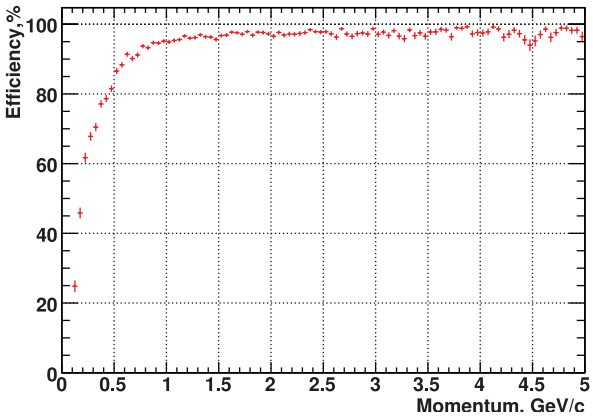

Figure 1: Track reconstruction efficiency versus momentum

	w/o TBB	with TBB	
		1 core	2 cores
CPU time [μs/track]	575	278	321
Real time [μs/track]	576	286	233

Table 1: Execution time of the initial (w/o TBB) and the optimised (with TBB) versions of CAT

In addition, some tuning of the algorithm parameters was done, which reduced the time per event to 120 ms. Thus, a total speed-up by a factor of 5 was achieved. Further optimization and parallelization of the Cellular Automaton based track finder will be investigated.

References

[1] I. Kisel, Nucl. Instr. Meth. Phys. Res. A **566** (2006) 85

[2] Intel Threading Building Blocks, `http://www.threadingbuildingblocks.org`

SIMDized particle reconstruction in the CBM experiment

I. Kisel[1] and M. Zyzak[2,3]

[1]GSI, Darmstadt, Germany; [2]Goethe-Universität Frankfurt, Germany; [3]University of Kiev, Ukraine

The reconstruction of vertices is an inherent task in high-energy physics experiments. Both the primary vertex reconstruction and the reconstruction of decayed particles from their daughter particles are prerequisites for many physics analyses. Since the reconstruction algorithm is usually called frequently during the analysis, the parallelization - and thus speed-up - of this function is highly desirable.

Single instruction, multiple data streams (SIMD) allow to parallelize the operations. The basic data unit of SIMD is a vector – a row of individual numbers or scalars. Using a 4-element, a four-way single-precision floating-point calculation can be executed in parallel. The implementation of SIMD instructions can hence increase the program execution speed up to 4 times [1]. Since all modern processors support SIMD instructions, SIMDization of the code is a suitable way of program parallelization.

SIMD instructions were implemented into the scalar version of the particle reconstruction algorithm [2]. The algorithm was tested on p + C UrQMD events at 30 GeV for the primary vertex reconstruction case and on central Au + Au UrQMD events at 25A GeV using the Λ reconstruction procedure for the secondary particle case. A Pentium Dual E2180 2 GHz processor with 1 MB L2 cache was used for the tests.

The difference between the vertex coordinates obtained with the scalar and with the SIMDized version is of the order of 0.01 μm for primary vertices and 10 μm for Λ decay vertices, while the residuals and pulls are almost the same in both cases (see Tables 1 and 2). The speed-up factor obtained by the SIMDization is about 1.5.

	Residuals [μm]	Pulls
x	18.9 / 19.0 / 19.0	1.14 / 1.15 / 1.21
y	18.6 / 18.5 / 18.7	1.13 / 1.13 / 1.14
z	100.6 / 101.2 / 101.4	1.18 / 1.20 / 1.23

Table 1: Residuals and pulls of the vertex coordinates for the code versions scalar / SIMD / SIMD with field approximation in the case of primary vertex reconstruction in p+C events at 30 GeV

In the scalar version of the code, the full magnetic field map is used, which complicates the implementation of SIMD instructions. This is the reason for the speed-up factor being below 4. Thus, an approximation of the magnetic field was performed in order to SIMDize the algorithm in a more efficient way. All three components of the magnetic field were approximated with parabolas along the particle trajectory. The corresponding coefficients were stored as parameters of the particle. This step allows to reduce the number of the magnetic field map accesses and simplifies the SIMDization of the code. Currently, the magnetic field map is still accessed at the field approximation step.

This magnetic field approximation was implemented in the SIMDized version of the code. The residuals and pulls of the coordinates are similar to that of the code version using the full map (Tables 1 and 2). The speed-up factor with respect to the scalar version is about 3.

	Residuals	Pulls
x	0.011 / 0.013 / 0.011 cm	1.50 / 1.51 / 1.64
y	0.015 / 0.015 / 0.015 cm	1.42 / 1.50 / 1.48
z	0.18 / 0.18 / 0.20 cm	1.63 / 1.69 / 1.74
M	1.2 / 1.2 / 1.5 MeV/c^2	1.54 / 1.54 / 1.67

Table 2: Residuals and pulls of the vertex coordinates and of the reconstructed invariant mass for the code version scalar / SIMD / SIMD with field approximation in the case of Λ reconstruction in central Au + Au collisions at 25A GeV

In summary, the SIMDization of the particle reconstruction code was performed, resulting in a speed-up factor of about three. A further increase in speed can be achieved by the full magnetic field approximation, also on the detector stations.

References

[1] S. Gorbunov *et al.*, Comp. Phys. Comm. **178** (2008) 374

[2] S. Gorbunov and I. Kisel, CBM-SOFT-note-2007-003 (2007)

Scalability of the SIMD Kalman Filter track fit based on vector classes

I. Kisel[1], M. Kretz[2], and I. Kulakov[3,4]

[1]GSI, Darmstadt, Germany; [2]Universität Heidelberg, Germany; [3]Goethe-Universität Frankfurt, Germany; [4]University of Kyiv, Ukraine

The core of event reconstruction in the CBM experiment is the Kalman filter (KF) [1]. Therefore, the speed of KF-based algorithms is of crucial importance for on-line data processing. One of the processors features which can speed up computations is the SIMD instruction set [2], which allows to pack several data items in one register and to operate on all of them in one go, thus achieving more operations per clock cycle.

A standalone benchmark for the Kalman Filter track fit, using the SIMD header interface, is described in [3]. Recently, a user-friendly interface to the SIMD instructions, the vector classes library (Vc) was developed [4]. The Vc library supports all types of CPU instructions and also the GPU LRBni instructions set, thus expanding the development possibilities. We adapted the KF track fit benchmark to make use of the Vc library, which necessitated the redefinition of some data types and constants to use the correspondent Vc types. Moreover, a procedure for input data packing into the SIMD vectors was added. The final version of SIMD KF track fit was tested on the 8-core computer lxir039 with two Xeon X5550 2.7 GHz processors and 8 MB L3 cache. The gcc 4.4.2 compiler was used for the tests. The Intel Threading Building Blocks (TBB) software package was employed for execution parallelization between cores.

Fit quality tests show good results with residuals of 49 μm and 44 μm for the x and y track parameters, respectively, and a relative momentum resolution of 0.7 %. In order to compare with the initial version, the fitting time per track was measured for both versions (see Table 1). In addition, each version was run both on one core and on all 8 cores by usage of TBB. As Table 1 shows, the version based on Vc shows almost the same results as with the initial version. This is expected because the SIMDized operations in the benchmark are simple enough not to be very sensitive to the implementation.

	SIMD header		Vc	
	w/o TBB	TBB	w/o TBB	TBB
Time [μs]	0.448	0.053	0.422	0.052

Table 1: Fitting time per track for different SIMD KF track fit versions executed with and without TBB on a 8-core computer. 1,000 tracks per thread were fitted.

The scalability of the benchmark on the lxir039 machine was also investigated. For this purpose, two possibilities were added to the benchmark: to run the SIMD KF fit on any set of cores, and to specify different distributions of tasks between cores. Each physical core on lxir039 has two logical cores because of the hyper-threading technology. The track fitting was run on various numbers of cores. Figure 1 shows the scalability on the physical cores. Here, track fitting was parallelized by execution of one thread per one logical core. We tested the fitting of 10, 100 and 1000 tracks per thread.

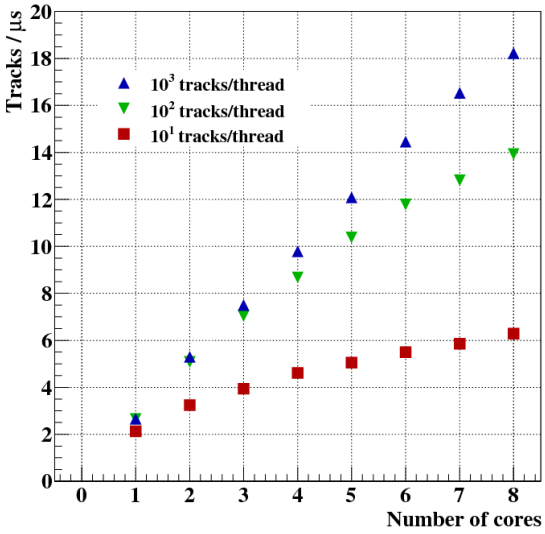

Figure 1: Scalability of the SIMD KF track fit

Our results show that for a small number of tracks per thread, the speed-up does not scale with the number of used cores. This can be understood by the large overhead with respect to the execution time. The maximum speed-up of a factor of 8 was reached for the case of 1,000 tracks per thread, which is in a good agrement with what is expected for a 8-core computer. The dependence of the speed on the number of cores is linear in this case, which proves that the tasks are performed independently on each core.

References

[1] I. Kisel, Nucl. Instr. Meth. Phys. Res. A **566** (2006) 85

[2] IA-32 Intel Architecture Optimization Reference Manual, Intel, June 2005

[3] S. Gorbunov *et al.*, Comp. Phys. Comm. **178** (2008) 374

[4] `http://gitorious.org/vc`

Fast parallel tracking algorithm for the muon detector of the CBM experiment

A. Lebedev[1,2], C. Höhne[1], I. Kisel[1], and G. Ososkov[2]
[1]GSI, Darmstadt, Germany; [2]JINR, Dubna, Russia

The tracking algorithms of the CBM experiment have to process terabytes of input data produced in particle collisions. Therefore, the speed of the tracking software is extremly important for data analysis. In this contribution, a fast parallel track reconstruction algorithm for the muon detector (MUCH) which uses available features of modern processors is presented. These features comprise a SIMD instruction set and multithreading. The first one allows to pack several data items into one register and to operate on all of them in parallel, thus achieving more operations per cycle. The second feature enables the routines to exploit all available CPU cores and hardware threads.

MUCH track reconstruction in CBM is based on track following and Kalman filter methods using reconstructed tracks in the STS as seeds [1]. In the STS, track reconstruction is based on the fast cellular automaton method [2] and a SIMDized Kalman filter based track fit [3]. In order to use SIMD and multithreading for tracking in MUCH, the LIT tracking algorithm was significantly modified, including necessary changes in the track propagation and track fitting routines for optimization and SIMDization.

The optimization of propagator and track fitter includes several steps. First, the access to the magnetic field was optimized using a local approximation of the field by polynomials. It was found to be sufficient for the track propagator to use a 2D polynomial of fifth order to approximate the field in the planes of each station. The field behavior between two stations within the same absorber gap is approximated by a linear interpolation. The track parameters obtained with the polynomial approximation of the magnetic field are as precise as those calculated using the full magnetic field map. Second, a simplified detector geometry and an optimized geometry navigation algorithm were developed. The simplified geometry is created by converting the detailed Monte-Carlo detector geometry into a reduced one which only consists of planes perpendicular to the beam direction. The navigation in such a simplified geometry was significantly optimized.

Then, the propgation and track fitting algorithms were SIMDized by changing the data representation from scalar to vector form. After packing the corresponding four scalar track parameters from different tracks into a vector, four tracks can be propagated and fitted in parallel.

The track fitter algorithm was tested using simulated muon tracks which were transported through the CBM setup using GEANT3. Table 1 shows the computational times and speed-up factors for the track fitter and track finder algorithms in the muon detector for a computer with a 2×core i7 processors at 2.66 GHz. An acceleration by a factor of 92 is achieved by the substantial optimization of the algorithms described above. Changing the data representation from the scalar to the vector (SIMD) format results in a three times faster algorithm. Running several threads of the SIMDized track fitter routine in parallel gains another speed-up of 8.8 for the 8 core machine. In total, a speed-up factor of 2,400 (from 1,200 μs/track to 0.5 μs/track) is achieved.

	Track fitter		Track finder	
	Time	Speedup	Time	Speedup
Initial	1200	-	730	-
Optimization	13	92	7.2	101
SIMDization	4.4	3	4.9	1.5
Multithreading	0.5	8.8	1.5	3.3
Final	0.5	2400	1.5	487

Table 1: Speedup of the track fitting (time is shown per track in μs) and track finding algorithms (time is shown per event in ms)

The track finding algorithm was also significantly modified to use the SIMDized track propagator and track fitter. Multithreading capabilities were implemented to the tracking algorithm, too. In order to test the parallel tracking algorithm, central Au+Au collisions at 25A GeV beam energy were simulated with UrQMD and propagated through the CBM setup using GEANT3. In addition, 5 μ^+ and 5 μ^- were embedded in each event at the primary vertex. The comparison of the initial serial scalar version and the parallel version of the tracking shows that on account of a minor loss in the momentum-integrated track reconstruction efficiency (from 94.7% to 94.0%), the parallel tracking algorithm is much faster (see Table 1). A speed up of 101 is achieved by optimization of the algorithm and the use of the optimized Kalman filter routines. SIMDization and multithreading give less speed-up factors than for the track fitter, which can be explained by the fact that some parts of the track finder are not completely SIMDized and parallelized. In total, the parallel tracking algorithm is 487 times faster than the initial serial scalar algorithm (from 730 ms/event to 1.5 ms/event).

References

[1] A. Lebedev et al., PoS(ACAT08)068 (2008)

[2] I. Kisel, Nucl. Instrum. Meth. Phys. Res. **A 566** (2006) 85

[3] S. Gorbunov *et al.*, Comp. Phys. Comm. **178** (2008) 374

Status of the global track reconstruction algorithm for the CBM experiment

A. Lebedev[1,2], C. Höhne[1], I. Kisel[1], and G. Ososkov[2]
[1]GSI, Darmstadt, Germany; [2]LIT JINR, Dubna, Russia

In this report, the status of the LIT global track reconstruction package for the CBM experiment is presented. The package is organized to be flexible with respect to feasibility studies of different physics channels and to the optimization of the detector geometry. Global track reconstruction in the electron and muon setup of the CBM detector, i. e. with either the TRD or the MUCH system, is based on track following using reconstructed tracks in the STS as seeds. In the STS, track reconstruction is based on the cellular automaton method [1] and provides initial track parameters as starting point for the following track prolongation. This track following is based on the standard Kalman filter technique and is used for the trajectory recognition and estimation of track parameters in TRD and MUCH. Tracks are prolongated subsequently from one detector station to the next adding hits in the detector stations. The global tracking algorithm uses the track propagation algorithm described in ref. [2].

The detailed layout of the detectors is still under investigation. In the high track density region of the TRD and MUCH stations, a pad layout is foreseen based on MWPC or GEM technology. For the upstream detector stations in MUCH, where track densities are low, straw tube chambers are under discussion. Moreover, the first TRD station can be used as tracking station after the last MUCH absorber.

The track reconstruction algorithm was tested for the standard TRD setup with segmented detector chambers and for four different MUCH geometries: 1) `MUCH1` is the standard MUCH with 6×3 detectors with pad readout; 2) `MUCH2` comprises 3×3 detectors with pad readout and straw tube detectors in the last 3×3 stations; 3) `MUCH3` is the same as `MUCH1` but with TRD after the last absorber (see sketch in Fig. 1); 4) `MUCH4` is the same as `MUCH2` but with the TRD after the last absorber.

The algorithm was tested with central Au+Au collisons at $25A$ GeV beam energy from UrQMD. In addition, for the reconstruction in TRD, 5 primary e^+ and 5 primary e^- with momenta 1 GeV/c $\leq$ p $\leq$ 10 GeV/c were embedded in each event. The performance in the muon system was evaluated by embedding 5 primary μ^+ and 5 primary μ^- per event with momenta 2.5 GeV/c $\leq$ p $\leq$ 25 GeV/c.

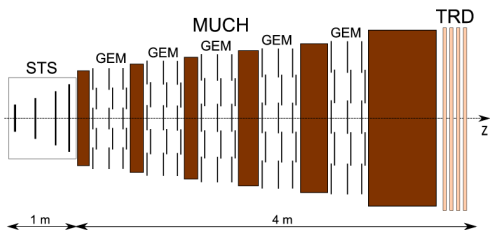

Figure 1: Sketch of the silicon tracking system (STS) and the muon detector (MUCH) with 5×3 GEM stations and the first TRD station after the last absorber

Geometry	`MUCH1`	`MUCH2`	`MUCH3`	`MUCH4`
Efficiency [%]	95.2	94.1	94.7	94.0

Table 1: Track finding efficiency for muon tracks for four different MUCH geometries.

The mean TRD track finding efficiency for reference tracks (primary tracks with $p > 1$ GeV/c) is 93% at a ghost rate of 3%. The reconstruction efficiency for electrons is 89%. The MUCH track finding efficiency for the four discussed geometries is presented in Table 1. Figure 2 depicts the global tracking efficiency in dependence on momentum for the geometry `MUCH3`.

In summary, the LIT track reconstruction package provides good tracking efficiency for both, the electron and muon setup of CBM. It is suitable for layout studies of different MUCH setups. The reconstruction efficiency is only slightly different for the different MUCH layout options.

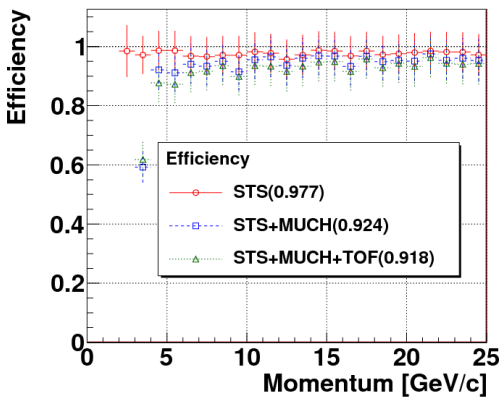

Figure 2: Global track finding efficiency for muon tracks in dependence on momentum for the `MUCH3` geometry

References

[1] I. Kisel, Nucl. Instrum. Meth. Phys. Res, **A 566** (2006) 85

[2] A. Lebedev and G. Ososkov, CBM-SOFT-note-2008-002 (2008), `http://www.gsi.de/documents/DOC-2008-Dec-182-1.pdf`

Primary Vertex Finding in Multivertex Events

I. Kisel[1] and M. Zyzak[2,3]
[1]GSI, Darmstadt, Germany; [2]Goethe-Universität Frankfurt, Germany; [3]University of Kiev, Ukraine

For the CBM experiment [1], the Kalman filter based algorithm of primary vertex reconstruction is implemented [2]. This algorithm is developed for the case of single primary vertex events: all found tracks are used for the primary vertex reconstruction. Multi-vertex events, like pile-up of several interactions within one readout frame, are assumed by the physics program of the CBM experiment. In case of such multi-vertex events, the situation is more complicated: the number of interaction points is unknown, and there is no information about the belonging of a certain track to a certain vertex.

Another problem is related to events with low track multiplicity. In this case, the currently implemented algorithm will be very sensitive to each measurement, where measurements are tracks included to the clusters of primary tracks. If tracks created by the secondary particles are included into these clusters, the errors of the reconstructed primary vertex position can be increased dramatically, and the vertex position can be determined incorrect.

The goal of this investigation is therefore to develop an algorithm which determines the number of primary vertices and find the clusters of primary tracks forming each vertex. The developed cluster finder algorithm is based on two assumptions: there is only one target, and all primary vertices are positioned on this target. The algorithm consists of the following steps:

1. Extrapolate all tracks to the target plane and estimate their positions in this plane and the corresponding errors (σ).

2. Define a track weight proportional to the number of tracks around it. Find the track with the maximal weight and use it as the central track of the cluster.

3. Form the cluster around this track. All tracks within a distance of less than 3.5σ are included into the cluster; they are rejected from the array of considered tracks for the next step as well.

4. The procedure is continued as long as there are remaining tracks, which could form clusters.

5. Then, all found track clusters are passed to the Kalman filter reconstruction routine [2].

The algorithm was tested on proton-carbon UrQMD events at $30A$ GeV. The residuals and pulls for single-vertex events were obtained by the algorithm [2] with and without cluster finder and are presented in Table 1 and in Fig. 1 with all coordinates having similarly shaped distributions. The results with the cluster finder are more accurate. This is due to the fact that secondary tracks are rejected from the cluster of tracks used for primary vertex reconstruction in this case.

	Residuals, μm	Pulls
x	18.9 / 21.2	1.14 / 1.28
y	18.6 / 20.6	1.13 / 1.28
z	100.6 /116.8	1.18 / 1.36

Table 1: Residuals and pulls with/without the cluster finder routine for single vertex events

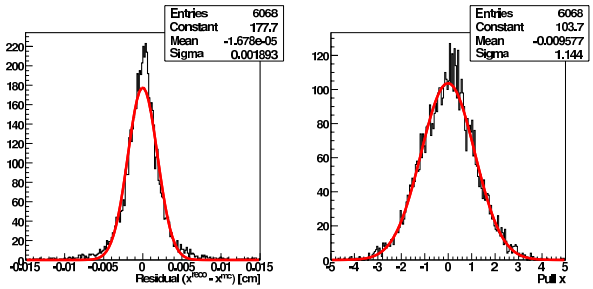

Figure 1: Residuals and pulls of the x coordinate for single-vertex events with the cluster finder algorithm

The quality of the reconstruction of primary vertices in case of two and more vertices in one event is the same as in the single-vertex case. The algorithm reliably distinguishes vertices with distances larger than 100 μm in the target plane. At smaller distances, the reconstructed vertices show the tendency to merge.

Concluding, the developed algorithm allows the reconstruction of more than one primary vertex in one event. The cluster finder routine gives better residuals and pulls also for the case of one primary vertex by rejecting secondary tracks from the primary track cluster, which is particularly important in case of small track multiplicity. The algorithm is built in such a way that it can be easily extended to the case of multiple targets at different z-positions.

References

[1] CBM Progress Report 2008, Darmstadt 2009

[2] S. Gorbunov and I. Kisel, *Reconstruction of decayed particles based on the Kalman filter*, CBM-SOFT-note-2007-003 (2007)

Fast parallel ring reconstruction algorithm for the RICH detector of CBM

S. Lebedev[1,2], C. Höhne[1], and G. Ososkov[2]
[1]GSI, Darmstadt, Germany; [2]JINR, Dubna, Russia

The high interaction rates and, consequently, the huge amount of data in the CBM experiment call for very fast event reconstruction. Fast algorithms require a smaller number of computers both for on-line and for off-line computing. In this contribution, the fast parallel ring recognition algorithm for the CBM RICH detector is presented.

Modern CPUs provide two features for parallel programming. First, the SSE technology allows to use the SIMD execution model. Second, multi-core CPUs give rise to the use of multi-threading. Both features were implemented in the parallel ring reconstruction algorithm.

RICH ring reconstruction in CBM [1] consists of two stages: 1) a local search of ring candidates, based on the Hough transform (HT) method; 2) a global selection algorithm, which compares all ring candidates and selects only good rings while rejecting clone and fake rings.

In order to use parallel features, the ring reconstruction algorithm was significantly modified. It was found that 99 % of the calculation time is consumed in the local ring candidate search. This part was optimized in several ways, including combinatorial and mathematical optimization of the HT, software optimization, memory usage optimization etc.

Then, the algorithm was SIMDized by changing the data representation from scalar to vector form. The idea is to calculate parameters of four rings from triplets in parallel by packing four scalar hit parameters into one vector.

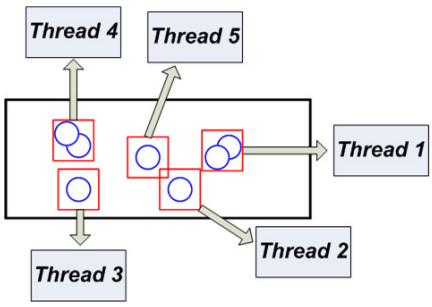

Figure 1: Illustration of the approach for many independent local ring-candidate reconstructions in the photo-detector plane

Multi-threading parallelization of the Hough Transform algorithm was implemented on different levels. Since the upper and lower part of the RICH photodetector are physically separated, they can be treated completely independently. The ring reconstruction procedure can thus be executed for each photo-detector halfplane in parallel in two different threads. Furthermore, localized Hough Transform enables many independent local ring candidate reconstructions in the photo-detector plane (see Fig. 1). Third, hits can be divided into several groups for independent HT execution for each group in parallel.

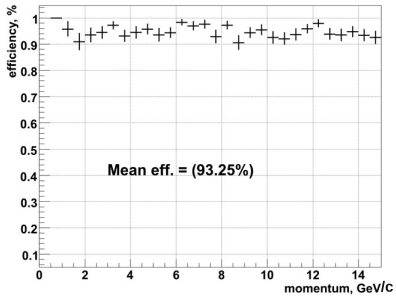

Figure 2: Efficiency for the reconstruction of primary electron rings in central Au+Au collisions at 25A GeV beam energy

In order to test the parallel ring reconstruction algorithm, central UrQMD Au+Au collisions at 25A GeV beam energy with 10 embedded primary e^+ and e^- were simulated. A computer with Core2Duo processors at 2.13 GHz was used for the timing tests. The comparison of the initial serial scalar version and the parallel version of the ring finding shows similar performances in terms of ring reconstruction efficiency (93 %), number of fake rings per event (3.5) and number of clone rings per event (1.0). The ring finding efficiency is shown in Fig. 2 as a function of momentum. A speed-up by a factor of 55 is achieved by the optimization of the algorithm. Using SIMDization and multi-threading, the speed of the algorithm is increased further by a factor of two. In total, a speed-up factor of 107 was achieved (from 750 ms/event to 7 ms/event) for the optimized parallel version in comparison to the initial algorithm. Larger speed-up factors from multi-threading are expected when using modern many-core CPUs.

	Time per event [ms]	Speed-up
Initial version	750	-
Optimization	13.6	55
Parallelization	7	1.95

Table 1: Time per one event (central Au+Au at 25A GeV) for different versions of the ring reconstruction algorithm

References

[1] S. Lebedev *et al.*, CBM Progress Report 2008, Darmstadt 2009, p. 84.

Taubin based ellipse fitting algorithm for CBM-RICH at FAIR

A. Ayriyan[1], N. Chernov[2], V. Ivanov[1], S. Lebedev[1,3], and G. Ososkov[1]

[1]Laboratory of Information Technologies, JINR, Dubna, Russia; [2]Department of Mathematics, University of Alabama at Birmingham, Birmingham, USA; [3]GSI Helmholtzzentrum für Schwerionenforschung GmbH, Darmstadt, Germany

Ring fitting in the CBM RICH detector uses an elliptic model of the Cherenkov radiation rings instead of the previously employed circular one, taking into account distortions of the rings due to imperfect optics. A first approach to this ellipse fitting problem [1] was based on the Kepler equation of the ellipse and minimization by the well known MINUIT package. We will denote this algorithm by Minuit Fitter. We developed and tested an alternative approach based on the Taubin method [2], which we henceforth refer to as Taubin fitter. Here, we report on a comparative analysis of this new method with the previously used Minuit fitter. It is important to stress that the Taubin method is direct (non-iterative) and thus much faster then the Minuit Fitter. Besides, it is statistically more accurate [2, 3].

For the comparison of the two ellipse fitting methods, a set of points distributed along ellipses was simulated with different rotation angles of the ellipse axes and various numbers of points. Each point was simulated with normally distributed errors in the $X-$ and $Y-$coordinates with $\sigma = 0.3$, where σ is roughly $1/20$ of the ellipse size. We find the Taubin Fitter to be 5÷25 times faster than the Minuit Fitter. Moreover, the speed of Taubin Fitter is practically independent of the number of ellipse points and this fitter gives also better estimates of the ellipse parameters [4].

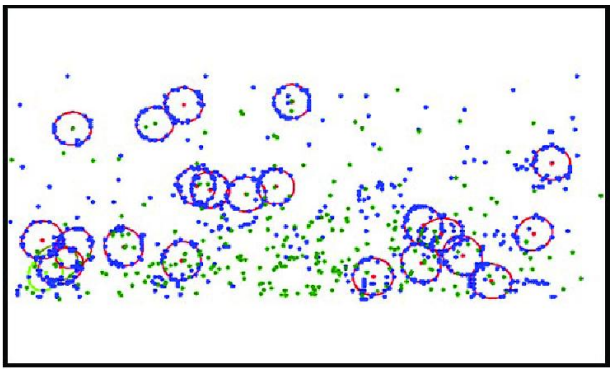

Figure 1: Part of a typical event in the RICH detector. RICH hits are displayed in blue, found rings in red, and track projections in green. On average, there are 80 rings per event.

To be closer to the experimental situation, 500 Au+Au UrQMD events at 25A GeV with additional 5 e^- and 5 e^+ per event were simulated and reconstructed to check the RICH ring finding efficiency. Figure 1 displays a part of a typical event in the RICH detector. The performances of the ring finder obtained with both fitting methods are given in Table 1. The Taubin Fitter provides an increase in the ring finding efficiency by 2.69 % while reducing the number of fake rings.

The comparison of the two ellipse fitting methods shows the advantages of the Taubin Fitter. On the basis of our studies, the Taubin Fitter was chosen as default algorithm for RICH ring fitting. The Taubin method is intended to fit a general conic section equation by points on a plane, but in rare cases the Taubin Fitter will result not in an ellipse, but in a hyperbola or even a parabola, while the Minuit Fitter gives only ellipse solutions. Therefore, we propose to apply a hybrid approach, where the ellipse is generally fitted by the Taubin method, but if it fails, the Minuit Fitter can be used. Such a hybrid approach is the topic for future investigations.

Ring Finder with	**Eff. %**	**Fakes %**	**Clones %**
Minuit Fitter	90.33	8.44	0.53
Taubin Fitter	93.02	7.49	0.88

Table 1: Ring finding performance for electrons and positrons embedded into central Au+Au events at 25A GeV

References

[1] S. Lebedev and G. A. Ososkov, PEPAN Letters Vol. 6, No. 2(151) (2009) 258 (in Russian)

[2] G. Taubin, IEEE Trans. Pattern Analysis Machine Intelligence **13** (1991) 1115

[3] N. Chernov, Journal of Mathematical Imaging and Vision **27** (2007) 231

[4] A. Ayriyan *et al.*, Bulletin of PFUR: series "Mathematics, Information Systems, Physics" No. 2 (2010) 3 (in Russian)

Systematic investigations of the influence of RICH and TRD detector parameters on electron identification in the CBM experiment

S. Lebedev[1,2], C. Höhne[1], G. Ososkov[2], and F. Uhlig[2]
[1]GSI, Darmstadt, Germany; [2]JINR, Dubna, Russia

Several new features were implemented in the RICH detector simulation to improve the realistic detector response: mirror surface inhomogeneities, photodetector coverage with wavelength shifter (WLS) films, and collection efficiency of the photodetectors. These features mostly influence the ring finder, which was tested in order to investigate limitations for the detector parameters. For this study, central Au+Au collisions at $25A$ GeV beam energy from UrQMD with 10 embedded primary e^+ and e^- were simulated.

The effect of light scattering due to mirror surface inhomogeneities was implemented as additional error with Gaussian distribution to the hit measurement. As a reference point, $\sigma_{gauss} = 0.6$ mm was taken, which is expected for the new CBM-RICH mirror prototypes. Different values of σ_{gauss} were tested, results of which are presented in Table 1.

σ_{gauss} [mm]	0.4	0.6	1.0	2.0	4.0	6.0
Eff. [%]	91.0	90.4	91.4	90.0	87.5	84.7
Fakes/ev.	3.8	3.7	3.9	4.3	5.8	7.6

Table 1: Ring finding performance vs. σ_{gauss}

The quantum efficiency (QE) of the photomultipliers is typically limited by the window material and extends down to 250 – 300 nm. In order to enhance the QE in the near UV region, the coverage of photomultiplier tubes (PMTs) with WLS films as e. g. p-terphenul (PT) was studied [1]. In addition, a reduced photoelectron collection efficiency (CE) of about 70% due to the construction of the photodetector Hamamatsu H8500 was considered. The ring finding efficiency in dependence on these photodetector effects is presented in Table 2.

In TRD simulations, the dependence of the pion suppression factor on different radiator parameters was studied. In the `cbmroot` framework, energy losses due to ionization are taken from GEANT, and transition radiation (TR) is calculated by an implemented model [2]. Three parameters for the radiator are used as input for the model: the number of foils, the thickness of the foils, and the distance between two foils. The radiator parameters used in our study are presented in Table 3. The first set overestimates preliminary experimental results, the second set underestimate these results. The third set was tuned to describe the experimental results [3].

	No WLS		WLS (PT)	
CE [%]	100	70	100	70
Efficiency [%]	90.4	85.5	91.5	88.2
Fakes/event	3.6	2.6	5.5	3.9

Table 2: Ring finding performance in dependence on different photodetector parameters

	set1	set2	set3
Number of foils	130	60	70
Foil thickness [cm]	0.0013	0.0015	0.0014
Distance between foils [cm]	0.02	0.05	0.04

Table 3: Three sets of parameters for TR simulation

To calculate the pion suppression factor, 10^6 electrons and 10^6 pions were simulated with parameters $\theta \in (2.5°, 25°)$, $\phi \in (0°, 360°)$ for certain momenta (1, 1.5, 2, 3, 4, 5, 7, 9, 11, 13 GeV/c). The BDT method was used for this study [4]. The results are presented in Table 4.

p [GeV/c]	1.5	3	5	9	13
set1	2892	2621	2149	1591	1189
set2	400	593	529	421	314
set3	660	845	690	525	395

Table 4: Pion suppression for different radiator parameters

The robustness of the pion rejection factor to experimental factors such as the calibration of the energy loss measurements, pile-up of signals etc. was studied by implementing an additional error with Gaussian distribution to the energy loss for each hit: $E_{loss} = E_{loss} + Gauss(0, \sigma_{error})$. Note that the most probable value of E_{loss} for pions with 1.5 GeV/c momentum is around 1.1 keV. The results on pion suppression assuming 90 % electron efficiency for different σ_{error} are presented in Table 5 (p = 1.5 GeV/c, radiator parameters set3). The study showed that the tested method for electron identification is very robust.

σ_{error} [keV]	0.01	0.025	0.05	0.1	0.25	0.5
pion supp.	659	636	626	637	585	466

Table 5: Pion suppression in dependence on σ_{error}

References

[1] P. Koczon *et al.*, CBM Progress Report 2008, Darmstadt 2009, p. 26

[2] M. Castellano *et al.*, Comp. Phys. Comm. **61** 1990

[3] A. Andronic *et al.*, GSI Scientific Report 2006, p. 233.

[4] G. Ososkov *et al.*, "e^-/π separation with TRD", https://www.gsi.de/documents/DOC-2009-Oct-232-1.pdf

Methods for e/π identification with the Transition Radiation Detector

E. P. Akishina , T. P. Akishina , O. Yu. Derenovskaya , and V. V. Ivanov
LIT JINR, Dubna, Russia

The problem of e/π identification using the n-layered transition radiation detector (TRD) in the CBM experiment is considered [1]. With this aim, we elaborated algorithms and implemented various approaches. The characteristic properties of the energy losses by electrons and pions in the TRD layers and special features of applying artificial neural networks (ANN) and statistical methods to the particle identification (PID) are considered. A comparative analysis is performed on the power of the statistical criteria and ANN for π and e with momenta 1 GeV/$c \leq$ p $\leq$ 11 GeV/c.

In the *mean value* (MV) method, the PID is based on the variable $\overline{\Delta E} = \frac{1}{n}\sum_{i=1}^{n}\Delta E_i$, where ΔE_i is the energy loss in the i-th TRD layer and n is the number of layers in the TRD.

The ω_n^k *test* is based on the comparison of the distribution function corresponding to the preassigned null-hypothesis (H_0) with an empirical distribution function:

$$\omega_n^k = - \frac{n^{\frac{k}{2}}}{k+1}\sum_{j=1}^{n}\left\{\left[\frac{j-1}{n} - \phi(\lambda_j)\right]^{k+1} - \left[\frac{j}{n} - \phi(\lambda_j)\right]^{k+1}\right\}, \quad (1)$$

where $\phi(\lambda)$ is a Landau distribution function which describes the pion energy losses and corresponds to the H_0-hypothesis, with a new variable λ:

$$\lambda_i = \frac{\Delta E_i - \Delta E_{mp}^i}{\xi_i} - 0.225, \qquad i = 1, 2, ..., n, \quad (2)$$

ΔE_i being the energy loss in the i-th absorber, ΔE_{mp}^i the value of most probable energy loss, and $\xi_i = \frac{1}{4.02}$ FWHM of the distribution of energy losses for π.

The *combined method* involves a successive application of two statistical criteria: 1) the MV method, and 2) the ω_n^k-test.

While applying the *likelihood functions ratio* (LFR) test to the PID problem, the value

$$L = \frac{P_e}{P_e + P_\pi},\ P_e = \prod_{i=1}^{n} p_e(\Delta E_i),\ P_\pi = \prod_{i=1}^{n} p_\pi(\Delta E_i)$$

is calculated for each set of energy losses, where $p_\pi(\Delta E_i)$ is the value of the density function p_π in the case when π loses the energy ΔE_i in the i-th absorber, and $p_e(\Delta E_i)$ is a similar value for e. The approximations of the density functions which with a good accuracy reproduce the distributions of energy losses of π and e are described in [2].

The main idea of the *modified* ω_n^k test consists in the following. When calculating ω_n^k, in eq. 1, we may use only that part of the $\{\lambda_i\}$ sample which corresponds to indices $i > 6$, i. e. to large values of particle energy losses; for details see [3].

We also applied the ANN – a three-layered perceptron from the JETNET3.0 and ROOT packages – to estimate the efficiency of PID [4]. Table 1 shows the pion rejection factor obtained by the various methods for 90 % efficiency of electron selection.

p [GeV/c]	1	3	4	5	7	9	11
MV	10	14	14	14	14	14	14
ω_{12}^6	43	39	31	25	19	16	14
MV + ω_{12}^6	87	148	134	120	101	93	85
mod $\omega_6 6$	81	250	281	265	244	211	196
LFR	272	567	509	481	403	363	320
root	294	478	549	456	524	448	323
jetnet	273	682	697	477	541	506	364

Table 1: Pion suppression factor for various methods of electron identification

This table clearly demonstrates that the MV method, the ω_n^k criterion and the composite (MV + ω_n^k) test do not meet the required level of the pion suppression ($\sim$ 100 – 150). The modified ω_n^k criterion permits to achieve the needed level of pions suppression using only information about the distribution of pion energy losses. The best pion suppression level is achievd by using: i) the LFR method with the energy losses approximated by a log-normal distribution for pions and by a weighted sum of two log-normal distributions for electrons, and ii) the ANN method when transforming from the initial energy losses in the TRD layers to a new variable (eq. 2) typical for the ω_n^k criterion.

References

[1] *Compressed Baryonic Matter Experiment. Technical Status Report*, Darmstadt 2005 (http://www.gsi.de/documents/DOC-2005-Feb-447.html)

[2] E. P. Akishina *et al.*, *Distribution of energy losses for electrons and pions in the CBM TRD*, JINR Communications E10-2007-158, Dubna 2007

[3] T. P. Akishina *et al.*, *On a modification of the ω_n^k criterion for e/π identification in the TRD*, this report

[4] T. P. Akishina *et al.*, *On electron/pion identification using a multilayer perceptron in the transition radiation detector of the CBM experiment*, JINR Communication P10-2009-61, Dubna 2009

On a modification of the ω_n^k criterion for e/π identification in the TRD

T. P. Akishina , O. Yu. Derenovskaya , and V. V. Ivanov
LIT JINR, Dubna, Russia

The particle identification problem (PID) in the Transition Radiation Detector (TRD) of CBM with the help of a ω_n^k criterion is considered. For PID we use Monte Carlo simulations for the n-layered TRD realized in the `cbmroot` framework for momenta in the range of 1 GeV/c to 11 GeV/c. The character of the electron energy losses permits to modify the procedure of the input sample preparation for the ω_n^k criterion. This, in turn, makes it possible to significantly increase the criterion power.

The ω_n^k test is based on the comparison of the distribution function corresponding to the preassigned null-hypothesis (H_0) with the empirical distribution function [1]

$$\omega_n^k = - \frac{n^{\frac{k}{2}}}{k+1} \sum_{j=1}^{n} \left\{ \left[\frac{j-1}{n} - \phi(\lambda_j) \right]^{k+1} - \left[\frac{j}{n} - \phi(\lambda_j) \right]^{k+1} \right\}. \quad (1)$$

Here, $\phi(\lambda)$ is a Landau distribution function which describes the pion energy losses and corresponds to the H_0-hypothesis, with a new variable λ:

$$\lambda_i = \frac{\Delta E_i - \Delta E_{mp}^i}{\xi_i} - 0.225, \qquad \text{i = 1,2,...,n}, \quad (2)$$

where ΔE_i is the energy loss in the i-th absorber, ΔE_{mp}^i the value of most probable energy loss, and $\xi_i = \frac{1}{4.02}$ FWHM of the distribution of the pion energy losses.

Let us consider in more detail the origin of the electron energy losses in the TRD. They are caused by ionization and by transition radiation (TR) (Fig. 1).

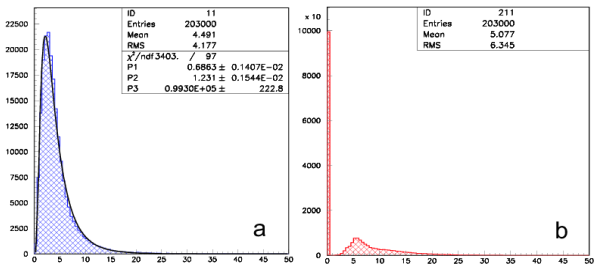

Figure 1: Distribution of electron energy losses by ionization and its approximation by a log-normal function (a) and by transition radiation (b)

Figure 1b clearly demonstrates that in approximately 50 % of the cases, we do not have a TR count in the TRD layer (left peak in the figure). The distribution of events with a different number of TR counts is presented in Fig. 2. This distribution shows that the most probable value of the TR counts in the 12-th layered TRD is 6, and we almost do not have the events with TR counts in all 12 layers.

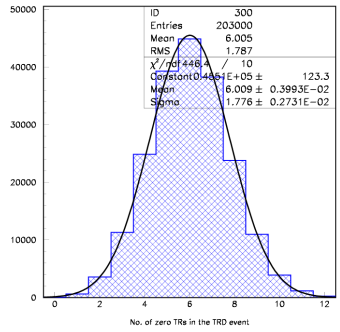

Figure 2: Distribution of events with a different number of TR counts and its approximation by a Gaussian distribution

It must be noted that when the electron passes the i-th layer with TR=0, its energy loss follows the distribution of dE/dx losses (Fig. 1a). In this case, it is practically impossible to distinguish electrons from pions on the basis of their energy losses. In the opposite case, we have the TR count in the i-th layer, and the electron energy loss corresponds to the sum of dE/dx + TR. So only such cases may permit us to distinguish electrons from pions.

When calculating ω_n^k in eq. 1, one uses a set of λ_i variables (eq. 2) which are ordered according to their values. The λ_i value is proportional to the energy loss value of a particle registered in the i-th layer of the TRD. In this connection and taking into account that the most probable value of TR counts in the TRD with 12 layers is 6 (Fig. 2), we may use in the ω_n^k criterion only that part of $\{\lambda_i\}$ sample which corresponds to indexes $i > 6$, i. e. to large values of particle energy losses. Table 1 clearly demonstrates that the proposed modification of the ω_n^k criterion permits to achieve a high level of pion suppression using only information about the distribution of pion energy losses.

p [GeV/c]	1.5	3	4	5	7	9	11
ω_{12}^6	56	39	31	25	19	16	14
mod ω_6^6	170	250	281	265	244	211	196

Table 1: Pion rejection factor for 90 % efficiency of electron selection for the standard and the modified ω_n^k tests

References

[1] P. V. Zrelov and V. V. Ivanov, Nucl. Instr. Meth. Phys. Res. A **310** (1991) 623

Symposium "The physics of dense baryonic matter" and the 13th CBM Collaboration meeting, March 9- 13, 2009, GSI

More than 160 scientists from 12 countries met at GSI from 9 – 13 March 2009 in order to attend the symposium "The physics of dense baryonic matter" and the 13th CBM Collaboration meeting. The symposium was jointly organized by the experiments STAR, PHENIX (RHIC Brookhaven) and CBM (FAIR), and was sponsored by the "HIC for FAIR" programme. The discussions at the symposium concentrated on experimental observables of the phase transition from nuclear matter to the quark-gluon plasma, and on their measurements in future experiments. At the CBM collaboration meeting the status of the experiment preparations and next steps were discussed in working groups and plenary sessions. The CBM Collaboration Board elected Subhasis Chattopadhyay (VECC Kalkutta) and Yuri Zaitsev (ITEP Moskau) as deputy spokespersons of the CBM Collaboration, and Jürgen Eschke (GSI Darmstadt) as resource coordinator.
More info: http://www-aix.gsi.de/conferences/CBM2009_Mar/

"Indian Participation in FAIR: Science and Technology"
Meeting in Hyderabad, India, April 18-19, 2009

On 18th and 19th April 2009 the Electronics Corporation of India Limited (ECIL) in collaboration with the DAE-DST Coordination Committee organized a meeting on the possible Indian contributions to FAIR in Hyderabad, India. More than 100 scientists and engineers from 8 Indian research institutes and 14 universities, from ECIL, from GSI and several members of the DAE-DST Task Force on the India-FAIR project with the Chairman Prof. VS Ramamurthy participated in the discussions. The purpose of the meeting was to showcase the details of the FAIR project so that the ECIL management could decide whether they could fruitfully participate in the project. The other objective of the meeting was to comprehensively judge the preparedness of various groups for participating in the FAIR programme, especially to obtain from them the list of items for *in kind* contributions to FAIR.

After two days of intensive discussions, the following viewpoints emerged. The participation of a Company like ECIL in the FAIR project would facilitate interaction with the FAIR Company in Germany. Apart from formal aspects, ECIL would be able to bring into the project valuable elements of corporate-like project management which would be extremely useful in running a time-bound and company-model project like FAIR. ECIL has strength in several areas of electronics and instrumentation which could be useful to the FAIR project at large. It would be able to function effectively as a mass-production agency. While ECIL has in-house design capabilities in several areas, it would require active collaboration with other R&D institutions in some specific areas. In addition, ECIL could also be a window to other industries in the country, wherever required.

Various groups proposed Indian in-kind contributions to FAIR. The official minutes of the meeting note that among these projects, the Energy Buncher Magnet and the Beam Stopper for the SFRS, and the Muon System for CBM were on reasonably solid footing. PANDA and NuSTAR groups are in the process to firm up their plans. India's participation in the p-linac could still be possible and this matter is needed to be pursued and clarified at the earliest.

During the discussions it became clear that the "Indian Cost" of producing the proposed items may be considerably higher than the prices given in the "FAIR Cost-Book Cost". While the cost estimates obtained during the meeting were still preliminary for several projects and needed to be firmed up further, it was clear that the "Indian Costs" would be certainly higher for the "magnet components" and, at best, be equal for the "experiment-related components". Therefore, it would be extremely important for ECIL to find some additional large-volume and, perhaps, not-so-sophisticated items which could off-set the extra cost that would be incurred for producing the items identified so far. It would be necessary to send an Indian delegation to FAIR with strong contingent from ECIL to enable ECIL to identify and bid for additional items which were more cost-effective.

Workshop "Nuclear Matter Physics at SIS100"
April 27, 2009, GSI Darmstadt

The goal of the workshop was to discuss and to prepare an internationally competitive physics programme which will become possible with the HADES detector and the CBM setup using the beam of SIS100. About 60 scientists participated in the meeting, and discussed experiments to explore the equation-of-state of nuclear matter at neutron star core densities, to study the hadron properties in dense baryonic matter using penetrating probes like lepton pairs, to search for heavy multi-strange objects, and to investigate the production mechanisms of charm at threshold energies.
More Info: https://www.gsi.de/documents/FOLDER-9871240454693.html

1st CBM Russia-JINR collaboration meeting, May 19-22, 2009 in Dubna

More than 70 scientists attended the 1st meeting of the CBM-Russia-JINR Collaboration which took place in Dubna from May19 to 22, 2009. The presentations and discussions addressed the physics potential of the CBM detector using beams from SIS100 and SIS300. Moreover, the status and perspectives of the joint development of detector components for CBM at FAIR and MPD at NICA have been discussed.
More info: http://cbm2009-may.jinr.ru/

3rd Workshop of the CBM-MPD STS Consortium, June 1- 4, 2009, Sortavala, Karelia, Russia

The 3rd workshop “Challenges of the CBM and MPD Silicon Tracking Systems - 2009” was held from 1st – 4th June 2009 in Sortavala, Republic of Karelia, Russia. About 30 scientists discussed in several working groups the joint R&D activities on the Silicon Tracking Systems for the experiments CBM at FAIR and MPD at NICA. The goal of the meeting was to define the work plans and responsibilities for the development of radiation-hard double-sided Silicon micro-strop sensors, ultra-light support structures, prototype detector modules, and the mechanical mainframe and cooling system.

More info: http://sts-karelia09.jinr.ru/

Workshop on "Event reconstruction in the CBM experiment", June 15 – 17, 2009, GSI Darmstadt

A CBM Tracking Workshop had been organized on 15 – 17 June at GSI. In total, 23 participants from Germany, India and Russia have taken part in the discussion on the status of tracking activity and on the strategy of further tracking developments in the CBM experiment. In addition to general and CBM specific tracking presentations, great interest of all participants was attracted to the presentation “Intel Processor and Platform Roadmap” given by R. Ratering from Intel. The ALICE HLT group from the Kirchhoff Institut of the University of Heidelberg has shared the experience with many-core computer architectures by presenting a programming model for the OpenCL parallel language and giving a whole-day tutorial on multithreading with Intel Threading Building Blocks (ITBB) and on vectorization with SIMD classes. The next tracking workshop is foreseen for November this year. Those, who are interested in the workshop, please contact Dr. Ivan Kisel (i.kisel@gsi.de).

CBM-INDIA collaboration meeting and workshop on Object Oriented Programming with C++ during 23-29th June 2009 at VECC-Kolkata, India

A 5-day workshop was held at VECC-Kolkata during 23/6/09 to 27/06/09 on Object Oriented Programming using C++ and their application in HEP using ROOT. About 25 participants from the collaborating institutes attended the lectures and hands-on arranged in the afternoons. The CBM-India collaboration meeting was held at VECC during 28th and 29th June’09. Participants from VECC, BHU-Varanasi, Gouhati Univ, IIT-Kharagpur, Sikkim-Manipal Institute of Technology, Punjab University, Kashmir University attended the meeting. The goal of the meeting was to discuss the status of simulations, detector and electronics R&D, and the physics of CBM. Detailed and long discussions took place on the development of GEM chambers for the CBM muon detection system, and on the upcoming test beam at GSI. Moreover, it was decided that quotations will be obtained from different Indian industries for assembly of CBM Read-out Controlers including production of the PCBs. The next CBM – India collaboration meeting will take place at BHU Varanasi in Jan. 2010

Successful beam test of various prototype detectors for CBM and PANDA

An international team of scientists from the CBM and PANDA collaborations (left picture) studied the performance of a variety of prototype detectors using the GSI proton beam in Cave C in August/September 2009. The PANDA Cherenkov group studied three different prototype Cherenkov detectors. The CBM scientists tested several prototypes of double-sided Silicon micro-strip detectors, gas-electron multipliers (GEM's), and a ring-imaging Cherenkov detector module. All detectors were read-out via a free-streaming read-out electronics by a common data-acquisition system.

Various prototype time-of-flight detectors based on the Resistive Plate Chamber (RPC) technology have been successfully tested with a proton beam at GSI in Cave B. The goal is to develop large-area high-rate detectors for the CBM experiment, in a collaboration of groups from Beijing, Bucharest, Heidelberg, GSI, and Hefei (right picture).

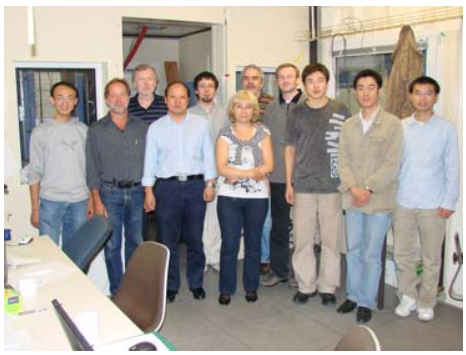

The 14th CBM Collaboration meeting, October 6 - 9, 2009, Split, Croatia

More than 120 scientists from 12 countries participated in the 14th CBM Collaboration meeting which took place in Trogir near Split (Croatia) from 6th to 9th October of 2009. The discussions included the future CBM/HADES research program at SIS-100 within the FAIR modular start version, and the preparation of an Interim Memorandum of Understanding defining the responsibilities of the collaborating institutions for R&D and construction of the CBM components.

More info: https://www.gsi.de/documents/FOLDER-9871255142704.html

CBM China Meeting, November 2 - 4, 2009, Tsinghua University, Beijing, China

DEUTSCH-CHINESISCHES
Jahr der Wissenschaft und Bildung
德中科学教育年
2009/10

About 60 scientists participated in the recent CBM China meeting which took place at the Tsinghua University in Beijing, China, from 2nd to 4th November 2009. Prof. Kang Kejun, the vice director of the Tsinghua University, opened the meeting which was attended also by Prof. Liu Minhua, the vice director of the Bureau of Basic Sciences from the Chinese Academy of Science (CAS), and Prof. Ji Peiwen, the director of the Department of Mathematical and Physical Science from the National Science Foundation of China (NSFC). The scientific discussions concentrated on the development of high-rate, large-area, and high-resolution time-of-flight detectors based on the Resistive Plate Chamber technology, and of the corresponding read-out electronics. Such a detector system is under consideration as a Chinese in-kind contribution to the CBM experiment. Groups from the Department of Engineering Physics of the Tsinghua University in Beijing, and from the University of Science and Technology in Hefei have already built a similar detector system for the STAR experiment at RHIC.

More info: https://www.gsi.de/documents/FOLDER-9871257424499.html
The meeting was supported by the German Ministry for Education and Research BMBF (Program: German-Chinese year of scientific cooperation).

CBM publications 2009

- N. Abel *et al.*
  Increasing Design Changeability using Dynamical Partial Reconfiguration
  Proceedings of IEEE-NSS-RT-2009, May 2009, Beijing, China
- J. Adamczewski-Musch *et al.*
  Data Acquisition Backbone Core DABC release v1.0
  Proceedings of CHEP'09, March 2009, Prague, Czech Republic, to appear in J. Phys. Conf. Ser.
- J. Adamczewski-Musch *et al.*
  First release of Data Acquisition Backbone Core
  Proceedings of IEEE-NSS-RT-2009, May 2009, Beijing, China
- T. Armbruster, P. Fischer and I. Peric
  A Self Triggered Amplifier/Digitizer Chip for CBM
  Proceedings of TWEPP-09, September 2009, Paris, France
- E. Berdermann *et al.*
  Diamond Start Detectors
  Proceedings of IEEE-NSS-MIC-09, October 2009, Orlando, USA
- S. Chatterji, A. Lymanets and J. Heuser
  Development of radiation hard silicon sensors for the CBM Silicon Tracking System using simulation approach
  Proceedings of IEEE-NSS-MIC-09, October 2009, Orlando, USA
- J. M. Ciobanu *et al.*
  PADI-2,-3 and-4: The second iteration of the Fast Preamplifier Ð Discriminator ASIC for Time-of-Flight Measurements at CBM
  Proceedings of IEEE-NSS-MIC-09, October 2009, Orlando, USA
- M. Deveaux *et al.*
  Radiation Tolerance of CMOS Monolithic Active Pixel Sensors with Self-Biased Pixels
  Proceedings of the 11th European Symposium on Semiconductor Detectors, June 2009, Wildbad Kreuth, Germany
- W. Gao *et al.*
  Active Buffer for DAQ in CBM Experiment
  Proceedings of IEEE-NSS-RT-2009, May 2009, Beijing, China
- M. Golubeva *et al.*
  Longitudinally Segmented Lead/Scintillator Hadron Calorimeter with Micropixel APD Readout
  Nucl. Instr, Meth. Phys. Res. A **598** (2009) 268
- M. Golubeva *et al.*
  Use of Micropixel Avalanche Photodiodes for readout of Lead/Scintillator Hadron Calorimeter
  Nucl. Instr, Meth. Phys. Res. A **610** (2009) 366
- D. Gonzalez-Diaz *et al.*
  The role of the resistive plate response function in bringing an RPC to a stationary situation
  Nucl. Instr, Meth. Phys. Res. A **602** (2009) 713
- J. Heuser and the CBM collaboration
  The Compressed Baryonic Matter Experiment at FAIR: Progress with feasibility studies and detector developments
  Nucl. Phys. **A 830** (2009) 563c
- C. Höhne
  SPS energy scan results and physics prospects at FAIR
  Nucl. Phys. **A 830** (2009) 369c
- C. Höhne
  The International Facility for Antiproton and Ion Research FAIR: Challanges and Opportunities
  Proceedings of CIPANP 2009, May 2009, San Diego, USA

- D. Kresan
  Event-by-Event Partical Ratio Fluctuations in the CBM and NA49 Experiments
  Proceedings of CPOD-2009, June 2009, Brookhaven, USA, to appear in PoS
- F. Lemke *et al.*
  A Unified Interconnection Network with Precise Time Synchronization for the CBM DAQ-System
  Proceedings of IEEE-NSS-RT-2009, May 2009, Beijing, China
- S. Löchner, H. Deppe and H. Flemming
  Radiation Studies on the UMC 180 nm CMOS Process
  Proceedings of RADECS-2009, September 2009, Bruges, Belgium
- A. Lymanets, S. Chatterji and J. Heuser
  The Silicon Tracker of the CBM experiment at FAIR: detector developments and first in-beam characterizations
  Proceedings of IEEE-NSS-MIC-09, October 2009, Orlando, USA
- P. Senger
  CBM/FAIR capabilities for charm and dilepton studies
  Proceedings of CPOD-2009, June 2009, Brookhaven, USA, to appear in PoS

CBM presentations 2009

http://cbm-wiki.gsi.de/cgi-bin/view/Public/PublicPresentations2009

Doctoral, diploma, master and bachelor theses 2009

http://cbm-wiki.gsi.de/cgi-bin/view/Public/Thesis2009

Doctorates 2009

CBM

Anna Kiseleva

Saint-Petersburg State Polytechnical University

Development of a muon system for CBM and muon simulations for the different beam energies

The Fundamental Library of Polytechnical University

Melanie Klein-Bösing

Westfälische Wilhelms-Universität Münster

Development of a Transition Radiation Detector and Reconstruction of Photon Conversions in the CBM Experiment

www.gsi.de/documents/DOC-2009-Oct-168.html

Tetiana Galatyuk

Goethe-Universität Frankfurt

Di-electron spectroscopy in HADES and CBM: from p + p and n + p collisions at GSI to Au + Au collisions at FAIR

www.gsi.de/documents/DOC-2009-Oct-252.html

CBM member institutions

- **Aligarh**, India, **Department of Physics, Aligarh Muslim University**
- **Beijing**, China, **Department of Engineering Physics, Tsinghua University**
- **Bergen**, Norway, **Department of Physics, University of Bergen**
- **Bhubaneswar**, India, **Institute of Physics**
- **Bucharest**, Romania, **National Institute for Physics and Nuclear Engineering (NIPNE)**
- **Bucharest**, Romania, **Atomic and Nuclear Physics Department, University of Bucharest**
- **Budapest**, Hungary, **Eötvös University**
- **Budapest**, Hungary, **KFKI Research Institute for Particle and Nuclear Physics (KFKI-RMKI)**
- **Chandigarh**, India, **Department of Physics, Panjab University**
- **Coimbra**, Portugal, **Laboratório de Instrumentação e Física Experimental de Partículas (LIP)**
- **Darmstadt**, Germany, **GSI Helmholtzzentrum für Schwerionenforschung GmbH**
- **Dresden**, Germany, **Institut für Strahlenphysik, Forschungszentrum Dresden-Rossendorf (FZD)**
- **Dubna**, Russia, **Veksler and Baldin Laboratory of High Energies, Joint Institute for Nuclear Research (JINR-VBLHE)**
- **Dubna**, Russia, **Laboratory of Particle Physics, Joint Institute for Nuclear Research (JINR-LPP)**
- **Dubna**, Russia **Laboratory of Information Technologies Joint Institute for Nuclear Research (JINR-LIT)**
- **Frankfurt**, Germany, **Institute for Computer Science, Frankfurt Institute for Advanced Studies, Universität Frankfurt**
- **Frankfurt**, Germany, **Institut für Kernphysik, Universität Frankfurt**
- **Gatchina**, Russia, **Petersburg Nuclear Physics Institute (PNPI)**
- **Guwahati**, India, **Department of Physics, Gauhati University**
- **Hefei**, China, **Department of Modern Physics, University of Science & Technology of China (USTC)**
- **Heidelberg**, Germany, **Kirchhoff-Institut für Physik, Universität Heidelberg**
- **Heidelberg**, Germany, **Physikalisches Institut, Universität Heidelberg**
- **Heidelberg**, Germany, **Zentrales Institut für Technische Informatik, Universität Heidelberg**
- **Jaipur**, India, **Physics Department, University of Rajasthan**
- **Jammu**, India, **Department of Physics, University of Jammu**
- **Katowice**, Poland, **Institute of Nuclear Physics And Its Application, University of Silesia**
- **Kharagpur**, India, **Department of Physics and Meteorology, Indian Institute of Technology**
- **Kolkata**, India, **High Energy Physics Division, Saha Institute of Nuclear Physics**
- **Kolkata**, India, **Department of Physics and Department of Electronic Science, University of Calcutta**
- **Kolkata**, India, **Variable Energy Cyclotron Centre (VECC)**
- **Kraków**, Poland, **Faculty of Electrical Engineering, Automatics, Computer Science and Electronics, Department of Measurement and Instrumentation, AGH University of Science and Technology**
- **Kraków**, Poland, **Marian Smoluchowski Institute of Physics, Jagiellonian University**
- **Kyiv**, Ukraine, **Department of Nuclear Physics, Taras Shevchenko National University of Kyiv**
- **Kyiv**, Ukraine, **High Energy Physics Department, Kiev Institute for Nuclear Research (KINR)**
- **Moscow**, Russia, **Institute for Nuclear Research (INR)**
- **Moscow**, Russia, **Alikhanov Institute for Theoretical and Experimental Physics (ITEP)**
- **Moscow**, Russia, **Skobeltsyn Institute of Nuclear Phyiscs, Moscow State University (SINP-MSU)**
- **Moscow**, Russia, **Kurchatov Institute**
- **Moscow**, Russia, **Moscow Engineering Physics Institute (MEPhI)**
- **Münster**, Germany, **Institut für Kernphysik, Westfälische Wilhelms Universität Münster**
- **Obninsk**, Russia, **Obninsk State Technical University for Nuclear Power Engineering**
- **Prag**, Czech Republic, **Czech Technical University (CTU)**
- **Protvino**, Russia, **Institute for High Energy Physics (IHEP)**
- **Pusan**, Korea, **Pusan National University**
- **Řež**, Czech Republic, **Nuclear Physics Institute, Academy of Sciences of the Czech Republic**
- **Seoul**, Korea, **Department of Physics, Korea University**
- **Split**, Croatia, **University of Split**
- **Srinagar**, India, **Department of Physics, University of Kashmir**

- **St. Petersburg**, Russia, **V.G. Khlopin Radium Institute (KRI)**
- **St. Petersburg**, Russia, **St. Petersburg State Polytechnic University (SPbSPU)**
- **Strasbourg**, France, **Institut Pluridisciplinaire Hubert Curien (IPHC), IN2P3-CNRS and Univesité Louis Pasteur Strasbourg**
- **Varanasi**, India, **Department of Physics, Banaras Hindu University**
- **Warszawa**, Poland, **Institute of Experimental Physics, Warsaw University**
- **Wuhan**, China, **Institute of Particle Physics, Hua-zhong Normal University**
- **Wuppertal**, Germany, **Fachbereich Physik, Bergische Universität Wuppertal**
- **Zagreb**, Croatia, **Rudjer Bošković Institute**

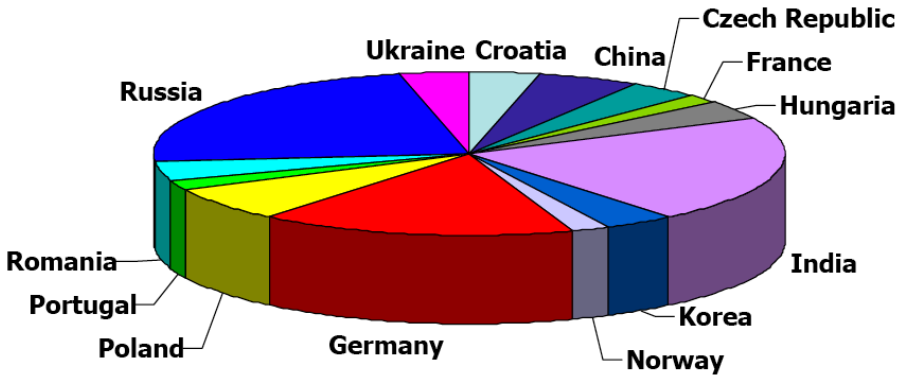

Contacts

Chairman of the Collaboration Board
Mihai Petrovici mpetro@ifin.nipe.ro

Spokesman
Peter Senger p.senger@gsi.de

Deputy Spokesmen
Yuri Zaitsev zaitsev@itep.ru
Subhasis Chattopadhyay sub@veccal.ernet.in

Technical Coordinator
Walter Müller w.f.j.mueller@gsi.de

Physics Coordinator
Volker Friese v.friese@gsi.de

Ressource Coordinator
Jürgen Eschke j.eschke@gsi.de

Management Board
S. Chattopadhyay, N. Herrmann, F. Rami, D. Röhrich, J. Stroth, J. Wessels, Y. Zaitsev

http://www.gsi.de/fair/experiments/CBM

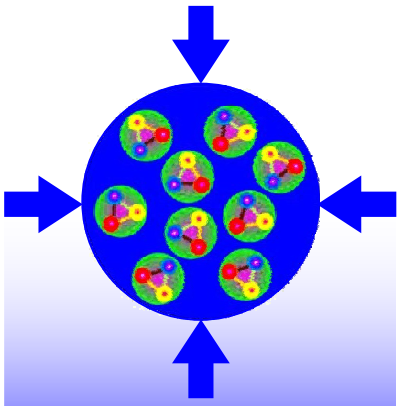

CBM

FAIR

HELMHOLTZ GEMEINSCHAFT

GSI

Bundesministerium für Bildung und Forschung

HIC for FAIR
Helmholtz International Center

HadronPhysics2

DEUTSCH-CHINESISCHES
Jahr der Wissenschaft und Bildung
2009/10